

A SEARCH FOR SUPERNOVA TYPE IA PROGENITORS IN THE MAGELLANIC CLOUDS

by

Kelly Lepo

A thesis submitted in conformity with the requirements
for the degree of Doctor of Philosophy
Graduate Department of Astronomy and Astrophysics
University of Toronto

© Copyright 2015 by Kelly Lepo

Abstract

A search for supernova type Ia progenitors in the Magellanic Clouds

Kelly Lepo

Doctor of Philosophy

Graduate Department of Astronomy and Astrophysics

University of Toronto

2015

While it is generally agreed that type Ia supernovae are thermonuclear explosions of carbon-oxygen white dwarfs, there is still an ongoing debate whether the explosions originate from two white dwarfs merging (the double degenerate or DD scenario) or a white dwarf accreting material off of a normal star companion (the single degenerate or SD scenario). In addition, observed number of suitable progenitor systems is significantly smaller than what is required to match the observed supernova rate.

White dwarfs with high mass transfer rates from their companion objects have been suggested as one type of type Ia supernova progenitor. I performed a survey looking for rapidly accreting white dwarfs (RAWD) in the central core of the SMC. I detect no candidate RAWD. The upper limits from this non-detection are 10 – 14 RAWD in the SMC, assuming they resemble the LMC source LHA 120-N 66 or fainter versions of Wolf-Rayet stars.

I conducted a second survey of the SMC to identify new symbiotic stars – white dwarfs accreting off of a giant star companion, usually via winds. They are another possible type Ia supernova progenitor. All of the stars identified as candidates in the survey are false positives. We conclude that there are about 12 – 18 bright symbiotic stars in the SMC. Even under optimistic assumptions, this is too few objects to make up for the 25 – 130 missing SD progenitors in the SMC.

I also briefly discuss LHA 115-S 18, a peculiar B[e] supergiant in the SMC, which was observed in the symbiotic star survey. S18 is both photometrically and spectroscopically variable. The system likely contains an approximately 12 solar mass B supergiant, along with a hot compact object. The identity of the hot object remains unclear since either a neutron star or a white dwarf could be formed through normal stellar evolutionary processes and are consistent with the observed properties of the hot object.

Contents

1	Introduction:	
	Accreting White Dwarfs and Type Ia supernovae	1
1.1	Type Ia Supernova	1
1.2	Observational Constraints on Progenitor Systems	2
1.3	Accretion Regimes	3
1.3.1	“Just Right” Accretion: Super Soft Sources	5
1.3.2	Slow Accretion: Novae	6
1.3.3	Rapid Accretion	17
1.4	Type Ia Progenitors in the Magellanic Clouds	19
1.4.1	The Expected Number of Type Ia Progenitors in the SMC	20
1.4.2	The hunt for missing Ia progenitors in the LMC and SMC	21
2	Rapidly Accreting White Dwarfs	23
2.1	Introduction	23
2.2	Expected numbers of RAWD	24
2.3	A hunt for RAWD in the SMC	24
2.3.1	Selecting candidate sources	25
2.3.2	Possible Mis-matches between the UIT and MCPS Catalogs	28
2.4	Observations	28
2.4.1	Expectations	30
2.5	Limits to the Number of RAWD	32
2.6	Conclusions	33
2.7	Appendix: Interesting objects found in the survey	34
3	A search for symbiotic binaries in the SMC	39
3.1	Introduction	39
3.2	Observational properties of symbiotic systems	41
3.2.1	Identifying Symbiotic Stars	41
3.2.2	Symbiotic Stars in the Magellanic Clouds	42
3.3	Selecting Candidate Symbiotics	42
3.4	Observations	47
3.5	Results	48
3.5.1	Known Objects	48
3.5.2	Candidate New Emission Line Objects	53

3.6	The Fraction of Symbiotics in the SMC	61
4	New observations of the peculiar emission line supergiant S18	64
4.1	Introduction	64
4.2	B[e] supergiant stars	65
4.3	Photometric and spectroscopic variability	66
4.3.1	Optical spectra and photometry	66
4.3.2	UV spectra and photometry	66
4.3.3	X-ray photometry	67
4.4	Is S18 a Luminous Blue Variable?	67
4.5	The nature of the cool star in S18	71
4.6	The nature of the hot component in S18	71
4.6.1	A White Dwarf Companion?	75
4.6.2	A Neutron Star?	75
4.7	A complete picture of the S18 system	76
4.8	Other B-star/White Dwarf Binaries	77
4.9	The fate of the S18 system	77
5	Conclusion	79
5.1	Understanding RAWDs	79
5.2	Designing a better symbiotic survey	80
5.2.1	Selecting hot objects	80
5.2.2	Better candidate identification	81
5.2.3	Deeper Spectroscopy	81
5.3	Implications for Type Ia Supernova Progenitors	81
	Bibliography	83

Chapter 1

Introduction:

Accreting White Dwarfs and Type Ia supernovae ¹

1.1 Type Ia Supernova

Type Ia supernovae (SN Ia) are thermonuclear explosions of carbon-oxygen white dwarfs (CO WDs). They show remarkably uniform correlations between duration, color, and luminosity, which allow their use as important standard candles in extragalactic astronomy. Despite much observational and theoretical work, however, it is unclear what type of progenitor white dwarf systems explode and how exactly the explosions proceed.

In all models, the explosion is thought to be triggered by the interaction of a white dwarf with a binary companion. The nature of the typical companion, however, remains to be determined. Usually, two scenarios are considered. In the first, the single degenerate (SD) scenario, the companion is a normal, non-degenerate star, and the trigger is related to mass transfer, either via Roche-lobe overflow or a strong wind. In the second, the double degenerate (DD) scenario, the companion is another white dwarf, and the trigger is associated with unstable mass transfer between and subsequent merger of the two white dwarfs. In most models, the white dwarf is assumed to explode as it approaches the Chandrasekhar limit of about $1.4 M_{\odot}$, when the strong increase in central density inevitably leads to runaway fusion. But ignition at lower density may also be possible, if the temperature can be raised on a short timescale, e.g., using a shock from a detonation of an overlying helium layer, or vigorous heating in a merger.

In this thesis, I focus on the question of the progenitors of type Ia supernovae, and in particular on the number of suitable SD systems. I first discuss the observational constraints currently available, and then describe how the behaviour of SD binaries depends on the accretion rate to the white dwarf, discussing what we can learn from observed counterparts. Then, I describe our reasoning for turning to the Magellanic Clouds for trying to measure the number of suitable progenitors.

¹Parts of this chapter were published as the introductory sections of Lepo & van Kerkwijk (2013).

1.2 Observational Constraints on Progenitor Systems

Constraints on models for SN Ia arise both from observations of individual events and from the overall properties of the ensemble. For the latter, the most basic property is the SN Ia rate, of about 2 SN Ia per Hubble time per $1000 M_{\odot}$ of stars formed (for reviews, Maoz & Mannucci 2012; Maoz et al. 2014). For both scenarios, the observed number of suitable progenitor systems appears significantly too small to match this rate. In particular, for the DDs, the SPY survey has failed to find the rather large expected number of binaries with a combined mass above the Chandrasekhar mass (Napiwotzki et al., 2007), and hence the DD scenario may only be viable if systems with a lower combined mass can be made to explode (van Kerkwijk et al., 2010; Badenes & Maoz, 2012). For SD models, the best-suited sources, the so-called super-soft sources are far too few to reproduce the SN Ia rate (Di Stefano 2010a; Gilfanov & Bogdán 2010; see Section 1.3 below).

A more precise constraint can be made by considering the types of stellar populations SN Ia occur in. For instance, although SN Ia are seen in both very young and old stellar populations, more SN Ia are seen in star-forming galaxies than in passively evolving ones (Sullivan et al., 2006). From detailed comparisons of the supernova rate for a galaxy (or an average of galaxies at a certain red shift) to its star formation history (or a mean star formation age based on the type of galaxy), one can infer the delay time distribution (DTD) — the supernova rate per unit time and unit mass as a function of time after an instantaneous burst of star formation. From current evidence, the DTD is proportional to t^{-1} for $1 < t < 10$ Gyr (Maoz & Mannucci, 2012), and at younger ages either continues or slightly turns over (e.g., Pritchett et al. 2008 find $t^{-1/2}$).

Comparing this to models, one finds a relatively poor fit for most SD scenarios, which yield a DTD that peaks between a few 100 Myr and 1–2 Gyr, the time range within which both a sufficient population of white dwarfs have formed and the 2–3 M_{\odot} companions needed to get the favored accretion rates still exist. For DD models, the DTD is expected to be a $\sim t^{-1}$ power law, beginning after a suitable number of white dwarfs have been made. This shape nicely matches the observed one, although, as noted above, standard DD models fail to match the normalization. Here, a cause for caution is that the predicted DTDs depend strongly on assumptions about initial conditions such as the initial mass function and the binary fraction, as well as the relatively poorly constrained physics of mass loss, accretion, and common envelope evolution. Overall, it seems there is still room for a significant SD contribution, especially at delay times of $\lesssim 1$ Gyr, where there DTD is not well constrained (see Maoz et al., 2014, and the references therein).

Turning now to constraints from individual events, arguably the best ones are from SN 2011fe (Nugent et al., 2011), a type Ia supernova in the galaxy M 101. At 6.4 Mpc, this was the closest SN Ia in 25 years. It occurred in a direction with low galactic and host extinction, and had the benefit of several pre-explosion observations. Combined with its exceedingly normal light curve, it is a nearly ideal test case to set limits on the nature of the progenitor system. The pre-explosion data seem to rule out SD systems with red giant and He-star donors (but not lower mass main-sequence companions), bright super-soft X-ray sources (although faint sources such as Cal 83 are not excluded; Liu et al., 2012) and accreting WDs that produce significant He II emission nebulae (Graur et al., 2014). Radio non-detections show that the environment around SN 2011fe has a low density, $n_{\text{CSM}} \lesssim 6 \text{ cm}^{-3}$ (Chomiuk et al., 2012). This rules out SD progenitors, such as rapidly accreting white dwarfs, that leak a significant amount of mass to the circumbinary environment during mass transfer. A recurrent nova, such as U Sco, would fall under the detection limits (Chomiuk et al., 2014). However, even if the WD did have a small main-sequence

companion (as is likely for many SD progenitors including SSS and novae), the blast by the supernova ejecta would likely puff up the companion and leave it over-luminous; if so, it should be visible in a few years as the supernova fades (Shappee et al., 2013; Chomiuk et al., 2014).

Observations of other supernovae show no evidence of interaction of the supernova ejecta with a large companion (Hayden et al., 2010; Nugent et al., 2011; Brown et al., 2012), and no bright former companions have been found in any SN Ia remnant (e.g., Schaefer & Pagnotta 2012; Kerzendorf et al. 2012, 2014). Similarly, strong, pre-explosion mass loss is excluded for the majority of progenitor systems, since neither most type Ia supernovae nor most of their remnants show signs of interaction with a dense circumstellar medium (Panagia et al., 2006; Chomiuk et al., 2012; Badenes et al., 2007).

The above suggests double degenerates as attractive progenitors for most, if not all SN Ia. Except for the basic problem that although there are many double white dwarf systems that have been identified, none have both an orbital period short enough to create a merger in a Hubble time and also have a combined mass that exceeds the Chandrasekhar limit (Napiwotzki et al., 2004). Indeed, this is confirmed by other observational statistics (Badenes & Maoz, 2012) and expected from basic population arguments (van Kerkwijk et al. 2010, and references therein). This rate problem may be solved if mergers with a sub-Chandrasekhar total mass lead to SN Ia (van Kerkwijk et al., 2010), but it remains unclear whether nuclear fusion would start in such mergers and, if so, whether it would lead to an explosion (e.g., Schwab et al. 2012).

Given this basic problem with merging white dwarfs, it seems wise to check also for SD scenarios. There are two basic questions that determine whether SD progenitors provide a viable mechanism for producing type Ia supernovae. First, are there enough progenitor systems to reproduce the observed type Ia supernova rate? This is not a trivial question, since there is a menagerie of accreting white dwarf systems with different observational signatures that could form type Ia supernovae under the right conditions. While basic arguments demonstrate that the total rate of interacting systems easily suffices (van Kerkwijk et al., 2010), the rate of occurrence of many of the individual types of systems is not well known, making it difficult to constrain the likelihood of any particular SD scenario.

The second question is whether the accreting white dwarfs that we know of actually produce type Ia explosions. Even if there were enough SD progenitor systems to produce the type Ia rate, this is no guarantee that the white dwarfs in such systems will accrete enough material to explode and that explosions of SD will look like a type Ia supernova. For instance, many of the proposed accretion scenarios should leave rather dense circumbinary environments as the white dwarf ejects some of the material that it accretes through various means. Will a white dwarf exploding in such an environment look like a type Ia supernova or something else? Do some type Ias explode with more surrounding material than others?

In this thesis, I chiefly seek to establish the answer to the first question — how many SD progenitor systems exist? This may also help us answer the second question. For example, if SD candidates can only account for 20 percent of the observed type Ia rate, then we may expect that the 20 percent of type Ia supernova that arise from SD progenitors should have unusual observational properties.

1.3 Accretion Regimes

A basic requirement for nearly all single-degenerate progenitors is that there must be enough mass in the binary system to get the white dwarf to the Chandrasekhar limit, setting a minimum to the companion

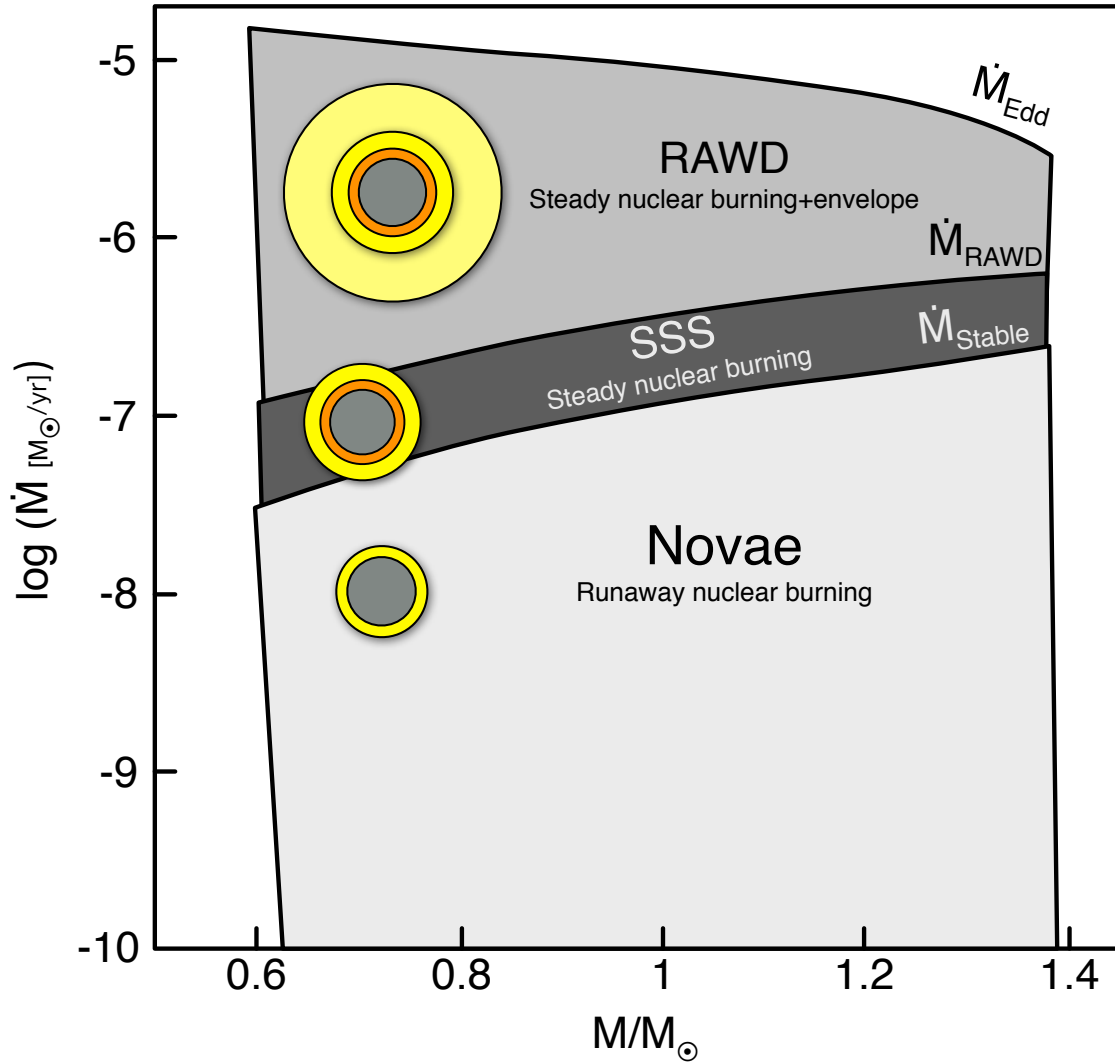


Figure 1.1

The possible states of a nuclear-burning, accreting white dwarf, based on the mass of the white dwarf and the accretion rate from its binary companion. If the white dwarf can accumulate enough mass, it may explode as a type Ia supernova. A sketch (not to scale) shows the rough structure of the white dwarf in each state, showing the white dwarf (grey), the (stable?) helium layer (orange), the hydrogen-burning shell (inner yellow ring), and the extended hydrogen envelope (outer yellow ring). Adapted from Nomoto et al. (2007).

mass. In addition, a sufficiently large fraction of this mass should not just reach the white dwarf (rather than be lost in winds), but also be processed and retained (rather than lost in outbursts). This in turn depends on how fusion proceeds in the matter that reaches the white dwarf.

As outlined in Nomoto et al. (2007) and Wolf et al. (2013), nuclear burning on white dwarfs can occur in three modes, depending on the accretion rate \dot{M} (see Fig. 1.1). In most known systems, cataclysmic variables and symbiotics, white dwarfs accrete below the steady nuclear burning rate ($3.066 \times 10^{-7} (\frac{M}{M_{\odot}} - 0.5357) M_{\odot} \text{ yr}^{-1}$, Nomoto et al. 2007). This slow accretion rate results in a shell that, at the time hydrogen burning ignites, is degenerate and thin, and hence cannot expand sufficiently to counteract the heating due to fusion, leading to a thermonuclear runaway and a nova outburst (Warner, 1995; Prialnik, 1986).

The most popular single-degenerate progenitors are systems where accretion rates are within a narrow range, of about a factor of 2.5 in \dot{M} , where stable nuclear burning occurs on the surface of the white dwarf (with \dot{M} between the limit listed above and $6.68 \times 10^{-7} (\frac{M}{M_{\odot}} - 0.4453) M_{\odot} \text{ yr}^{-1}$, Nomoto et al. 2007). Unlike in a nova, the hotter hydrogen shell is thicker and sufficiently non-degenerate to allow stable burning. For white-dwarf masses above $\sim 0.8 M_{\odot}$, the temperatures become high enough for the peak of the spectrum to move to the soft X-ray range, and these systems can be observed as so-called super-soft sources (SSS, van den Heuvel et al., 1992). With fast accretion and no mass loss (and barring any eruptions caused by instabilities in the He layer, see Idan et al., 2013), white dwarfs in such systems can grow to the Chandrasekhar mass within an interval that reproduces the short end of the known delay-time distribution, as long as the initial WD is sufficiently massive (Di Stefano, 2010a).

White dwarfs may also accrete at a rate above that needed for steady nuclear burning. Such white dwarfs will have a stable hydrogen burning layer over the degenerate core, and an extended envelope. The WD should retain all of the material it fuses on its surface (again barring instabilities in the He layer) and the high accretion rate will give such systems a sufficiently prompt delay time. They will not be super-soft X-ray emitters, since their envelope and/or winds cause the photosphere to move out, and the emission to peak at longer wavelengths, likely the (far) UV. For lack of a better name, we have dubbed these systems rapidly accreting white dwarfs (RAWD; Lepo & van Kerkwijk, 2013).

I now discuss the three groups in more detail, starting with the super-soft sources, as these have generally been considered the best SN Ia progenitors and thus have received most attention.

1.3.1 “Just Right” Accretion: Super Soft Sources

Most super soft sources (SSS) are thought to be short-period, semi-detached binaries, similar to cataclysmic variables (CV) but with a higher accretion rate. These systems consist of a late-type main-sequence or subgiant mass donor and a white dwarf with a surrounding accretion disk. The mass donor overflows its roche-lobe and transfers mass to the accretion disk via a stream from the inner (L1) Lagrange point. Symbiotic stars — binaries that consist of a giant star that transfers mass onto a hot, compact object (usually a white dwarf) via a stellar wind or Roche-lobe overflow in a wide ($\sim 200 - 1000$ day) binary — can also form SSS if their accretion rate is high enough.

For the white dwarf to approach or exceed the Chandrasekhar limit, it must accrete and retain a sufficient amount of mass from its companion and convert the accreted hydrogen into helium through shell burning (and also further helium fusion to carbon and oxygen, which is usually ignored; cf., Idan et al. 2013). Shell burning on the surface of a white dwarf produces luminosities of $10^{37-38} \text{ erg s}^{-1}$ with

spectra that peak at 30–100 eV — i.e., in the soft X-ray regime (Wolf et al., 2013). This nuclear burning luminosity overwhelms any accretion luminosity onto the white dwarf (Di Stefano, 2010a).

Since soft X-rays are easily absorbed by circumstellar material, steadily burning white dwarfs will only be observed as SSS if they are nearly naked. This limits SSS to a narrow range of accretion rates where the white dwarf burns hydrogen in its outer shell as fast as it accretes it from its companion. This also adds to the appeal of SSS as SN Ia progenitors, as it avoids the complications and potential mass loss associated with the accretion regimes above and below the range suitable for SSS.

Unfortunately, the number of SSS observed is too small to reproduce the SN Ia rate: both counts of SSS in nearby galaxies (Di Stefano, 2010a) and total X-ray flux measurements in nearby elliptical galaxies (Gilfanov & Bogdán, 2010) find that the number of SSS are a factor of 10 to 50 short of what is needed. The shortage is made even worse when one includes that, of course, not all of the soft X-ray emission, or even the soft X-ray point sources detected in a galaxy will be from white dwarfs. For instance, Orio et al. (2010) find that of the 89 super-soft X-ray sources in M31, about 30 percent are known novae in the SSS phase at the end of their outbursts, around half are likely novae, and only about 20 percent are the type of persistent, stellar soft X-ray sources that could be steadily accreting white dwarfs.

Thus, either single degenerates do not produce (most) SNe Ia as SSS, or the SSS phase is shorter than expected. The latter would imply less mass gained in the SSS phase, as could be the case if explosions are triggered at sub-Chandrasekhar masses, as in the double detonation model of Woosley & Weaver (1994). But it could also mean that only part of the mass was gained in the SSS phase. According to Hachisu et al. (2010), the latter is expected: they argue the X-ray fluxes observed in elliptical galaxies are consistent with those expected for the single degenerate scenario, as long as one takes into account that the SN Ia progenitor will be a SSS only part of the time, after a phase in which the accretion rate is above that required for producing SSS, and followed by a phase as a recurrent nova.

1.3.2 Slow Accretion: Novae

White dwarfs that accrete below a rate of about $3.066 \times 10^{-7} \left(\frac{M}{M_{\odot}} - 0.5357 \right) M_{\odot} \text{ yr}^{-1}$ from their companion objects will go through cycles of periodic, unstable nuclear burning observed as novae. Depending on the properties of the system, the period between nova outbursts is predicted to vary smoothly, from ~ 1 to 10^8 yr (Yaron et al., 2005). Observationally, however, novae are generally categorized as either classical novae (exactly one observed nova outburst) and recurrent novae (more than one observed nova outburst). Since the oldest photographic plate collections only go back ~ 100 yr, recurrent novae all have recurrence periods of roughly less than once per century. Of course, observational bias also plays a part in whether a system is categorized as either a classical or a recurrent nova — a classical nova may have a recurrence period less than a century if it had an unobserved outburst. Schaefer (2010) estimates that in the Galaxy as many as 60–100 objects classified as classical novae are recurrent novae with outbursts that were missed.

During an nova outburst, the white dwarf system will increase ~ 6 to 19 magnitudes over its pre-nova brightness (Warner, 1995). In general, the larger the peak magnitude, A , of the nova, the shorter the decay time, t_3 (the time it takes the nova to fall 3 mag below the maximum amplitude). While most nova systems will be cataclysmic variables, symbiotic stars can form novae too.

While it can be difficult to determine whether something is a SSS or a RAWD, classifying an object as a nova tends to be fairly straight forward once it has an outburst. This ostentatiousness, combined

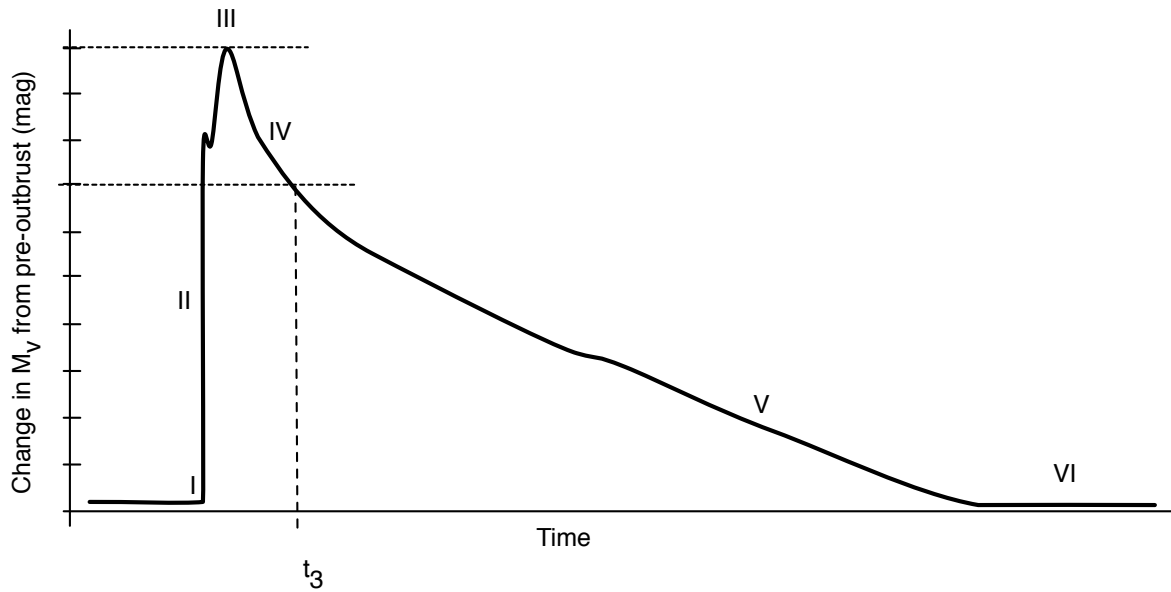


Figure 1.2

Schematic light curve of a nova outburst. Adapted from McLaughlin (1960). Roman numerals correspond to the steps in the nova cycle described in Section 1.3.2.

with what was assumed to be a fairly mature theoretical understanding of the nova cycle, make novae the most straight forward SD progenitors. However, as we will see, these objects tend to be just as messy and hard to understand as their higher accretion rate cousins.

Independent of their possible nature as SN Ia progenitors, novae give us an important way to test our theoretical understanding of shell burning on white dwarfs. By observing the system before outburst, we can determine the accretion rate onto the white dwarf; combined with the time between outbursts, this should give us an observational measure of the shell mass necessary to trigger thermonuclear runaway. By observing the system during and immediately after outburst, we can determine the total amount of the envelope ejected, the amount of mixing between the accreted envelope and the underlying white dwarf and the amount of mass retained on the surface of the white dwarf after outburst. Of course, many of these measurements are easier said than done. For instance, measuring the timescale and amount of mass ejected from the system requires a dedicated campaign of multi-wavelength observations of what are (somewhat) unpredictable transient events.

Below, I describe classical nova theory in some detail and review the observational evidence regarding the key question of whether there is net mass gain or loss over nova cycles, focussing on the well-studied case of T Pyx. I then discuss expected differences for symbiotic novae, and systems with non-standard composition of either the white dwarf or the accreted material.

Classical Nova theory

A simplified model of the nova cycle proceeds as follows (adapted from Warner 1995; Prialnik 1986):

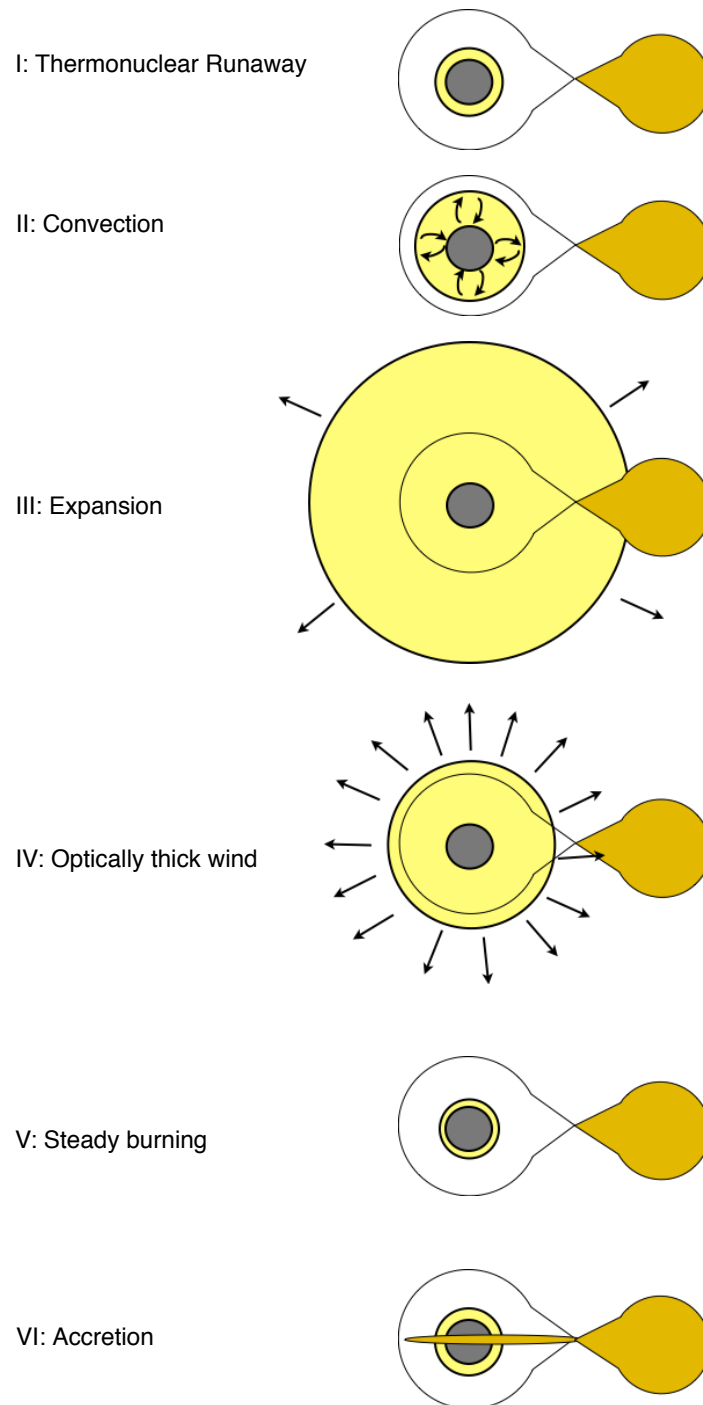


Figure 1.3

Cartoon (not to scale) showing the structure of a nova shell during outburst. Roman numerals correspond to the steps in the nova cycle described in Section 1.3.2.

- I: **Thermonuclear Runaway.** Material accretes onto the WD and undergoes gravitational contraction until the temperature and density at the base of the shell are high enough for ignition of nuclear fusion. This leads to a thermonuclear runaway (TNR) both because the material is somewhat degenerate, and hence raising the temperature a small amount will greatly increase energy output via the CNO cycle but not lead to much of an increase in pressure; and because the shell is thin, which means that, unlike in thick shells or cores of stars, any lifting of the outer parts due to increased pressure will not lead to a reduction in temperature.
- II: **Convection.** As in the cores of massive stars, the temperature sensitivity of the CNO cycle will cause the burning to be highly concentrated, resulting in a large temperature gradient. This in turn leads to convection in the shell, which transports heat to the surface and deposits unstable nuclei produced in intermediate steps of the CNO cycle to the top of the envelope, where they decay and deposit energy. The bolometric luminosity increases sharply, and the shell expands, lifting its degeneracy.
- III: **Expansion.** (~ 5 hr after the beginning of TNR.) The shell will undergo hydrodynamic expansion, while nuclear burning continues. The maximum bolometric luminosity happens at the peak of runaway, which is generally a few hours after its onset. The maximum visual magnitude, where the nova is most likely to be discovered by observers, happens when the photosphere of the expanding ejecta reaches its largest radius. The delay between the two depends on the expansion rate. At this point, the shell can reach over $100 R_{\odot}$, which is generally far beyond the Roche lobe of the WD. An outer shell, containing 10 to 50% of the total envelope mass is ejected and the remaining shell contracts.
- IV: **Optically thick wind.** (a few days after expansion.) If there was no further mass loss, the H-envelope would burn for ~ 100 yr before it ran out of fuel. This may be the case in symbiotic novae, which have very long decay times. In classical novae, the expansion phase is followed by a phase of steady mass loss, probably through radiation-pressure driven winds, which eject most or all of the shell. The photosphere shrinks due to the mass loss, and the flux begins to be dominated by free-free emission by optically thin ejecta located outside of the photosphere (Hachisu & Kato, 2006). As the photosphere shrinks, the spectral energy distribution of the nova shifts to higher energies, leading to a decline in the nova's visual magnitude.
- The presence or absence of optically thick winds depends on the shell mass, which itself depends on the mass of the white dwarf. For very small shell masses, the temperature at the photosphere of the expanding shell never reaches the opacity peak, largely due to iron lines, at $\sim 10^{5.2}$ K — the radiation-pressure gradient is too weak and no winds occur. For very large shell masses, Kato & Hachisu (2009) find that hydrostatic equilibrium can occur when a density inversion layer appears, in which the gas pressure gradient balances the radiation pressure gradient. They suggest this suppresses the optically thick winds and the envelope will quasi-statically expand without wind-induced mass loss.
- V: **Steady burning.** The winds will stop after a large part of the envelope has been ejected. Afterwards, the shell will return to hydrostatic equilibrium and steadily burn hydrogen. This is sometimes referred to as the super-soft source phase. This will continue until the envelope mass reaches the minimum mass required for steady hydrogen burning. The time scale for the wind

phase and the steady burning phase will depend strongly on the mass of the WD and weakly on the total fraction of CNO in the nova envelope. More massive WDs evolve faster, as will envelopes with a higher CNO fraction (Hachisu & Kato, 2006). The surface temperature in this phase is determined by the WD mass – white dwarfs with larger masses have smaller radii and thus higher potentials, leading to higher effective temperatures (Wolf et al., 2013).

Observations indeed show the emergence of soft X-rays, but only after a sufficiently large amount of the original envelope mass has been ejected, so that the soft X-rays produced near the surface are no longer absorbed (Schwarz et al., 2011). Generally, this will be well after the theoretical steady burning phase of the nova cycle has begun, with the delay determined by the total mass of the envelope — larger envelope masses will take longer to be removed (Schwarz et al., 2011). Schwarz et al. (2011) find that for the novae in their sample, the SSS phase generally lasts less than three years, with a mean time of 1.4 yr.

VI: **Accretion.** After hydrogen burning ends, the white dwarf will cool, accrete fresh material, and the nova cycle begins again. Hydrogen may be diffused or mixed into the degenerate core of the WD, while material from the core of the WD may be mixed outward, to an extent that likely depends on the cycle time.

Note that all these phases depend to smaller or larger degrees on both the parameters of the white dwarf and of the accreted material. A summary of the expected effects is provided in Table 1.1.

Do novae gain or lose mass over many cycles?

During the accretion phase of a nova system, some hydrogen (and helium) is diffused or mixed inward from the envelope into the core of the WD and some carbon and oxygen is mixed out. During the TNR, the hydrogen in the core ignites first, causing convection. This dredges up further material from the core into the envelope and increases the metallicity of the nova ejecta (Kovetz & Prialnik, 1985). Calculations by Shen & Bildsten (2009) yield ejecta composed of $\sim 10\%$ core material and $\sim 90\%$ accreted material. Many (but not all) nova spectra indeed show enrichments of one or more of the CNO elements. Other novae (such as Nova Vel 1999) show strong neon lines, suggesting material dredged up from an ONe core. The enhanced CNO abundance in the ignition layer also helps understand some fast novae on smaller WDs (see Table 1.1).

An overall effect of the envelope mass including not just accreted mass but also dredged up material, is that novae could erode the WD. Indeed, from numerical simulations, Yaron et al. (2005) infer that only nova systems with high accretion rates ($\sim 10^{-8} - 10^{-7} M_{\odot} \text{ yr}^{-1}$) will retain mass. Thus, while recurrent novae are often considered good candidate SN Ia progenitors. To know whether this is indeed the case requires one to determine whether, on average, white dwarfs gain rather than lose mass over a nova cycle, and, if they do gain mass, whether this will continue as the WD approaches the Chandrasekhar limit.

To reproduce the short recurrence times of recurrent novae, the nova system must have both massive WD ($M_{\text{WD}} \gtrsim 1.2 M_{\odot}$) and a relatively high accretion rate ($\dot{M} \gtrsim 10^{-7} M_{\odot} \text{ yr}^{-1}$), with the latter implying relatively massive companions. Observational evidence for this, however, is conflicting. Two recurrent novae, U Sco and CI Aql, are double-lined eclipsing systems, allowing reasonable estimates for their mass. U Sco has a $1.55 \pm 0.24 M_{\odot}$ white dwarf and a $0.88 \pm 0.17 M_{\odot}$ companion in a 1.23 d orbit (Thoroughgood et al., 2001), while CI Aql has a $1.00 \pm 0.14 M_{\odot}$ white dwarf and a $2.32 \pm 0.19 M_{\odot}$ companion, likely a

Table 1.1
Parameters that effect the evolution of a nova light curve

Shell mass	The shell mass depends on the mass of the WD, the temperature of the white dwarf, the accretion rate, and the composition of the shell. In general, thicker shells will be denser and more degenerate at the surface of the white dwarf, and thus produce more violent outbursts. The mass of the shell also may determine wether the nova forms a optically thick wind in its decay phase.
M_{WD}	Less massive white dwarfs have lower gravity and a larger radius. They need to accrete more mass in order to reach the temperatures and densities needed for TNR, and thus have thicker shells. Smaller WD have longer recurrence times and longer decay times. The mass of the white dwarf is also a factor in wether a WD will form an optically thick wind.
T_{WD}	White dwarfs with hotter temperatures at the base of the shell need to accumulate less mass before triggering a TNR. They will have thinner shells and less violent outbursts.
\dot{M}	Slower accretion rates will lead to lower temperatures and thus more massive shells and longer recurrence times. This may also allow more mixing between the WD and the accreted shell.
WD composition	For CO white dwarfs, carbon will be dredged up into the nova shell which catalyzes the CNO cycle, allowing a TNR at lower temperature and lower shell mass than would otherwise be the case. Novae on He and ONeMg WDs should thus have thicker, more degenerate envelopes and have ejecta with different abundances WD (both from dredge-up and nuclear burning). While the exact ratios of C, N and O are important for setting the ignition temperature, only the total amount of CNO determines the evolution of the nova at latter times, with more CNO leading to shorter decay times (Hachisu & Kato, 2006).
Shell composition	Hydrogen burns via the CNO cycle, and He via the triple- α process. He burning has a much higher ignition temperature, so for given WD parameters, He novae will have thicker, more degenerate shells.

slightly evolved A star, in a 0.62 d orbit (Sahman et al., 2013). Both of these observations are consistent with theoretical predictions. However, T Pyx (discussed below) likely has a significantly smaller mass than is expected for a recurrent nova, and also has a short period.

Experimentally, to measure the mass retained after a nova requires one to measure the total accreted envelope of a white dwarf (through measuring the time between outbursts and the accretion rate) and then measure the total ejected mass. Especially the latter is difficult and highly model dependent, and currently we only have reasonably good estimates of or constraints on the ejected masses for three recurrent nova outbursts. Based on non-detections of a change in the orbital period after outbursts, Schaefer (2011) find an upper limit on the ejected mass of $\sim 1 \times 10^{-6} M_{\odot}$ for the 2000 outburst of CI Aql and an upper limit of $1.1 \times 10^{-5} M_{\odot}$ for the 1999 outburst of U Sco. Preliminary results from a similar analysis of the 2010 eruption of U Sco suggest that the system ejected $2.5 \times 10^{-5} M_{\odot}$. Given the accretion rate onto the object of $\sim 2 \times 10^{-7} M_{\odot} \text{ yr}^{-1}$, and the recurrence time of about a decade, U Sco is probably losing mass (Schaefer, 2013). CI Aql, on the other hand, with its similar accretion rate of $\sim 1 \times 10^{-7} M_{\odot} \text{ yr}^{-1}$, longer recurrence time, yet smaller ejected mass, may be gaining mass overall (Hachisu et al., 2003; Schaefer, 2011).

Observations of the 2011 T Pyx outburst

T Pyx had outbursts in 1866, 1890, 1902, 1920, 1944 and 1966/1967. Schaefer et al. (2010, 2013) suggest that T Pyx was a normal CV with a fairly small accretion rate until the 1866 outburst irradiated its companion star, triggering a period of rapid mass loss from the companion and an increased accretion rate onto the white dwarf. The accretion rate has been slowing down ever since, which is evident in the increased period between outburst of the system.

In the late 1980s and early 1990s, observing programs were put in place in anticipation of another outburst, ~ 22 years after that of 1967. However, T Pyx did not erupt on schedule. There was much speculation about the reason for the delay and as the early 2000s approached, doubts rose as to whether another nova would happen on T Pyx in our lifetimes. Schaefer (2005), in the same paper that correctly predicted that U Sco would erupt in 2010, predicted that T Pyx would not erupt again until 2052 ± 3 ; later, Schaefer et al. (2010) revised this estimate to the year 2225. This diminished the enthusiasm for monitoring T Pyx, leading to, e.g., the cancellation of the long-running *HST* target of opportunity program for the object. T Pyx surprised everyone when it began to increase in brightness in April 2011 (Schaefer et al., 2013), starting an outburst that proved the Schaefer et al. (2010) predictions were very wrong very shortly after they were published.

One byproduct of the extensive pre-outburst monitoring is that there are a fair number of photometric and spectroscopic observations of the object in quiescence. The interpretation of these observations is still subject to some debate, but it is clear that T Pyx has a small orbital period (1.83 hours; Uthas et al., 2010), which is under the period gap for CVs, and a relatively low inclination, between 10 and 30 degrees (Patterson et al., 1998; Selvelli et al., 2010; Uthas et al., 2010). Recent measurements of a light echo sweeping through the nova remnant after the 2011 outburst show the system is at 4.8 ± 0.5 kpc (Sokoloski et al., 2013).

Less well constrained, however, are the most important parameters: the white-dwarf mass and the mass accretion rate. Uthas et al. (2010) use the separation between peaks in emission line profiles of T Pyx in quiescence, assuming to originate in an accretion disk surrounding the white dwarf, to conclude that the system likely consists of a $0.7 \pm 0.2 M_{\odot}$ white dwarf with a $0.14 \pm 0.03 M_{\odot}$ companion. However,

as Schaefer et al. (2013) note, this estimate relies on assuming the companion is a normal, slightly inflated main-sequence star. Relaxing this requirement or assuming that the emission peaks seen by Uthas et al. (2010) do not come from a disk, one can reproduce the observations with a white dwarf mass of $1.25 - 1.30 M_{\odot}$. This is more consistent with the theoretical prediction that recurrent novae should have a mass $> 1.2 M_{\odot}$ to produce frequent outbursts. Indeed, interpolating the models by (Yaron et al., 2005), can reproduce the observed recurrent time and ejected mass (Schaefer et al., 2010).

For the mass accretion rate, Schaefer et al. (2013) use the change in the orbital period of T Pyx over the period of 1985 to 2011 to determine the mass loss rate from the secondary. Assuming that the white dwarf retains most of this accreted material, this gives an accretion rate of $(1.7-3.5) \times 10^{-7} M_{\odot} \text{ yr}^{-1}$ or a total mass of $(0.75-1.5) \times 10^{-6} M_{\odot}$ accreted over the 44 years since the last outburst. They also obtain an accretion rate by calculating the total mass the white dwarf in T Pyx must have accumulated to trigger a nova, based on several theoretical nova models. This gives a total accreted envelope mass of $10^{-5.9 \pm 0.6} M_{\odot}$ (for a mass-accretion rate of $10^{-7.5 \pm 0.6} M_{\odot} \text{ yr}^{-1}$), reasonably consistent with the rate inferred from the period change.

Although these pre-outburst parameters still have large observational uncertainties, they are perhaps better known than for any other recurrent nova system. Even though the 2011 outburst came as a surprise, several groups were able to make high cadence, multi-wavelength observations of the nova during its entire outburst. We can look at these observations to test our models of the nova cycle, and establish (within observational uncertainties) whether T Pyx gains or loses mass over its nova cycles.

Schaefer et al. (2013) report that while T Pyx maintained a steady $V = 15.5 \pm 0.14$ during quiescence, in April 2011, roughly 18 days before the outburst, its brightness increased by 1.1 mag. This pre-eruption event is puzzling, since there is no theoretical reason for this bump in the light curve to exist. Neither the accretion stream onto the white dwarf (which dominates the luminosity of the system in quiescence), nor the outer layers of the accreted envelope should know that the hydrogen nearest to the white dwarf is about to undergo a TNR.

A combination of radio and X-ray observations suggest that the system likely expelled less than 10 percent of its accreted envelope mass at around the time of the optical rise. The remaining envelope puffed up, creating a large quasi-stable envelope around the white dwarf. This may be the reason for the plateau seen in the optical light curve (Chomiuk et al., 2014; Shore et al., 2013). But around day 75 (~ 2 months after the thermonuclear runaway), the bulk of the envelope mass is expelled. At around day 117, the two shells hit each other, with the shocks leading to X-ray emission (Chomiuk et al., 2014). The cause of this second, delayed ejection is unclear.

Chomiuk et al. (2014) note two possibilities from the literature for creating a delayed ejection of material from a nova. The first, from Kato & Hachisu (2011), is that slow novae may transition from a non-wind steady state (no mass loss) to an optically thick wind state (rapid mass loss) during an outburst. This is caused by frictional drag from the secondary star as it moves through a common envelope surrounding both the WD and the secondary. However, they claim this mechanism only works for WD masses below $0.7 M_{\odot}$; thus, it should not apply to T Pyx.

The second, from Williams (2012) is that the bulk of the mass loss from a nova comes from the binary companion star, rather than the white dwarf. In this scenario, the nova causes the secondary star to inflate above its Roche lobe and eject mass. This can be caused by either irradiation from the WD or the blast from the nova ejecta hitting the secondary star.

In any case, the delayed ejection of the majority of the envelope in the outburst suggests that the secondary star may play more of a role in the evolution of a nova outburst than is traditionally assumed.

Estimates of the total mass ejected were made in several ways. First from the emergence of soft X-rays in *Swift* observations at about day 123, an ejected envelope mass of $\gtrsim 10^{-5} M_{\odot}$ was inferred (Chomiuk et al., 2014). Radio observations suggest a larger mass, between $\sim 10^{-5}$ and $10^{-4} M_{\odot}$ (Nelson et al., 2014), while measurements of the increase in the period of T Pyx after the eruption put the ejected mass at $3 \times 10^{-5} M_{\odot}$ (Patterson et al., 2013). This suggests that the white dwarf T Pyx lost mass during this nova cycle, at least under the assumption that the ejecta was primarily expelled from the white dwarf and not the companion star. This is contrary to the predictions of Yaron et al. (2005), who predict that high mass, high accretion rate systems should gain rather than lose mass.

Black body fits to the soft X-ray spectrum of T Pyx show a temperature of $4 - 5 \times 10^5 K$ (Chomiuk et al., 2014), which is significantly cooler than the black body temperatures measured for RS Oph and U Sco ($\sim 0.7 - 1.0 \times 10^6 K$; Osborne et al., 2011; Orio et al., 2013). This, along with the rather large ejected mass, suggests that T Pyx has a smaller white dwarf ($\sim 1 M_{\odot}$) than other recurrent novae (Wolf et al., 2013).

The 2011 outburst exposes some of the limits of our theoretical understanding of novae and other accreting white dwarfs. For instance: How should we determine the mass of the white dwarf in T Pyx? What is the pre-outburst accretion rate? What was that pre-outburst bump in the light curve? Why were there two mass ejection events? How similar to the 2011 outburst of T Pyx are other nova explosions?

It also shows how messy and frustrating the study of accreting white dwarfs can be. Clearly the cycle of accretion onto a white dwarf (that may or may not have strong magnetic fields), explosively burning hydrogen and then ejecting some or all of the nova shell is more complex than the current models allow. This makes interpreting and connecting observations made at various wavelengths difficult and leads to contradictory claims using the same data of the same object.

Symbiotic Novae

Symbiotic stars consist of an evolved giant that transfers mass to a hot, compact companion — usually a white dwarf. The binary is typically surrounded by nebular material which is lost from the giant and ionized by the WD. Symbiotic systems are identified by their spectra which have characteristics of both a cool component (molecular absorption features like TiO) and a hot component (high ionization emission lines like He II 4686).

The majority of symbiotic systems do not show evidence of outbursts and seem to steadily burn the hydrogen accreted onto the WD. However, some symbiotics form novae. Of course, there is likely some observational bias — symbiotics that steadily burn hydrogen will be much brighter than quiescent symbiotic novae, making systems with higher accretion rates much easier to find.

There are two classes of symbiotic novae — extremely slow novae with outbursts that last for a decade or more, and fast, recurrent novae with outbursts that last for days. The term “symbiotic nova” is usually reserved for sources in the former class, while those in the latter are generally referred to as symbiotic recurrent novae.

Compared to normal novae, outbursts in symbiotic novae proceed very slowly. Rather than days, the rise time is months to years, and the decline time can be a decade or more (Hachisu et al., 2010). The 1979 outburst of the symbiotic nova PU Vul has been extensively studied and was recently modeled by Kato et al. (2011). The outburst began in 1977, reaching its maximum brightness of $V = 8.6$ in 1979. It

maintained this brightness for eight years, except for a deep minimum in 1980. There was no evidence of shell ejection during this time, neither from emission lines nor from shell absorption lines (Yamashita et al., 1982). The nova began to decrease in brightness in 1988, but has not yet reached its pre-outburst state, of $V \simeq 15$. From their modelling, Kato et al. (2011) estimate a mass of the WD component of $\sim 0.6 M_{\odot}$; they find no evidence of any strong mass loss during the outburst.

Symbiotic recurrent novae systems are rare (only 9 out of ~ 200 symbiotic binaries known), and also seem to have unusual components. Most symbiotic stars have a giant with a mass of $\sim 1.6 M_{\odot}$ and a WD with a mass between 0.4 and $0.6 M_{\odot}$. However, for those symbiotic recurrent novae where the masses of the components are known (RS Oph and T CrB), the giant is less massive ($0.4\text{--}0.8 M_{\odot}$) than the rather massive WD ($1.2\text{--}1.4 M_{\odot}$). As in normal recurrent nova, the short decay and recurrence time of the symbiotic variant probably reflect outbursts originating in thin shells on massive white dwarfs.

It was thought that the components of symbiotic binaries do not fill their Roche lobes and interact through winds. However, ellipsoidal variability detected in the light curves of some classical symbiotics, and the relatively high accretion rates needed for recurrent symbiotic novae ($\sim 10^{-7} M_{\odot} \text{ yr}^{-1}$) suggest that some mass transfer via Roche lobe overflow occurs (Schaefer, 2009; Mikolajewska, 2010).

The differences seen between slow classical and symbiotic novae are probably due, at least in part, to the very different orbital separations of the system and thus the different sizes of their Roche lobes. Classical novae arise in cataclysmic variable systems that typically have orbital periods of hours and Roche lobe radii for the WD of $\sim 1 R_{\odot}$. During the expansion phase of the novae, the shell will easily expand past this Roche lobe, causing rapid ejection of the envelope. Symbiotic systems, on the other hand, are wide binaries and the Roche lobe of the WD can be well over $100 R_{\odot}$. Thus, even during the nova expansion, the envelope will not extend beyond the Roche lobe, thus avoiding ejection. Instead, these systems will burn the material in a long, stable hydrogen-burning phase (Iben & Tutukov, 1996).

Indeed, symbiotic novae (and symbiotics in general) are considered good SN Ia progenitors because the white dwarf will tend to retain more mass over the course of many nova cycles than would be the case in a tighter binary, making it easier for the system to grow in mass.

Novae on He WD

Novae on the surface of He white dwarfs (not to be confused with He novae) occur when He white dwarfs accrete hydrogen from a companion. He white dwarfs have a mass less than $0.5 M_{\odot}$. For stable mass transfer to occur, mass donors should have masses less than about two thirds of the WD mass, i.e., $< 0.315 M_{\odot}$. Thus, the companions will be M dwarfs or brown dwarfs (unless mass is transferred via a stellar wind).

The stable mass accretion rate onto a He WD is quite low. Shara et al. (1993) use a mass transfer rate of $< 10^{-9} M_{\odot} \text{ yr}^{-1}$, while Shen et al. (2009), citing dynamical calculations, use a rate of $< 4 \times 10^{-11} M_{\odot} \text{ yr}^{-1}$. The low mass of the WD and the slow accretion rate imply that the shell mass required for TNR is very large, $\sim 10^{-3} M_{\odot}$, and that the recurrence times are very long, 10^7 to 10^8 yr. Because of the long timescales, the He core will equilibrate thermally with the accreted hydrogen layer. The long recurrence time will also allow relatively large amounts of hydrogen to be diffused or mixed into the helium core.

With a helium core, no enhancement of C or O in the accreted shell will happen, and hence the nova ejecta should have roughly solar metal abundances, i.e., an excess of He and a deficit of CNO compared to novae on CO WD (Shen et al., 2009). He nova should follow the same general cycle as a classical

CO WD nova, but perhaps without the optically thick wind phase, due to the large envelope mass and the small WD mass. The envelope may instead expand quasi-statically (Kato & Hachisu, 2009). Even in the presence of other mass loss, the shell will contract and reestablish hydrostatic equilibrium with a mass of $\sim 10^{-4} M_{\odot}$, and steadily burn the remaining hydrogen over ~ 1000 yr.

It is not clear whether the WD will gain mass over time: this depends critically on the amount of mass loss during the nova event, which as yet, with neither observed examples nor good theoretical understanding, remains unknown. In principle, if the WD could grow in mass, at some point He will be ignited, similar to the He flash in a red giant. Given the low accretion rates, however, this will take a long time.

Novae on ONe WD

Stars with masses just below the limit required for core-collapse supernovae, pass through a super-AGB phase and produce ONe WD, with masses over $1 M_{\odot}$. Few calculations of novae on such WDs have been done (instead, most nova models for massive WD assume CO WD – presumably grown in mass due to earlier mass transfer). But generally speaking novae on ONe and CO WDs should be similar, except that there will be less carbon to catalyze the CNO cycle, implying that at low temperatures there will be less nuclear energy released, delaying the onset of TNR. Given this, ONe WDs should accrete somewhat thicker, denser, more degenerate shells, and have somewhat more violent nova explosions, with higher peak temperatures and a more luminous maximum. Because of the higher peak temperature, the ejecta will have higher Z nuclei than expected for CO WDs, as well as enhanced neon due to dredge-up from the core, as is indeed seen in some nova spectra (José & Hernanz, 1998). Since the duration of the optically thick wind phase and the steady nuclear burning phase of the nova weakly depends on the total amount of CNO available to catalyze H burning, ONe should have somewhat longer decay times late in the nova cycle (Hachisu & Kato, 2006).

He novae

He novae (not to be confused with He WD core novae), occur when a white dwarf accretes He from a H-deficient companion, and then explosively burns the accreted He shell. These novae were predicted by Kato et al. (1989) and Iben & Tutukov (1994) and modeled by Kato & Hachisu (2003) and Kato et al. (2008).

He shells will be thicker than H shells because of the much higher ignition temperatures required for the triple-alpha process. The thicker shell may suppress optically thick wind formation and lead to longer decay times. If so, this would allow accreted helium to burn into carbon and oxygen, and remain on the WD after the eruption. Models by Kato et al. (2008) put the mass retention efficiency at up to 50%, suggesting that He nova systems are good SN Ia supernova progenitors.

It is possible, however, that ignition of helium does not lead to a nova-like eruption, but rather to the detonation of the helium layer. Indeed, this underlies the so-called double-detonation model of Woosley & Weaver (1994), where the shock from the helium detonation converges in the center of a CO WD, triggering a carbon detonation there. A similar mechanism is also invoked for mergers of relatively massive white dwarfs, where the accretion of helium at the start of the merger leads to the helium shell detonation that triggers carbon ignition (Pakmor et al., 2013; Shen & Bildsten, 2014).

Observations of helium novae that fail to trigger a SN Ia could test these models. So far, the only clear example of a He nova is V445 Puppis, which erupted in December 2000 (Ashok & Banerjee, 2003;

Kato & Hachisu, 2003; Kato, 2005). Spectra taken during and after the outburst in the optical (Wagner et al., 2001; Iijima & Nakanishi, 2008), near-infrared (Ashok & Banerjee, 2003) and mid-infrared (Lynch et al., 2001) showed lines typical of slow classical novae, with the exception of the absence of hydrogen lines and unusually strong carbon emission lines, the latter presumably from He fusion. The nova was blacked out by carbon-rich dust grains about 7.5 months after the initial discovery of the nova.

There were no spectroscopic observations or measurements of the period of the progenitor of V455 Pup. However, it is present in many photographic plate collections, as well as in more recent multi-band surveys like 2MASS, and hence we know the progenitor had a visual magnitude of 14.5, which at the distance of 8.5 kpc inferred from the expansion of its bipolar nebula, and correcting for extinction, implies it was very luminous, $\sim 2000 L_{\odot}$ (Woudt et al., 2009). While there is no evidence of a prior outburst between 1897-1955 (Woudt et al., 2009), there may be variability in the light curve of the progenitor of about 0.4 mag.

Based on the existing photometry, Kato et al. (2008) find it is unlikely that V445 Pup had a disk that contributed much to the total luminosity of the system. Instead, they suggest most of the luminosity probably came from the He star companion. They also find that the event can be reasonably well reproduced by their nova models, but only if the WD is massive, $\gtrsim 1.35 M_{\odot}$. This again suggests WDs accreting helium may grow in mass, and might eventually explode. Conversely, it suggests double detonations may be difficult to realize in nature, at least in systems where the WD accretes relatively slowly.

1.3.3 Rapid Accretion

The final accretion regime occurs when white dwarfs accrete at a rate above the range for which all of it can be burned steadily, sources we have dubbed rapidly accreting white dwarfs (RAWD, Lepo & van Kerkwijk 2013). Such white dwarfs will still have a hydrogen burning layer over the degenerate core, but likely with an extended envelope or wind through which material that cannot be burnt sufficiently fast is lost. In principle, since the WD should retain the material it fuses on its surface, the WD could grow in mass and ignite – relatively promptly given the high accretion rate.

Whether this indeed happens depends on how these systems really behave. From detailed simulations, Idan et al. (2013) recently found that hydrogen is not burnt steadily, but rather through many short cycles, in which rapid accretion alternates with fusion. Here, the cycles occur because Idan et al. assume that when the luminosity of the WD increases rapidly, accretion is turned off. It remains to be seen whether this indeed happens, or whether instead some stable configuration can be found where matter is simultaneously accreted, burnt, and ejected (perhaps in different locations). Independently, however, the work of Idan et al. (2013) brought attention to an often-ignored question, of the fate of the helium that is produced: Idan et al. (2013) found that once sufficient helium had accumulated to trigger a TNR, the resulting helium nova ejected most of the accreted mass on the WD. If so, RAWD would be unlikely SN Ia progenitors.

Observationally, a RAWD will likely not be a super-soft X-ray emitter, since the excess mass in the envelope and/or winds cause the photosphere to move out, and the emission to peak at longer wavelengths. There are two general ideas for what a RAWD might look like instead. The simplest and perhaps naive one would be that the white dwarf tries to become a red giant, but is limited by the orbit, and loses mass from the L2 Lagrange point and/or forms a common envelope (Nomoto et al., 1979; Iben, 1988). Given that most cataclysmic variables have periods of about 80 min to 10 hours, one thus

expects the envelope to be at most a few solar radii in size. With an expected luminosity of $\sim 10^{4.5} L_{\odot}$ (Nomoto et al., 2007), the effective temperature would be $\sim 10^{4.5}$ to 10^5 K, i.e., the sources might look like undersized OB stars. If the accretion rate is high enough for the white dwarf to overflow to its Roche lobe, the system will form a common envelope. While such systems may be interesting on their own, they will not be type Ia progenitors.

The second possibility is that the white dwarf will lose mass through optically thick winds (leading to the name of “accretion wind evolution system”), produced by the same strong peak in opacity (largely due to iron lines) at $\sim 10^{5.2}$ K that drives winds in late-time nova envelopes (Hachisu et al., 1996). Depending on the mass loss rate and the accretion rate, the white dwarf may or may not fill its Roche lobe. With such a wind, these sources may appear like Wolf-Rayet stars or Wolf-Rayet planetary nebula, of WN subtype, i.e., showing the products of the CNO cycle.

In either case, one might hope to identify a population of rapidly accreting white dwarfs by looking for sources that are bright in the ultraviolet and are hot, but are fainter than main-sequence stars of similar temperature. I present such a search elsewhere in this thesis. Here, I restrict myself to describing some of the better studied objects suggested to be RAWD, the V Sge stars and the [WN] core of the planetary nebula LHA 120-N 66 in the LMC.

V Sge Stars

V Sge is a peculiar double-lined binary that shows clear eclipses in its light curve, with a period of 0.541 days. There is no consensus on the exact nature of the system, and several models have been proposed to explain its light curve. Most relevant for our purposes is the suggestion by Hachisu & Kato (2003a) that V Sge may be a white dwarf accreting at a high rate from a Roche-lobe filling companion. Their models assume a $1.25 M_{\odot}$ WD and a 3.0-3.5 M_{\odot} companion, which would make the system an excellent SN Ia progenitor.

V Sge shows quasi-periodic optical high and low states of ~ 180 days, and is a SSS in the low state. In the optical high state, the WD accretes faster than it can burn hydrogen, and thus is a RAWD. Hachisu & Kato (2003a) suggest that during this state, the accretion disk around the white dwarf grows, becoming circumbinary and absorbing soft X-rays produced by the white dwarf. The white dwarf also accumulates matter on its surface, creating an extended envelope. The expanding photosphere pushes the peak of the white dwarf’s emission to longer wavelengths. During the optically low state, winds from the white dwarf suppress the mass accretion rate from the companion. The disk shrinks, as does the envelope of the white dwarf. This brings the peak of the emission from the white dwarf to shorter wavelengths, and it should behave much like a SSS. The smaller, less flared disk is less luminous, and thus contributes less to the total luminosity of the system.

The spectra of V Sge show numerous strong emission lines of highly ionized species, including both O VI (3434, 3811, 5290, 5584 Å) and N V (4945, 4603 Å). These lines are not present in most of the known Galactic Wolf-Rayet stars. It also has a He II 4686 line that is about twice as strong as its H β line, indicating a high degree of ionization. No He I is seen, which suggests the lines are formed by photoionization (Steiner & Diaz, 1998).

Stars with similar spectra, including QU Carinae, WX Cen, V617 Sgr, and RX J0513.9-6951, are considered members of the “V Sagittae” class of nova-like cataclysmic variables (Steiner & Diaz, 1998). While not as well studied, it is assumed that these objects are physically similar to V Sge. In particular, Hachisu & Kato (2003b) model the transient super-soft X-ray source RX J0513.9-6951 using the same

disk/wind model used for V Sge, and attribute differences in their observed properties to different viewing geometry.

The Planetary Nebula LHA 120-N 66 and its [WN] Core

LHA 120-N 66 (also known as WSPN 35 and SMP LMC 83, hereafter N 66) is a unusual planetary nebula with an early [WN] core, located in the Large Magellanic Cloud. It undergoes periodic outbursts, where its luminosity increases by about an order of magnitude for a period of years. In its quiescent state, its luminosity ($\log[L/L_{\odot}] = 4.5$) exceeds that of known [WC] planetary nebulae, and in outburst its luminosity ($\log[L/L_{\odot}] = 5.4$) is on par with galactic WN stars (Hamann et al., 2003). Two outbursts have been observed, with peak luminosities occurring in 1994 and 2007 (Peña et al., 1995; Hamann et al., 2003; Peña et al., 2008). There is no evidence in archival data that any outbursts occurred from 1955 to 1990, and it is not detected as an X-ray source (Hamann et al., 2003). We conclude that it is in its high state at most half the time, and never reaches a state similar to a SSS.

Spectra of N 66 show incompletely CNO-processed material — strong helium emission lines, some hydrogen, enhanced nitrogen and depleted carbon. From the width of the lines one infers a terminal wind speed $v_{\infty} = 2200 \text{ km s}^{-1}$ during outburst and 1600 km s^{-1} during quiescence. The model that has the fewest contradictions with the observed properties of N 66, is that the central object of the planetary nebula is a low-mass binary, with a WD primary and a non-degenerate secondary. In this model, the WD rapidly accretes mass, and loses some to winds, in other words, it is a RAWD. The outbursts — hard to explain with a single star model — may be due to hydrogen or helium shell flashes on the white dwarf (Hamann et al., 2003).

Very little work has been done to verify if the core of N 66 is in fact a binary. Hamann et al. (2003) find that there is no radial velocity variations in the observed spectra that would indicate a binary system. However, given the widths of the emission lines and the confusion by nebular material surrounding the central objects(s), this may not be surprising. Unless there is a systematic search for RV variations, looking preferentially at lines that originate from the irradiated atmosphere of a main-sequence companion, it is unlikely that one will see evidence of a periodic signal (see, e.g., Miszalski et al. (2011) for a successful spectroscopic detection of a binary-core planetary nebula).

Assuming the system consists of a white dwarf and a normal star, models by Hamann et al. (2003) put the radius of the photosphere of the WD at $0.52 - 1.38 R_{\odot}$. This is about what one would expect for the Roche lobe of a white dwarf in a close binary. They find the mass loss rate of the object varies from $\dot{M} = 10^{-5.7}$ during quiescence to $10^{-5.0} M_{\odot} \text{ yr}^{-1}$ during outburst. This would put the white dwarf in the high \dot{M} regime. Both the radius and \dot{M} estimates are consistent with our ideas of RAWD.

While V Sge seems to only be a RAWD during its optically high state, the cooler surface temperature and lack of X-ray detection of N 66 suggests it is a RAWD full time. This may be because the average mass loss rate from the secondary, and hence the accretion rate onto the WD and the mass loss rate from winds, is higher in N 66 than in V Sge.

1.4 Type Ia Progenitors in the Magellanic Clouds

In this thesis, I describe surveys for two types of candidate SN Ia progenitors, for neither of which there currently are good constraints: rapidly accreting white dwarfs and symbiotics. Both of these contain white dwarfs that accrete fast and thus should grow in mass relatively rapidly, like the super-soft sources

that have been the favored SN Ia progenitor candidate, yet for both types of sources there are good reasons to expect them to have escaped detection in previous surveys that focused on super-soft sources (and showed these were too few to reproduce the SN Ia rate; Section 1.3.1).

For my searches, I chose to conduct surveys of the Small Magellanic Cloud (SMC). Both Magellanic Clouds are ideal candidates for establishing the rates of various proposed type Ia progenitors because:

- 1 They have a small angular size and dense but still resolvable stellar fields. This means that a large number of candidates can be observed simultaneously with modern multi-object spectrometers.
- 2 There is very little extinction towards the MC, which avoids contamination by reddened stars.
- 3 They have a known distance, which simplifies, among other things, luminosity calculations.

While in the Milky Way one is able to observe fainter sources, the large amount of extinction along the galactic plane and usually poorly known distances prevent us from having a true understanding of the populations of white-dwarf binaries in our galaxy. And while in other galaxies one has larger samples within which to hunt for type Ia progenitors, both identification and follow-up is made difficult by the inability to resolve individual point sources, either for the entire galaxy, or for the inner portion of the galaxy for nearby spirals such as M31. Thus, the Magellanic clouds seem to offer good hope for studying the rate of various type Ia supernova progenitors. I chose to work primarily in the Small Magellanic Cloud because the better UV coverage of the galaxy is useful for spotting the hot sources expected for binaries with accreting white dwarfs.

The larger than Galactic yet not quite extragalactic distance of the Magellanic clouds has its downsides as well. For instance, their relatively large distance yet large area mean that surveys often cover only parts of the galaxies yet are relatively shallow. The Magellanic clouds were surveyed by the Ultraviolet Imaging Telescope (UIT) during two space shuttle missions in late 1990 and early 1995, using several FUV filters, including B5 at 162 nm (Cornett et al., 1997). UIT observations cover the central bar of the SMC, but exclude the central portion of the galaxy. The UIT catalog suffers from somewhat poor astrometry, gaps due to scratches on the photographic plates used to make the survey, and a depth only to $m_{162} \sim 14.5$. The LMC and SMC were also observed by GALEX, at the end of its lifetime (Bianchi et al., 2014). Those observations, only cover the outer portions of the two galaxies, since the MC are close enough to make the inner portions too bright. Unfortunately, the UIT and GALEX catalogs for the SMC do not overlap to a significant extent.

Despite the above difficulties, the UV catalogs of the SMC provide a good option to try to find single-degenerate systems, intriguing in particular since selection using ultraviolet criteria has not been attempted before. Below, I first discuss how many SN Ia progenitors should exist in the SMC, and then briefly introduce the two surveys I conducted.

1.4.1 The Expected Number of Type Ia Progenitors in the SMC

We follow Di Stefano (2010a) and calculate the number of accreting WDs expected in the SMC, based on a SN Ia rate estimated from the galaxy's blue luminosity (Eq. 4 from her work),

$$N_{\text{acc}} = 1500 \left(\frac{\Delta M}{0.4 M_{\odot}} \right) \left(\frac{8 \times 10^{-7} M_{\odot} \text{yr}^{-1}}{\beta \dot{M}_{\text{in}}} \right) \left(\frac{L_B}{10^{10} L_{\odot}} \right), \quad (1.1)$$

where \dot{M}_{in} is the mass transfer rate and β is a retention factor, which is a function of M_{WD} , the mass of the white dwarf, and \dot{M}_{in} .

The maximum accretion rate implicit in the derivation of this equation is $\beta\dot{M}_{\text{in}} = 8 \times 10^{-7} M_{\odot} \text{ yr}^{-1}$ for a solar mass white dwarf (or, equivalently, a $0.4 M_{\odot}$ gain in mass and an accretion lifetime of 5×10^5 years). This is approximately the upper limit for steady hydrogen burning on the white dwarf and thus the most rapid rate that mass can be added to the white dwarf (for higher accretion rates, the excess is lost through winds or outflows). Stars with smaller accretion rates than the steady burning limit will have longer lifetimes, and thus there will be more accreting systems to observe.

With the maximum rate, one can thus infer a rough lower limit on the number of accreting white dwarfs that we should observe. Using $\Delta M = 0.2$ to $0.8 M_{\odot}$, corresponding to initial masses from $1.2 M_{\odot}$ (the maximum possible for a CO white dwarf) to $0.6 M_{\odot}$ (the typical mass of WDs formed in isolation), and $L_B = 4.4 \times 10^8 L_{\odot}$ for the SMC, we find that the number of accreting white dwarfs needed to reproduce the SN Ia rate is $N_{\text{acc}} = 33\text{--}132$.

1.4.2 The hunt for missing Ia progenitors in the LMC and SMC

If most SN Ia arise in progenitors in which matter is burnt on the WD as it is accreted, the above numbers are rough expectations rather than lower limits. For this case, since there are only four (possibly five) known super-soft sources in the SMC (Greiner, 2000; Sturm et al., 2011), there should be dozens of missing systems in the SMC. So, where are the missing progenitors? Before abandoning the SD progenitor model entirely in favor of the DD model, it would be useful to have a complete census of all accreting white dwarfs in a particular galaxy (like the SMC). Even if not all of these white dwarf systems will eventually form SN Ia, understanding the formation rate of white dwarf binaries and the range of accretion rates onto the white dwarfs will help us understand the stellar evolution processes that lead to SD progenitors. Since DD progenitors will also go through a phase where one of the stars in the system is a white dwarf and the other is still a normal star, this may help us understand the distribution of DD progenitors as well. In the next two chapters, I describe searches for these missing systems.

In Chapter 2, I describe a search for rapidly accreting white dwarfs, which, as discussed in Section 1.3.3, would not be seen as X-ray sources but are likely bright UV sources, because they accrete more material than they can burn and have photospheres well above the white-dwarf surface. Combining data from the UIT (UV), MCPS (optical) and 2MASS (IR) catalogs, I created a multi-wavelength photometric catalog of point sources in the SMC. Then, selecting objects that were bright in the far UV and with blue far UV-V colors, I took followup spectra using the multi-object spectrographs VLT/FLAMES and AAO/AAOmega. Non-detections of any new RAWD in the SMC put upper limits of the number of high accretion rate white dwarfs in the galaxy.

Next, in Chapter 3, I describe a second survey, for symbiotics. There is a known population of symbiotics stars in the SMC, which seem to be concentrated in the outskirts of the galaxy. However, this sample suffers from observational biases since it is much easier to find bright symbiotics away from the dense stellar field in the central bar of the galaxy. Thus, there is almost certainly a population of unobserved symbiotics in the SMC, some of which could be SN Ia progenitors. Using similar strategy to the RAWD survey, I used GALEX and UIT (UV), MCPS (optical) and 2MASS (IR) colors to identify possible symbiotics and then took ~ 1000 followup spectra using AAO/AAOmega to look for new symbiotics in the SMC.

In chapter 4, I discuss the B[e] supergiant S18, which is not a symbiotic star, yet has emission lines (He II 4686 and Raman scattered OVI) that are rarely found in objects that are not symbiotic stars. I speculate on the nature of these lines and the implications for the nature of the S18 system.

Chapter 2

Rapidly Accreting White Dwarfs ¹

The nature of the progenitors of type Ia supernovae is still a mystery. While plausible candidates are known for both the single degenerate and double degenerate models, the observed numbers fall significantly short of what is required to reproduce the type Ia supernovae rate. White dwarfs with high mass transfer rates from their companion object have been suggested as one possible type of type Ia supernova progenitor.

We present a survey using multi-object spectrographs looking for rapidly accreting white dwarfs (RAWD) in the central core of the SMC, from objects selected to be bright in the far UV and with blue far UV-V colors. While we find some unusual objects, and recover a known planetary nebula and WR stars, we detect no candidate RAWD. The upper limits from this non-detection depend on our expectations of what a RAWD should look like, as well as assumptions about the internal extinction of the SMC. Assuming they resemble the LMC source LHA 120-N 66 or fainter versions of Wolf-Rayet stars we set an upper limit of 10 – 14 RAWD in the SMC. However, our survey is unlikely to detect objects like V Sge, and hence we cannot set meaningful upper limits if RAWD generally resemble these.

2.1 Introduction

As was discussed in chapter 1, the nature of the progenitors of type Ia supernovae is still a mystery. While plausible candidates are known for both the single degenerate and double degenerate models, the observed numbers fall significantly short of what is required to reproduce the type Ia supernovae rate.

Some of the most promising single-degenerate type Ia progenitors are recurrent novae and super-soft sources (SSS). White dwarfs with higher mass transfer rates can also be type Ia supernova progenitors. For these rapidly accreting white dwarfs (RAWD), more material than is needed for steady burning accretes on the white dwarf, and extends the white dwarf’s photosphere. Unlike super-soft sources, such objects will likely not be detectable at soft X-ray energies, but will be bright at longer wavelengths, such as the far ultraviolet (UV). Possible examples include LHA 120-N 66 in the LMC (hereafter, LMC N66) and the V Sagittae stars.

There are two general ideas for what a RAWD might look like. The simplest and perhaps naive one would be that the white dwarf tries to become a red giant, but is limited by its Roche lobe, and loses mass from the L2 Lagrange point and/or forms a common envelope (Nomoto et al., 1979; Iben, 1988).

¹Parts of this chapter were published as Lepo & van Kerkwijk (2013).

Given that most cataclysmic variables have periods of about 80 min to 10 hours, one expects the envelope to be at most a few solar radii in size. With an expected luminosity of $\sim 10^{4.5} L_{\odot}$ (Nomoto et al., 2007), the effective temperature would be $\sim 10^{4.5}$ to 10^5 K, i.e., the sources might look like undersized OB stars. If the accretion rate is high enough for the white dwarf to overflow its Roche lobe, the system will form a common envelope. While such systems may be interesting on their own, they will not be type Ia progenitors.

The second possibility is that the white dwarf will lose mass through optically thick winds, produced by the same strong peak in opacity (largely due to iron lines) at $T \simeq 150,000$ K that drives winds in late-time nova envelopes (Hachisu et al., 1996). Depending on the mass loss rate and the accretion rate, the white dwarf may or may not fill its Roche lobe. With such a wind, these sources may appear like Wolf-Rayet stars or [WR] planetary nebula (of WN subtype, i.e., showing the products of the CNO cycle).

In either case, one might hope to identify a population of rapidly accreting white dwarfs by looking for sources that are bright in the ultraviolet and are hot, but are fainter than main-sequence stars of similar temperature. Here, we present our search for such UV-bright sources in the Small Magellanic Cloud.

2.2 Expected numbers of RAWD

In order to search for RAWD, it is helpful to have dense but still resolvable stellar fields, so that many stars can be scrutinized, low extinction along the line of sight, allowing the ultraviolet to pass through, and known distance, so that one can use both color and luminosity for selection. The Magellanic Clouds fulfill these criteria best, and we picked the Small Magellanic Cloud (SMC) as it had better UV coverage.

In chapter 1, we calculated the number of accreting WDs expected in the SMC, based on a SN Ia rate estimated from the galaxy’s blue luminosity — $N_{\text{acc}} = 33\text{--}132$.

Since there are only four (possibly five) known SSS in the SMC (Greiner, 2000; Sturm et al., 2011), there should be dozens of missing progenitors in the SMC if single degenerates produce most SN Ia. From the models of Hachisu et al. (2008, 2010), such progenitors spend only 10% of their time as SSS; for all systems that have a secondary with a mass greater than $\sim 2.0 M_{\odot}$, most of the accretion will happen in a wind (or rapid accretion) phase early in their evolution that lasts $\sim 5 \times 10^5$ yr, i.e., while the sources are RAWD, before the accretion rate drops and the objects become SSS and later recurrent novae.

Of course, even if single degenerates are not responsible for most SN Ia, one would expect some rapidly accreting white dwarfs with high accretion rates to exist, in numbers likely not too dissimilar from those of the SSS.

2.3 A hunt for RAWD in the SMC

While some examples of possible RAWD are known, we cannot be sure these sample the full array of possibilities (or that these examples are genuine RAWD). Generally, one expects the emission to peak in the UV, since the luminosity is high, yet the effective radius is relatively small, as it is unlikely to exceed the Roche lobe. Hence, we aimed to select candidates that had unusual UV emission, indicative of a hot component. (We will return to the effectiveness of these estimates in Section 2.4.1.)

The Magellanic clouds were surveyed by the Ultraviolet Imaging Telescope (UIT) during two space shuttle missions in late 1990 and early 1995, using several FUV filters, including B5 at 162 nm (Cornett et al., 1997). Since the UIT observations cover the entire central bar of the SMC, while the LMC observations are in scattered fields, we chose to use the SMC data to simplify followup observations.²

2.3.1 Selecting candidate sources

We matched objects in the UIT SMC catalog with the optical Magellanic Cloud Photometric Survey (MCPS, Zaritsky et al., 2002). Since the astrometry given in the two catalogs is not on exactly the same system, we redid the astrometry using an iterative procedure, in which we: (1) found the object with the brightest U magnitude in the MCPS catalog within a given radius of each UIT point; (2) scaled, rotated, and translated all of the points in the UIT field, performing a least squared fit to minimize the distance between the matched UIT and MCPS points; and (3) decreased the search radius and repeated steps (1) and (2).

We first ran this algorithm on all points in the MCPS catalog with $U < 16$, and beginning with the resulting, revised positions, ran it on all points in the MCPS catalog with $U < 19$. We began with a search radius of 20 arcsec and finished with a radius of 3 arcsec. Using these final matches between the catalogs, we took the position of each point to be the position of the brightest source in the MCPS catalog within 3 arcseconds of a UIT point.

Unfortunately, due to a programming error, we actually selected the faintest rather than the brightest star in step (1), which effected our astrometric solution as well as the matches between the two catalogs. We chose our fiber positions before we noticed this error. However, since there are not that many MCPS points with $U < 19$ around each UIT point, this does not seem to have had a large effect. Re-running the matching code to correctly select the brightest star, we see almost identical numbers of matches between the two catalogs (with 6230 matches originally, 6228 with the correction). The same MCPS point was selected around a UTI point for 5907 sources, meaning a different point was selected only for about 5 percent of all points in our catalog. Our online data in Lepo & van Kerkwijk (2013) includes the revised UIT/MCPS catalog, and includes all MCPS points within 3 arcsec of the UIT point. From here on, we will only consider those sources for which the identification did not change.

The color-magnitude cuts for candidate sources were chosen to maximize the number of objects with a possible UV excess, while minimizing the number of normal main sequence stars in our survey. Figure 2.1 is a color magnitude diagram of $m_{162} - V$ vs V (here, magnitudes are on the ST system). Overlaid on this plot is the position of the main sequence calculated by Cornett et al. (1997).

The central, main sequence clump is by definition the densest region of Fig. 2.1. Thus, rather than using a color cut to identify the outliers, we used a density cut. To do this we calculated the number of neighboring points around each point in Fig. 2.1, within a radius of 0.3 mag in color-magnitude space. We selected candidate points that were more than 1.35σ outliers in the number of neighboring points. This essentially amounted to a cut in color of $m_{162} - V < -4$ for the points with a UV excess (shown in blue in Fig. 2.1). For sources with a UV deficit, however, the color limit varies much more with brightness (shown in red).

²The central regions of both Magellanic clouds are too UV bright for *GALEX*.

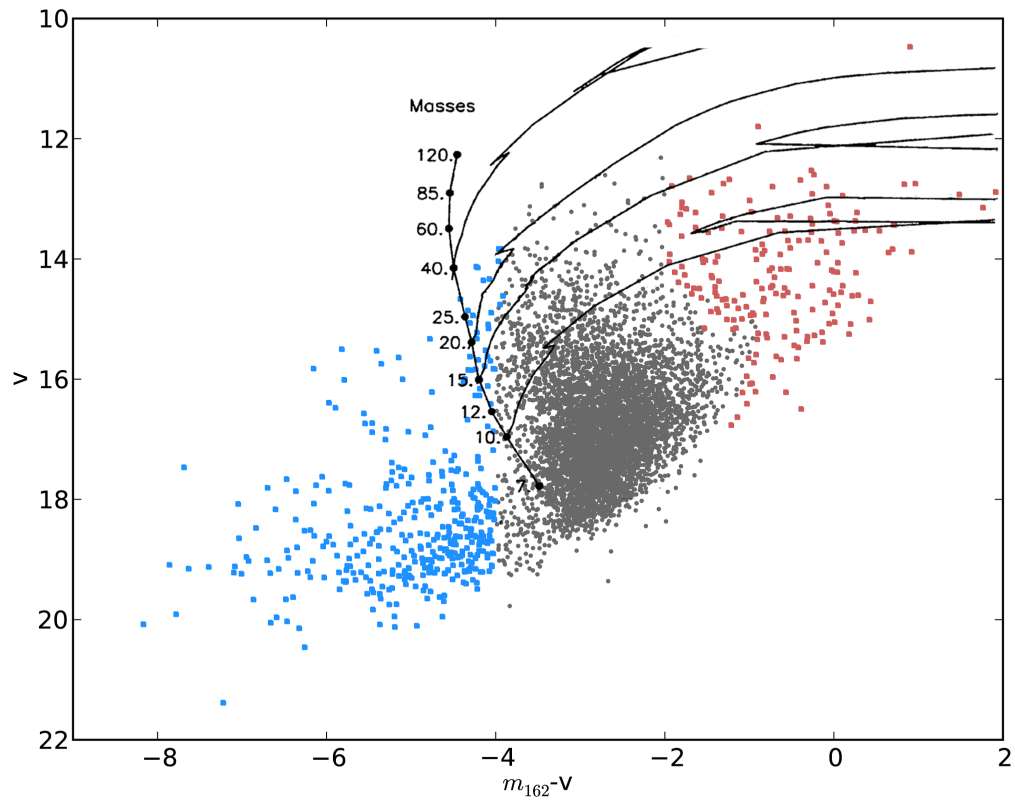


Figure 2.1
 Ultraviolet to visual color-magnitude diagram for stars in the bar of the SMC, using values from UIT and MCPS. There are 5670 sources in the central clump (circles), 175 sources redder than the central clump (squares) and 385 sources bluer than the central clump (squares). Overlaid are evolutionary tracks of OB stars (Fig. 4 from Cornett et al. 1997).

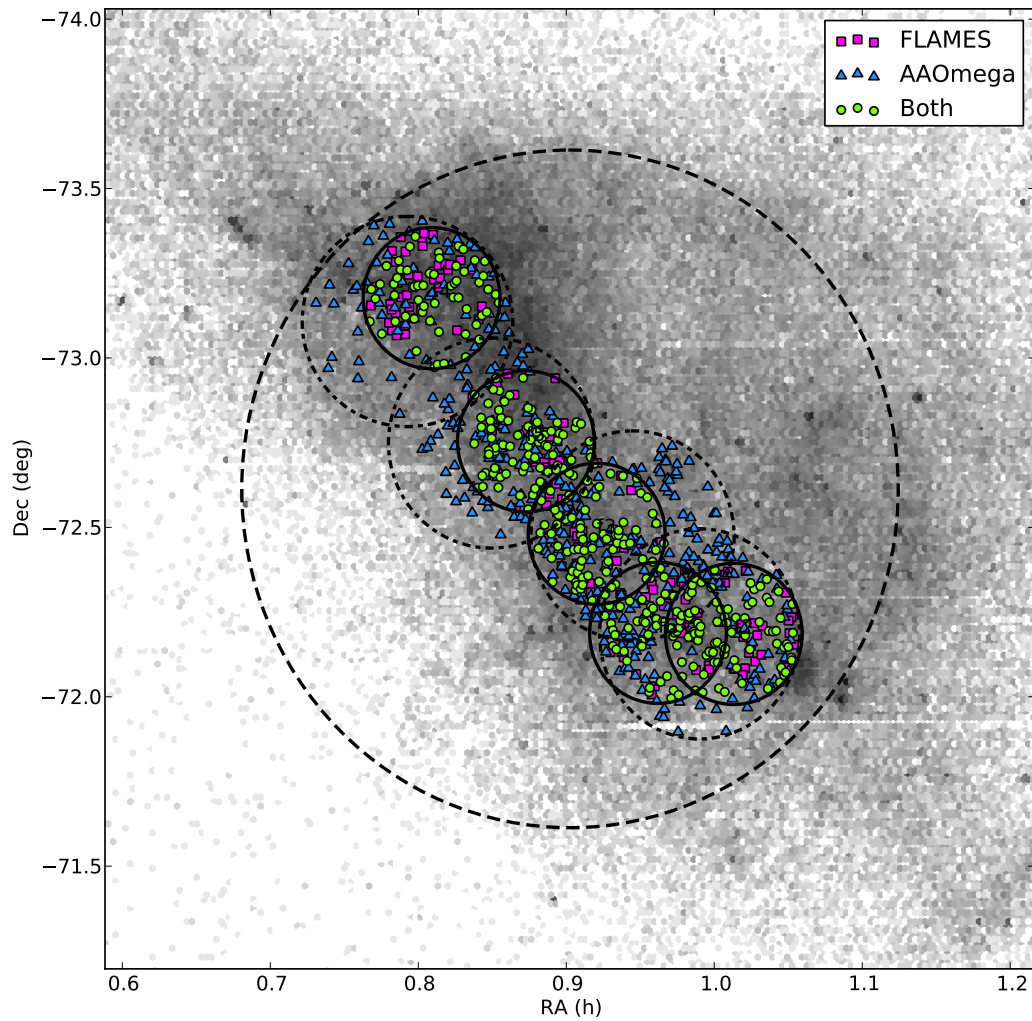


Figure 2.2

Objects observed in this survey. In the background is a density map of objects in the SMC MCPS survey, with $V < 19$, which traces the stellar density of the SMC. The dot-dashed lines represent the fields observed by UIT. The large, black dashed line is the AAOmega field, the smaller solid lines are the FLAMES fields. The purple square points are objects observe with FLAMES, the blue triangles are objects observed by AAOmega, and the green circular points are observed by both.

2.3.2 Possible Mis-matches between the UIT and MCPS Catalogs

An inherent problem in trying to find outliers by matching two catalogs of astronomical objects taken at two different wavelengths at two different times is that one will find not just objects with a true color excess but also variable sources and bad matches. For instance, for some of the objects that were outliers based on their $m_{162} - V$ color, we find unremarkable spectra, and it seems likely the UV emission was instead from a much brighter object just beyond our selection radius (for which typically the color would place it in the central, main sequence clump in Fig. 2.1).

To get a handle on the influence of mis-matches, we looked at each object in the MCPS (optical) catalog we matched to each UIT (FUV) point, as well as at the second closest star in the MCPS catalog. The second closest star should, in general, be the most likely match if the initial one was incorrect.

For our initial match, 233 of 5907 objects (4%) were bluer than the central clump of the CMD. Using the second closest MCPS point, we get 3333 out of 5907 objects (56.4%) bluer than the central clump. Clearly, the first match was much better. Using the second closest MCPS point moves 157 (67.4%) of the objects that were originally “blue” candidates into the central clump.

For comparison, we also assigned each UIT point a random point from the MCPS catalog. If the matching program were perfect, the second closest point should be identical to a random point, as there would be no miss-matches and hence no special significance to the second closest point in the MCPS catalog. After 500 runs, using the V magnitude from a random MCPS point and the original UIT m_{162} magnitude, 3251 (± 34) of 5907 objects (55%) were bluer than the central clump. Assigning a random point produces an almost identical CMD to the one produced using the second closest point, within errors. It seems that our matching program did a good job for the majority of the sources in the UIT catalog. However, using a random MCPS point only moves 63 (± 6 , 2%) of the objects that were originally bluer than the central clump into the central clump. The improvement seen using the second closest point over a random point suggests that $\sim 40\%$ of the original bluer outliers were due to bad matches between the UIT and the MCPS catalogs. Conversely, this suggests that $\sim 60\%$ of the blue outliers should be true matches. Of course, this does not prove a true excess (instead of measurement errors or variability), but does suggest that any RAWD with properties consistent with our selection criteria would likely be selected.

2.4 Observations

We took optical spectra of a majority of the objects outside of the main-sequence clump of Figure 2.1, using the multi-object spectrometers FLAMES on the VLT and AAOmega on the Anglo-Australian Telescope (AAT) (Pasquini et al., 2002; Sharp et al., 2006). We also took spectra of objects within the central clump using any extra fibers.

With FLAMES, we observed five, $25'$ diameter fields, which overlapped slightly, with ~ 110 objects in each field. Two fields were observed twice because the first observations were not taken within specified seeing conditions, but even these observations turned out to be usable. In the end, we had 503 unique objects and 745 spectra taken from Oct 2010 to Jan 2011.

The spectra were taken using Giraffe with its LR03 setting, covering 4501–5078 Å at a resolving power of $\lambda/\Delta\lambda \approx 7500$. This setting covers H β , several He I and He II lines (including He II at 4686 Å), [O III] at 4959 and 5007 Å, as well as the Bowen blend of N III and C III lines at 4640 Å. We chose this band as a compromise between being able to do stellar classifications of hot stars (H β , He I and/or

He II absorption lines), and having features relevant for ionized gas, be it nebular (strong, narrow $H\beta$ emission lines with strong [O III] lines) or from a wind powered by a hot central core (like WR stars or RAWD; strong He II, N and/or C lines).

The two degree diameter field of view of AAOmega allowed us to image the entire core of the SMC in one field. We took three observations of the same field, but targeting objects in different magnitude ranges with different exposure times. This left us with 857 spectra of 732 unique objects. Observations were taken from 4-5 June 2011, covering 3700–5800 Å in the blue with the 580V grating, and 5600–8800 Å in the red with the 385R gratings. The resolving power in each band is ~ 1300 . The blue spectra include the range covered by the FLAMES observations, and we looked for similar spectral features. In the red spectra, the most prominent line is $H\alpha$, which was useful for interpreting otherwise ambiguous spectra.

We assigned all objects in our combined UIT/MCPS catalog a priority based on their positions in the Figure 2.1 as well as their $B - V$ colors. In order of priority these were (1) stars bluer than the central clump with a $B - V < 0$, (2) stars bluer than the central clump with a $B - V > 0$, (3) stars redder than the central clump, and (4) all stars in the central clump. Stars were assigned fibers according to their priority and the instrumental limitations on fiber positions.

Of the 233 candidates bluer than the central clump, we observed 204 (88%; 14 only with FLAMES, 71 only with AAomega, 119 with both). Of the 171 objects redder than the central clump, we observed 150 (88%; 19 only with FLAMES, 52 only with AAomega, 79 with both). Finally, of the 5503 candidate objects from the central clump, we observed 376 (6.8%; 116 only with FLAMES, 206 only with AAomega, 54 from both). Limitations on fiber positions prevented us from observing 100 percent of the blue candidate sources.

We assigned all objects a rough classification by eye, using summary graphs such as those shown in Figure 2.3. In addition, since many cataclysmic variables including V Sge stars show eclipses, ellipsoidal variation or periodic irradiation effects due to the hot primary irradiating the secondary star, we looked for periodic variations using the Ogle microlensing survey of the SMC (Szymanski, 2005; Udalski et al., 1997). We found the most likely photometric period of the objects from FFT periodograms created by using the Lomb-Scargle method on Ogle II photometry data (of objects that were within the Ogle SMC fields). We were able to recover several known eclipsing binaries from the Ogle data, but no objects with short-period variations had unusual spectra, and no objects outside of the central clump showed any periodic variations.

We did recover some known objects that are similar to what we expect a RAWD to look like (discussed in more detail in Appendix 2.7): SMC-SMP 8, a [WC 8] planetary nebula, as well as SMC WR11 and WR 12, the two known Wolf-Rayet stars in the central core of the SMC. These objects have strong winds and a UV excess, which give us confidence that we would see a RAWD if it had Wolf-Rayet like features.

As expected, the majority of objects in the central “main sequence” clump were normal OB stars along with Be and B[e] stars. Stars to the red side of the central clump (that had abnormally low FUV emission) were generally O, B and A giants.

Stars to the blue side of the central clump (with a FUV excess) fell into a few broad categories. These include, in order of frequency, (A) About 50% of the objects that show a UV excess in their SED are in a crowded field, yet have unremarkable spectra. They are most likely a mismatch between the FUV and optical catalogs. An example is shown in Fig. 2.4. (B) About 20% appear to be main sequence stars, some with nebular lines such $H\alpha$ and [O III] that may arise from the star or the surrounding ISM. These sources were almost exclusively found near the edge of the central clump, so they likely belong to

that main sequence group. (C) About 20% appear to be misaligned fibers or objects with bad positions from the MCPS catalog — objects that do not have a counterpart DSS images, have little flux and show spectra more consistent with the ISM rather those of stars. And (D) the remaining 10% which includes extended objects like star clusters and nebulae, objects with a bad V -band magnitude in the MCPS catalog (or at least one highly inconsistent with the object’s U , B , and I -band magnitudes), as well as the three known WR stars discussed above.

Other than the two WR stars and the [WR] planetary nebula we observed, none of our candidate sources have He II emission lines, or are unusually hot for their luminosities, meaning it is unlikely we observed any RAWD.

2.4.1 Expectations

Our non-detection means that we can only set an upper limit to the number of RAWD in the SMC. To help establish these limits, we first describe a simple model and then turn to objects suggested to be RAWD.

Comparison with Models

To see what fraction of RAWD we should be able to detect, we created a simple model: a white dwarf with an extended envelope modeled as a black body and a main sequence star modeled with synthetic spectra from Pickles (1998). For the companion, we try a range of masses $6.5\text{--}0.21 M_{\odot}$, corresponding to spectral types B5–M5) and set the binary separation such that they fill their Roche lobe. For the white dwarf, we assume either (1) that the envelope extends to the white dwarf’s Roche lobe or (2) that it extends to half its Roche lobe. We also assume that the luminosity equals that of the upper edge of the steady burning region ($10^{4.64} L_{\odot}$; Nomoto et al. 2007); the temperature then follows.

In order to compare our results to the observations, we assume a distance modulus of 18.9 to the SMC. A source of uncertainty is the internal reddening of the SMC. Generally, for the SMC one has $E_{B-V} = 0.02$ to 0.12 , with about 0.02 to 0.04 coming from the Milky Way foreground and the rest from internal reddening (Bessell, 1991; Cornett et al., 1997). While Cornett et al. (1997) measure E_{B-V} for objects that are in both the SMC UIT catalog and the AzV catalog of SMC OB stars (Azzopardi & Vigneau, 1982), they assume a conservative $E_{B-V} = 0.1$ for the SMC when discussing their sample as a whole. This value may be too large for RAWD, which should be substantially older than most OB stars and thus mostly outside of star forming regions, in areas of low extinction. Hence, for our comparison in Figure 2.5, we show results both for the more conservative assumption, $E_{B-V} = 0.1$ (top panel) and for a more optimistic one, $E_{B-V} = 0.01$ (bottom panel). For both cases, this is assumed to include Galactic reddening. We take the SMC extinction curve from Gordon et al. (2003).

From Figure 2.5, one sees that for the Roche-lobe filling model, the flux from the white dwarf dominates the system, with only a small companion contribution at the earliest spectral types. For the half-filling case, however, the companion has a bigger influence, and the predictions merge with the main-sequence clump for companions earlier than spectral type A0, corresponding to a mass of $\sim 3.2 M_{\odot}$.

Comparison with Known RAWD Candidates

There are no UIT observations of any of the known RAWD candidates — the V Sge stars or LMC N66 — but several of these objects do have spectra in the IUE archive. We can use these IUE observations to

estimate UIT magnitudes fairly reliably, since IUE fluxes were used to calibrate UIT. UIT magnitudes are defined as: $m_\lambda = -2.5 \log F_\lambda - 21.1$, where F_λ is the flux in $\text{erg cm}^{-2} \text{s}^{-1} \text{\AA}^{-1}$ and for the B5 filter $\lambda = 1615 \text{\AA}$. For SMC objects, Parker et al. (1998) find that the difference in magnitudes obtained from IUE spectra and UIT photometry is 0.04 ± 0.25 mag.

Combining these UV magnitudes with visual observations contemporary to the IUE observations, we can approximate where these objects would be found on Figure 2.1. To transform the color and magnitude to the SMC, we first calculate absolute magnitudes with published distance and extinction estimates, and then estimate apparent magnitudes for the SMC. For the extinction curves, we use that of Gordon et al. (2003) for the LMC and that of Seaton (1979) as fit by Fitzpatrick (1986) for the Milky Way.

LMC N66

While there are several IUE spectra of LMC N66 during quiescence, there is only one with a published, contemporary V magnitude observation from Peña et al. (1995). At this time, the object was both faint ($V = 19.54$ at the distance of the SMC) and blue ($m_{162} - V = -5.89$). This suggests that if LMC N66 was able to pass the $U < 19$ magnitude cut of our survey (which is likely given its blue SED), then it would have been selected as a candidate source.

LMC N66 was observed by the MACHO micro-lensing survey from Jan 1993 to Dec 1999, capturing the object's first outburst. A HST image of the system published in Peña et al. (2004) shows a $\sim 5''$ diameter nebula surrounding the central object LMC N66. There are two MACHO objects that are within $5''$ of the central source, MACHO 61.9159.33 and MACHO 61.9159.42. Both sources show a rise and fall in their visual magnitude that coincides with the outburst. Comparing the positions given in the MACHO catalog (accurate to ~ 1 arcsec) with the HST image, it seems that MACHO 61.9159.33 is most likely the central source, and MACHO 61.9159.42 is a knot in the surrounding nebula. MACHO 61.9159.42 is brighter in V than MACHO 61.9159.33, but this is most likely due to strong emission from the nebular [O III] 4959 and 5007 lines, which fall within the MACHO blue band and can contain up to ten percent of the total flux seen from a planetary nebula.

LMC N66 is located at a distance modulus of 18.5 and $E_{B-V} = 0.16 \pm 0.03$ (Hamann et al., 2003). Using MACHO 61.9159.33, LMC N66 appears both brighter ($V = 16.51 \pm 0.23$ at the distance of the SMC) and redder ($m_{162} - V = -3.63 \mp 0.40$) during outburst than during quiescence. This puts LMC N66 at the edge of the main sequence clump (see Figure 2.5). Of the 9 observations, 4 fall within the region of our candidate sources using $E_{B-V} = 0.1$ for the SMC and 8 of 9 using $E_{B-V} = 0.01$.

V Sge

V Sge has AAVSO observations dating back to 1910, and has been tracked continuously since 1930. This means that there are visual observations of the object within at least a few days of when every IUE spectra was taken.

V Sge is reddened by $E_{B-V} = 0.3 \pm 0.1$ (Mader & Shafter, 1997). While the distance to V Sge is poorly constrained, Hachisu & Kato (2003a) use models of the system to estimate it at ~ 3 kpc. During its optical high state, V Sge has a similar visual luminosity to LMC N66 during outburst (corresponding to $V = 16.46 \pm 0.053$ at the distance of the SMC). During its optical low state, it is brighter than LMC N66 during quiescence (17.36 ± 0.28). Unlike LMC N66, the $m_{162} - V$ color of V Sge does not shift during its optical high and optical low state, remaining inside the central clump of Fig. 2.1 and much redder

than our candidate sources (see Fig. 2.5). It is not clear whether this is due to a large contribution from a cool disk or whether there is some internal extinction within the system. In either case, using $E_{B-V} = 0.1$ for the SMC, none of the observations of V Sge fall into the region of our blue candidate sources. Using the optimistic $E_{B-V} = 0.01$, 1 of 7 observations in its high state and 1 of 9 observations in its low state fall within this region. Thus, it is unlikely a star like V Sge would have been selected in our survey.

RX J0513.9–6951

RX J0513.9-6951 has two IUE spectra, one during its optical high state, and one during its optical low state, that also have simultaneous MACHO observations. It is located at a distance modulus of 18.5 and $E_{B-V} = 0.13 \pm 0.022$ (Gänsicke et al., 1998). RX J0513.9–6951 has a similar predicted V-band brightness to V Sge and LMC N66 during its optical high state, but has a much redder $m_{162} - V$ color. During its optical low state, its visual luminosity is similar to V Sge during its low state, but it has a bluer $m_{162} - V$ color, appearing at the edge of our main sequence clump (see Fig. 2.5). Assuming $E_{B-V} = 0.01$ for the SMC, it could be considered a candidate source, within uncertainties, but not with $E_{B-V} = 0.1$.

Hachisu & Kato (2003a) claim that the differences in optical and X-ray variability between RX J0513.9–6951 and V Sge is due to differences in viewing geometry. For V Sge, the inferred inclination is relatively close to edge-on, $i = 70^\circ - 80^\circ$, while RX J0513.9–6951 is suggested to be viewed closer to pole-on, $i = 20^\circ - 30^\circ$. With a lower inclination angle in RX J0513.9-6951, we observe less of the variability in the irradiated disk, and more of the change in photosphere of the WD. However, it is difficult to explain the color changes with this model, unless the expanding photosphere and winds of the white dwarf make the source appear very red for some reason.

QU Car

Several IUE spectra of QU Car are available, and we have visual observations within a few days of each thanks to it having been monitored continuously by AAVSO since 1987. A major uncertainty is the distance, which Drew et al. (2003) put at “ ~ 2 kpc or more”. Using 2 kpc and $E_{B-V} = 0.1 \pm 0.015$, the object is much fainter and redder than V Sge and LMC N66. A distance of ~ 4 kpc is needed to bring its visual luminosity in agreement with V Sge and LMC N66. Thus, either the published distance estimate is too low (which is plausible) or the system is not similar to V Sge. In either case, given its relatively red color, it would not be considered a candidate source.

2.5 Limits to the Number of RAWD

We did not detect any RAWD, and thus we are only able to establish an upper limit on the number of RAWD in the SMC, given our expectation of what such sources would look like, and the visibility limits of this survey.

For any RAWD, the probability that we would find it can be written as three factors, $p_{\text{det}} = p_{\text{infield}} \times p_{\text{cand}} \times p_{\text{fiber}}$, where the three factors are the probabilities that the source is in one of the UIT fields, that it would be identified as a blue candidate source, and that it would be assigned a fiber, respectively.³

³Strictly, there is the additional probability of showing a sufficiently unusual spectrum. We take this to be unity, given the known RAWD examples.

For a given number n of RAWD sources, the probability of not detecting any of them is $P(0|n) = (1 - p_{\text{det}})^n$, and, conversely, the probability of detecting at least one is $1 - P(0|n)$. Thus the number of RAWD in the SMC for which at some confidence $1 - P$ we should have detected one or more, is $n_{\text{max}} = \log P / \log(1 - p_{\text{det}})$. Below, we will quote 95% confidence limits (i.e., set $P = 0.05$).

Of the three probabilities that enter p_{det} , two are straightforward to estimate. The first is p_{infield} , which is simply the fraction of the SMC covered by the UIT images, i.e., most of the central bar (see Fig. 2.2). Since the UIT fields contain 30.6% of all $U < 19$ entries in the MCPS catalog, and since the MCPS catalog covers the central 4.5×4 degrees of the SMC, which is the vast majority of the dwarf galaxy, we infer that $p_{\text{infield}} = 0.306$. The second is p_{fiber} , which equals the fraction of 88.8% of objects identified as candidate sources that were observed by our survey (due to constraints on fiber positioning and the fields of view of AAOmega and FLAMES).

The final piece is the probability p_{cand} that a RAWD would be identified as a candidate source. We can divide our predictions into three cases, based on different assumptions on what a RAWD looks like and how much reddening there is internal to the SMC.

In our first, most optimistic case, RAWD resemble faint Wolf-Rayet stars, with very blue $m_{162} - V$ colors, and thus always fall within the region of blue candidate sources in Fig. 2.1. Thus, for this case $p_{\text{cand}} = 1$ and $p_{\text{det}} = 0.27$, and our non-detection sets a limit of 10 RAWD in the SMC at the 95% confidence level.

In the second case, RAWD resemble LMC N66. If so, detectability depends on state and reddening. LMC 66 should always be visible in quiescence, but in outburst the detectability depends on extinction: placed in the SMC with $E_{B-V} = 0.1$, LMC N66 in outburst would be selected as a candidate source in 4 of 9 observations. Hence, $p_{\text{cand}} \simeq \frac{1}{2} + \frac{1}{2} \frac{4}{9} \simeq 0.72$ and $p_{\text{det}} = 0.196$. This puts a limit of 14 RAWD similar to LMC N66 at the 95% confidence level. Assuming $E_{B-V} = 0.01$ for the SMC, it would be selected as a candidate source 8 of 9 times during outburst. Hence, $p_{\text{cand}} \simeq 1$ and the limit is (nearly) the same as for our first case.

In the third, most pessimistic case, RAWD generally resemble V Sge. If so, they would only be selected as candidates if the extinction is very low. V Sge spends about 180 days in its high state and 120 days in its low state. Assuming the most optimistic reddening of $E_{B-V} = 0.01$, V Sge placed in the SMC would be selected in 1 of 7 observations in its high state and 1 of 9 observations in its low state. Hence, $p_{\text{cand}} \simeq \frac{3}{5} \frac{1}{7} + \frac{2}{5} \frac{1}{9} \simeq 0.13$, $p_{\text{det}} = 0.035$, and one infers a very loose upper limit of 83 RAWD. However, V Sge would not be selected at all for our survey if E_{B-V} were higher.

Thus, for the first two cases, we can put an upper limit of 10–14 RAWD in the SMC. However, the upper limits from the third case are not useful, since even under extremely favorable reddening conditions, they still are consistent with even the upper end of the range of 33–132 expected type Ia progenitors in the SMC (Section 2.2).

2.6 Conclusions

We have described our attempt to find binaries containing RAWD among unusually UV-bright stars in the SMC. We had hoped to find at least some, to empirically constrain the range of observed properties, but found none. This either means that RAWD are substantially rarer than expected based on single-degenerate SN Ia progenitor models, or that most RAWD are not very blue, e.g., because most are like the V Sge stars and few like LMC N66.

To derive more stringent constraints would require using a more reliable indicator for a RAWD. Apart from the unobservable extreme-UV flux, best may be the presence of high ionisation lines in the spectra, such as He II, which are seen in all known examples (as well as in SSS). Suitable candidates might be found using a narrow-band imaging survey. Of course, He II is seen in other objects as well, but most are interesting on their own accord (e.g., X-ray binaries, Wolf-Rayet stars) or also relevant for the SN Ia progenitor question (e.g., symbiotics, progenitors on their own and a phase in the evolution to double degenerates).

Acknowledgements

We acknowledge with thanks the variable star observations from the AAVSO International Database contributed by observers worldwide and used in this research.

This paper utilizes public domain data obtained by the MACHO Project, jointly funded by the US Department of Energy through the University of California, Lawrence Livermore National Laboratory under contract No. W-7405-Eng-48, by the National Science Foundation through the Center for Particle Astrophysics of the University of California under cooperative agreement AST-8809616, and by the Mount Stromlo and Siding Spring Observatory, part of the Australian National University. This paper also utilizes public domain data from the Ogle-II microlensing survey on-line photometric database.

Some of the data presented in this paper were obtained from the Mikulski Archive for Space Telescopes (MAST). STScI is operated by the Association of Universities for Research in Astronomy, Inc., under NASA contract NAS5-26555. Support for MAST for non-HST data is provided by the NASA Office of Space Science via grant NNX09AF08G and by other grants and contracts.

This research has made use of the VizieR catalogue access tool and the SIMBAD database, operated at CDS, Strasbourg, France. This research has also made use of NASA's Astrophysics Data System

2.7 Appendix: Interesting objects found in the survey

While our survey did not detect any sources that could be a rapidly accreting white dwarf, we did detect several objects that have similar properties, including two Wolf-Rayet stars and a [WR] planetary nebula.

SMC USSC 131 = SMC WR11 (Fig. 3.35). Observed with FLAMES and AAomega, we find NIII-V emission lines at ~ 460 nm, a strong, wide He II 4686 emission line, a weaker $H\beta$ absorption line and a strong, wide $H\alpha$ emission line in the spectra of SMC WR11. $H\beta$ absorption lines are common in SMC WR stars — all but SMC WR 4 exhibit early-type absorption spectra superposed on the canonical WN emission lines. While the presence of absorption lines can be signs of either a binary companion or absorption from thin stellar winds, SMC WR 11 shows no periodic radial velocity variations, which makes it likely that WR 11 is a single object (Foellmi et al., 2003). Foellmi et al. (2003) give a V magnitude of about 15.7, this is consistent with $V = 15.845$ listed in MCPS. The absolute magnitude is $M_V \simeq -4.7$, using a distance modulus to the SMC of 18.9, which is similar to other SMC WN stars. Given this and the spectrum, it is very unlikely that SMC 11 is a [WR] planetary nebula core.

SMC USSC 482 = SMC WR12 (Fig. 3.178) is the most recent Wolf-Rayet star to be discovered in the SMC, a (likely) single and hydrogen-rich WN3 star (Massey et al., 2003; Foellmi, 2004). Observed

with AAOmega, we find strong, NIII-V emission lines at ~ 460 nm, a strong, wide He II 4686 emission line, with a weak, asymmetric, H β absorption and emission line and a strong, wide H α emission line in the spectra of SMC WR12. As with other SMC WN stars, WR12 shows signs of a weak early-type absorption spectra. Massey et al. (2003) give $V = 15.5$ for WR 12, somewhat brighter than the $V = 16.158$ listed by MCPS. This yields an absolute magnitude $M_V \simeq -4.0$, which is consistent with other SMC WN stars. Given this and the spectrum, it is very unlikely that the object is a [WR] planetary nebula core.

SMC USSC 276 = LIN 302 is a [WC 8] Wolf-Rayet type planetary nebula core. It is similar to the galactic [WC 8] NGC 40, a very low-excitation, evolved nebula (Barlow, 1987; Pena et al., 1997). While it is likely that the central object of the planetary nebula is responsible for the UV emission seen with UIT, a bad match between the MCPS and UIT catalog gave a optical position which is offset from the central object, and thus our spectrum is dominated by the nebula. Nonetheless, apart from the strong, narrow H β and [OIII] 4959 and 5007 emission lines characteristic of a planetary nebula, we also detect weak, wide He II 4686 and C III 4647 emission lines from the [WC] core of LIN 302.

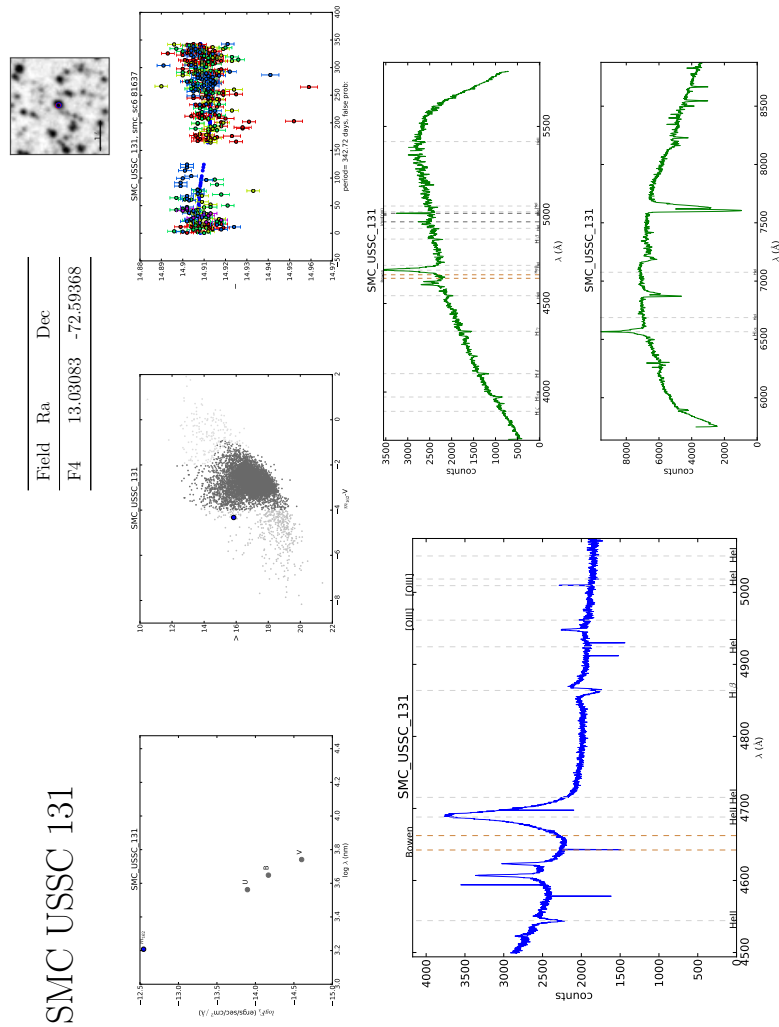


Figure 2.3

Summary of the observations for SMC USSC 131. **Top row:** Name of object in the survey. Survey field, ra (degrees), dec (degrees). Digital sky survey image of the area around the UV source, revised position of the UV source is shown in blue, position of the optical counterpart is shown in red. Circles are 3 arcsec in diameter. **Second row:** Spectral energy distribution of the object, showing the UV flux and several optical bands from MCPS and IR bands from 2MASS (if available). Color magnitude diagram similar to Figure 2.1 showing the position of the object in the large blue circle. If available, Ogle II lightcurve with a sine curve at the best-fit period overdrawn in blue. **Third row:** Spectra from FLAMES (left) and AAOmega (right). Wavelength is in Å.

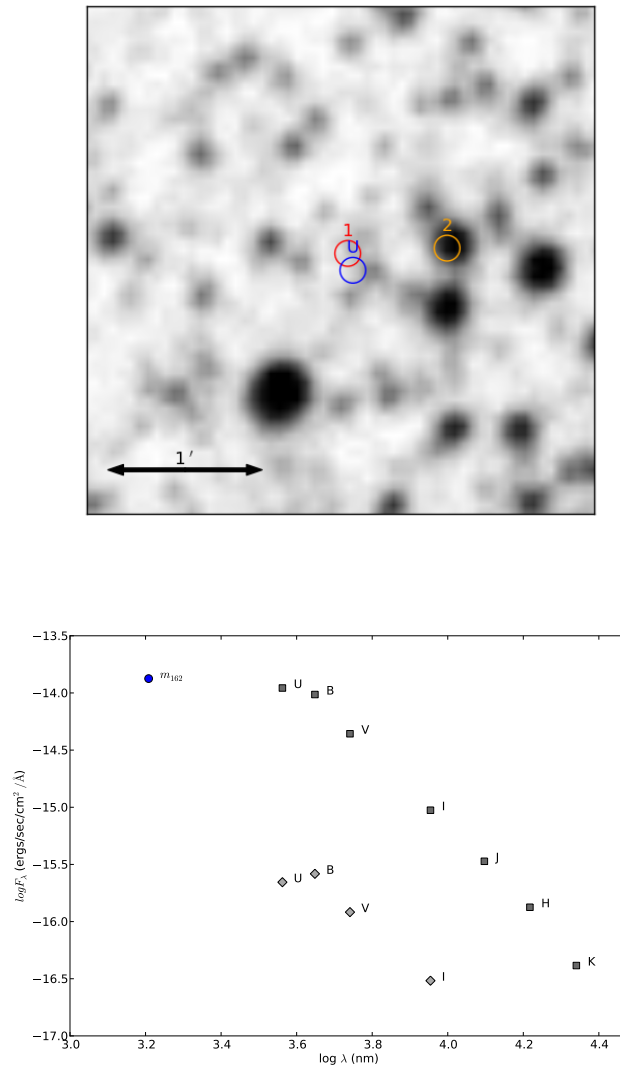


Figure 2.4

Example of a miss-match between the optical and UV catalogs. **Top:** Image from the digitized sky survey. The position of the UIT UV source, using our revised astrometry, is shown with a blue 3 arcsec radius circle labeled “U”. Our candidate optical counterpart, star 1, is shown with a red circle. Star 1 has a m_v of 19.14 in the MCPS catalog, which is near the magnitude limit of the DSS image, so no star is visible within the circle. Most likely, the the ultraviolet source corresponds to one (or more) of the brighter stars, possibly the star marked with the orange circle, star 2, with a m_v of 15.24. **Bottom:** SEDs for star 1 (diamonds) and star 2 (squares), with U , B , V , and I from MCPS, J , H , and K from 2MASS, and m_{162} from UIT. One infers a UV excess in the SED of star 1, but this is probably because the optical and UV fluxes come from different objects. Compared to all of the other nearby stars, the SED of star 2 is the most consistent with a single star that has the observed UIT m_{162} . Since the spectra of star 1 are unremarkable and inconsistent with a hot object, we conclude star 2 is the likely counterpart to the UV source.

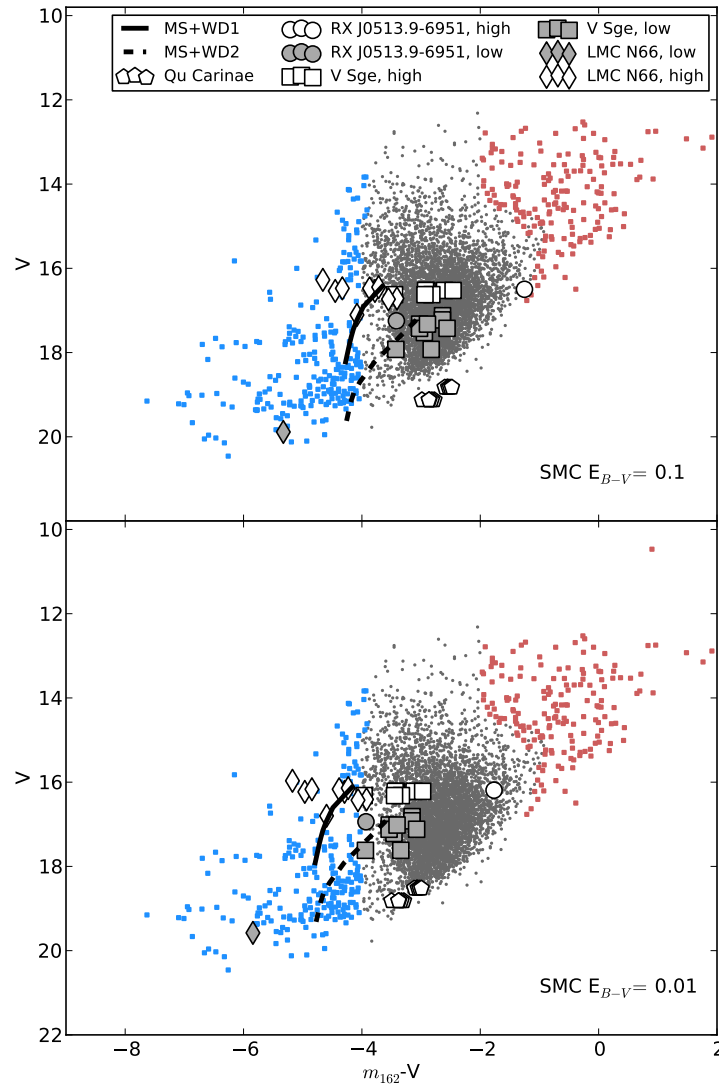


Figure 2.5

Same as Fig. 2.1, but also showing objects suggested to be rapidly accreting white dwarfs (as labeled). Two models are shown, with (1) the white dwarf filling its Roche lobe and (2) the white dwarf filling 50% of its Roche lobe. The top panel assumes a conservatively high reddening, $E_{B-V} = 0.1$, and the bottom panel assumes a very low reddening in the SMC, $E_{B-V} = 0.01$.

Chapter 3

A search for symbiotic binaries in the SMC

Symbiotic stars consist of a hot white dwarf and a giant companion. Their number is an important piece of evidence for solving the mystery of the nature of type Ia supernova progenitors — not only are they possible single degenerate progenitors themselves, but also all double degenerate progenitors should evolve through a symbiotic phase.

We try to construct a complete sample of symbiotics in the Small Magellanic Cloud by identifying candidates from ultraviolet, optical and infrared surveys. We then follow up these candidates using the multi-object spectrometer AAOmega. We find eight sources with spectral signatures consistent with those of symbiotics, including four showing what appear to be the 6825 Å feature resulting from Raman scattered O VI lines, which would normally be enough to classify these objects as symbiotics. Upon close inspection, however, we find the sources are almost certainly false positives (with the possible exception of one source), with the emission lines mostly originating from interstellar nebular emission. This includes the Raman features, which in our sources likely originates from O VI emission from a supernova remnant scattering on dense neutral hydrogen surrounding a strong H II region.

From the numbers and distribution of the known symbiotic systems, combined with the fact that we do not find any (secure) new ones, we conclude that there are about 12 – 18 bright symbiotic stars in the SMC. Even under optimistic assumptions, this is too few objects to make up for the 25 – 130 missing SD progenitors in the SMC.

3.1 Introduction

Symbiotic binaries consist of a giant star that transfers mass via a stellar wind or Roche-lobe overflow to a hot, compact companion (usually a white dwarf) in a wide ($\sim 200 - 1000$ day) orbit. Mass lost from the giant surrounds the system and is ionized by the hot white dwarf, producing nebular lines. There are two types of symbiotic systems, S-type (star), which have normal giant companions and D-type (dust), which have Mira variable companions and a significant amount of warm dust.

Symbiotic binaries are of interest not only on their own accord, but also as progenitors to other systems, in particular to type Ia supernovae, and for this purpose it would be very useful to have a better handle on their formation rate.

Type Ia supernovae are the thermonuclear explosions of carbon-oxygen white dwarfs. There are two main categories of possible progenitor binaries: two white dwarfs that merge (the double degenerate or DD scenario) and a white dwarf that accretes material off of a normal star companion (the single degenerate or SD scenario). For standard scenarios, in which the nuclear runaway is triggered when the (combined) mass of the white dwarf approaches the Chandrasekhar mass, the observed number of suitable progenitor systems is significantly smaller than what is required to match the observed type Ia supernova rate, of about 1% of the white-dwarf formation rate (for a review, Maoz et al. 2014).

Symbiotic systems are considered good SD progenitors, since the wide orbits imply that the white dwarf is likely to retain the material it accretes from its companion. Symbiotic stars are also important in the DD scenario, as the common-envelope event that produces a short-period DD system is likely preceded by a symbiotic phase. However, there seem to be too few symbiotics to produce the appropriate number of progenitor systems for either scenario (Di Stefano, 2010b). In both scenarios, a massive white dwarf burning hydrogen on its surface in the symbiotic should produce super-soft X-rays. However, both the total X-ray flux measurements in nearby elliptical galaxies (Gilfanov & Bogdan, 2010) and counts of soft X-ray point sources in nearby galaxies (Di Stefano, 2010a), show too few sources to account for the observed Type Ia supernova rate. The only way out of this conundrum would appear to be that the expected X-ray emission is hidden, either by absorption (but see Woods & Gilfanov 2013 for constraints based on the absence of He II emission in elliptical galaxies) or because the white dwarfs are not as massive – as would be expected for most “sub-Chandrasekhar” models (Maoz et al., 2014).

Given the above, an independent estimate of the rate of occurrence of symbiotics would provide a crucial constraint on both SD and DD progenitor models. Unfortunately, this rate is not well known. There are about 300 symbiotic stars known (Belczynski et al., 2000; Mikolajewska et al., 2014), but most were discovered as one-off unusual variable stars, rather than as part of any systematic survey. Hence, the current sample is incomplete and suffers from strong observational biases, making it difficult to infer much about the population as a whole.

Several attempts have been made in recent years to find new Galactic symbiotics (Miszalski et al., 2013; Baella et al., 2013; Miszalski & Mikolajewska, 2014). One such attempt (Corradi et al., 2008) used a magnitude-limited sample of candidates found by comparing data from the INT Photometric H α Survey (IPHAS) of the northern Galactic plane with 2MASS colors. In follow-up spectroscopy of 62 of the ~ 1000 candidates, however, Corradi et al. (2010) confirmed only 11 symbiotic systems; there was significant contamination by Be stars and young stellar objects (both of which show H α emission and infrared excess, due to their equatorial wind and proto-stellar disk, respectively).

Instead of focusing on our own Galaxy, we decided to survey the Magellanic Clouds. This may give us a more complete understanding of the true symbiotic rate because the stars have a known distance and typically very little extinction, which simplifies determining the luminosities of the systems, and avoids contamination by reddened stars. Furthermore, the clouds subtend a relatively small angular size and have dense but still resolvable stellar fields, making it practical to use multi-object spectrometers to follow up candidates, even when the criteria used to select these have large false-positive rates.

In this work, we focus on the Small Magellanic Cloud (SMC), since it has better UV coverage which we felt provided a relatively unbiased way to identify the hot component of a symbiotic star. In Section 3.2, we first give a brief overview of the observational properties of symbiotics, and of possible differences between ones in the Magellanic Clouds and those in the Galaxy, and then discuss in Section 3.3 the criteria with which we select candidates. We describe our observations of these candidates in Section 3.4

and present spectra of both known objects and interesting sources in Section 3.5. We discuss the implications for the occurrence rate of symbiotics in Section 3.6.

3.2 Observational properties of symbiotic systems

Symbiotic stars show, by definition, observational signatures of both a hot and a cool component in their optical spectra. For the majority of symbiotic systems, this means spectral features from a cool giant as well as high-excitation emission lines indicating optically thin material ionised by the hot component.

In most symbiotics, the hot component dominates the luminosity (100–10,000 L_{\odot}), with the main contribution arising from nuclear burning of accreted material on the surface of a white dwarf, with a typically more minor contribution from an accretion disk (Tutukov & Iungelson, 1976; Skopal, 2014, 2015). In the majority of systems, hydrogen is burned steadily (sometimes leading to the appearance as super-soft X-ray sources), but in a minority the accretion rate is too low for steady burning and nova eruptions occur instead (often followed by a long-lasting phase as a super-soft source). From models of shell-burning white dwarves, surface temperatures of 10^5 to 10^6 K are expected, with the precise value depending on the mass of the white dwarf (Nomoto et al., 2007). This is consistent with what, e.g., Muerstet et al. (1991) infer from the presence of ionization emission lines like He II 4686 (which peaks at temperatures of $10^{5.5}$ K; Nahar 1999), [O III] 5007 and the Balmer series. Of course, these emission lines are not unique to symbiotic stars, but are also seen in other sources with hot ionising emission, such as other types of super-soft sources, Wolf-Rayet stars, and B[e] stars (Mürset & Schmid, 1999).

In most symbiotics, the cool object starts to dominate the continuum flux somewhere in the optical band (Skopal, 2005, 2011, 2014), depending on the spectral type of the giant, the temperature and luminosity of the white dwarf, and whether the system is in an active or quiescent phase. If the cool object is a late K to M giant, the spectra will often show molecular absorption bands such as those from TiO and VO. Otherwise, there may be signatures of a G to early K giant such as absorption lines of Ca I 4227 or Fe I 4405 (Mürset & Schmid, 1999).

About half of all symbiotic stars show broad, asymmetric emission features around 6825 and 7088 Å (Allen, 1980), which are due to Raman scattering of O VI 1032, 1038 doublet photons in neutral hydrogen (Schmid, 1989, 2001). Thus, the Raman lines provide direct evidence of both a hot, ionizing object and a source of neutral hydrogen – in a symbiotic, the white dwarf and the cool giant with its wind, respectively. While not strictly unique to symbiotics (see Section 3.5), very few other sources show Raman lines.¹

3.2.1 Identifying Symbiotic Stars

Since symbiotics are a somewhat heterogeneous group, it is difficult to present iron-clad classification criteria, but a reasonable set would be the ones used by Belczyński et al. (2000) for their catalogue of symbiotic stars:

- 1 Strong emission lines of H I ($H\beta$ and $H\alpha$) and He I (5876, 6678, 7065 Å) as well as emission lines with a high ionization potential (such as [O III] 4363, 4959, 5007 or He II 4686) or an A- or F-type continuum (from the hot component in outburst).

¹An intriguing example of Raman scattering in a different context is the high-mass X-ray binary 4U 1700–37, which shows features near He II 1640 resulting from extreme ultraviolet emission lines originating near a neutron star Raman scattering off of singly-ionised helium in the wind of the companion O star.

- 2 Absorption features characteristic of late-type giants such as TiO (7054, 7088, 7126 and 7744 Å) or VO absorption bands.
- 3 **And/or** the presence of the Raman 6825 Å emission feature.

Note that some authors use more stringent criteria. For instance, Corradi et al. (2008) require objects to have He II emission lines in their survey, thus excluding lower-ionization symbiotics (where the white-dwarf temperature is $\lesssim 50000$ K). We choose to include cooler symbiotics, which will include systems with a lower-mass white dwarf ($\lesssim 1 M_{\odot}$) or those where the accretion rate on the white dwarf is too low for steady shell burning to dominate the system's luminosity.

3.2.2 Symbiotic Stars in the Magellanic Clouds

In their catalogue of symbiotics, Belczyński et al. (2000) lists six symbiotic stars in the SMC and seven in the LMC, as well as two candidates in the LMC. Since that time, two further confirmed and one candidate symbiotics have been found in the SMC; we summarize all systems in Table 3.1.

Muerset et al. (1996) classified the stellar components of twelve of the symbiotic stars in the Magellanic Clouds, and find both commonalities and intriguing possible differences with the galactic symbiotic population. For instance, symbiotics appear to be associated with old populations both in the Galaxy (Wallerstein, 1981) and in the Magellanic Clouds, where symbiotics have only been found far from the centers and therewith far from the younger stellar populations. But while most galactic symbiotic companions are thought to be either normal red giants (for s-type systems) or mira-type stars (for d-type systems), Muerset et al. (1996) suggest that most or all Magellanic Cloud symbiotics have an AGB companion.

The observed differences of Magellanic Cloud symbiotics with Galactic ones likely reflect differences in metallicity, which affects a giant's ability to form strong stellar winds. Muerset et al. (1996) suggest that means that (i) The Magellanic Clouds should have fewer symbiotic binaries per stellar mass than the Galaxy; (ii) The strong wind necessary for a symbiotic will require a more massive giant in the Magellanic Clouds; (iii) The lifetime of significant mass loss, and therefore the lifetime of the symbiotic, will be shorter in the Magellanic Clouds.

Muerset et al. (1996) caution, however, that the known symbiotics in the Magellanic Clouds likely only sample the upper end of the luminosity function, i.e., those with the highest accretion rates onto the white dwarf and the most massive cool companions. There may well be a population of unknown, fainter symbiotic stars. Furthermore, there may also be yet undiscovered symbiotics in the cores of the SMC and LMC, where symbiotics may be confused with early-type giants with emission lines (Oe or Be stars). A search for these fainter symbiotics may thus tell whether or not the bright Magellanic Cloud symbiotics are typical of the larger population.

3.3 Selecting Candidate Symbiotics

To select good candidate symbiotic systems, one needs evidence for both a hot and a cool component. Unfortunately, this is not easy to do with optical colors alone, since the wavelength where the cool component starts to dominate can occur anywhere in the optical, i.e., the overall colors could range anywhere from those of a hot object to those of a cool one. In the infrared, however, the cool component will dominate, so infrared colors can be used to ensure the presence of a giant. This is used by Corradi

Table 3.1
Known Symbiotic Stars in the Magellanic Clouds

Name	B00 entry	RA	Dec	V	MCPS V	Ref.
Small Magellanic Cloud						
SMC 1	001	00 29 10.9	-74 57 38.9	16.2		B00
SMC 2	002	00 42 48.1	-74 42 00.0	16.2	16.490 ± 0.062	B00
SMC 3	004	00 48 19.9	-73 31 54.9	15.5	14.858 ± 0.054	B00
LHA 115-N 60	005	00 57 12.0	-74 13 00.0	16.8	17.109 ± 0.034	B00
LIN 358	006	00 59 24.0	-75 04 59.9	15.2		B00
LHA 115-N 73	007	01 04 42.0	-75 48 00.0	15.5		B00
OGLE SMC-LPV-00861		00 30 07.40	-73 37 19.1	16.1 ^b	16.032 ± 0.034	M14
[OVS2013] 19		00 54 19.16	-72 29 09.6	18.27	18.388 ± 0.085^c	O13
[JD2002] 11 ^a		00 50 52.66	-72 52 16.7	19.043	19.059 ± 0.052	H14
Large Magellanic Cloud						
LMC 1	018	05 25 01.1	-62 28 47	15.9		B00
LHA 120-N 67	019	05 35 50.0	-64 45 09	15.9		B00
LHA 120-S 154	013	04 51 50.4	-75 03 36	15.7	15.709 ± 0.019	B00
LHA 120-S 147	014	04 54 04.6	-70 59 34.0	16.0		B00
LHA 120-N 19	015	05 03 24.0	-67 56 35.0	16.4	16.977 ± 0.034	B00
LHA 120-S 63	021	05 48 44.1	-67 36 12.9	15.2	15.709 ± 0.019	B00
SMP LMC 94	022	05 54 10.3	-73 02 39.0			B00
Sanduleak's star ^a	020	05 45 19.6	-71 16 06.72	16.9	17.055 ± 0.023	B00
[BE74] 583 ^a	s02	05 26 54.0	-71 06 00.0	16.1		B00

References. — B00: Belczyński et al. (2000), M14: Miszalski et al. (2014), O13: Oliveira et al. (2013), H14: Hajduk et al. (2014)

^aSuspected symbiotic

^b V during quiescence, during outburst $V = 14.75$

^cThe MCPS object with the brightest U within $2.5''$ has $V = 14.623 \pm 0.028$, however, as Oliveira et al. (2013) note, there is a blue star about $2''$ from the object they identify as a symbiotic. We use here the object with the next brightest U in the MCPS catalog

Table 3.2
UV Properties at Known Symbiotic Stars in the Magellanic Clouds

Name	UIT m_{162} GALEX	NUV	FUV
Name		Name		
Small Magellanic Cloud				
SMC 1		J002910.4–745739	18.96 ± 0.01	18.20 ± 0.02
SMC 2		J004247.9–744200	19.80 ± 0.07	19.77 ± 0.13
SMC 3	14.4 ± 0.63			
LHA 115-N 60	14.7 ± 0.6^b	J005705.6–741316	18.21 ± 0.03	16.57 ± 0.03
LIN 358	14.9 ± 0.8^b	J005912.2–750517	18.74 ± 0.04	18.52 ± 0.07
LHA 115-N 73	15.2 ± 0.6^b	J010439.2–754824	20.53 ± 0.16	19.91 ± 0.17
OGLE SMC-LPV-00861 [JD2002] 11 ^a	... ^c	J003007.8–733719	17.06 ± 0.02	17.52 ± 0.04
Large Magellanic Cloud				
LMC 1	14.8 ± 0.6^b	J052500.8–622848	18.84 ± 0.08	17.31 ± 0.05
LHA 120-N 67	15.2 ± 0.5^b	J053607.3–644321	18.97 ± 0.08	18.14 ± 0.080
LHA 120-S 154	15.5 ± 0.8^b	J045150.3–750335	17.34 ± 0.02	16.06 ± 0.02
LHA 120-S 63	13.2 ± 0.8^b			
SMP LMC 94	15.4 ± 0.7^b	J055410.5–730247	21.27 ± 0.33	
Sanduleak’s star ^a	15.8 ± 0.8^b	J054519.4–711607	19.09 ± 0.14	

^aSuspected symbiotic

^bEstimate from IUE spectra

^cWhile there is a UIT point source within 2.5 asec of this object, it is likely the bluer star Miszalski et al. (2014) identify near the symbiotic, not from the symbiotic star itself.

Note. — UIT magnitudes are in the ST system, i.e., $m_{ST} = -2.5 \log F_\lambda - 21.1$, where F_λ is the flux in $\text{erg cm}^{-2} \text{s}^{-1} \text{\AA}^{-1}$ and for the B5 filter $\lambda = 1615 \text{\AA}$. GALEX magnitudes are in the AB system, with $m_{AB} = -2.5 \log F_\nu - 48.6$, where F_ν is the flux in $\text{erg cm}^{-2} \text{s}^{-1} \text{Hz}^{-1}$ and where the effective wavelengths of the NUV and FUV bands are 227 and 152 nm, respectively. Roughly, therefore, one expects $FUV - m_{162} \simeq 3 \text{ mag}$.

et al. (2008), who combine a selection for a cool component using 2MASS colors with evidence for a hot component from H α emission (from IPHAS narrow-band imaging, see Section 3.1). While this technique leads to large numbers of false positives, e.g., from Be stars and pre-main sequence stars (Corradi et al., 2010), it does robustly select symbiotics, i.e., the false negative rate is fairly low. Unfortunately, no publicly available survey of H α point sources in the SMC is available, and at the larger distance of the SMC compared to the Galaxy, an H α survey would be more seriously hampered by nebular emission from the interstellar medium, particularly in the central core of the SMC.

An advantage of the Magellanic Clouds is that the reddening is relatively low, suggesting that it should be possible to look for the hot component directly, using ultraviolet emission. In the ultraviolet, the outskirts of the SMC have been surveyed by GALEX (Bianchi et al., 2014; Simons et al., 2014) and all symbiotics that were in its survey area were easily detected, with NUV and FUV magnitudes well above the 5σ detection limit of 20.8 and 22.7 in the NUV and ~ 22.6 in the FUV band (see Table 3.2; here, we selected the object with the brightest NUV magnitude within 5 arcsec of the symbiotic).

The core of the SMC was too bright for GALEX, but has been surveyed at 162 nm using the Ultraviolet Imaging Telescope (UIT; Cornett et al. 1997). Of the SMC symbiotic binaries, only [OVS2013] 19 and [JD2002] 11 fall within the UIT survey region. Near [OVS2013] 19, a UIT source is present, but this is almost certainly associated with the bright, hot star close to the symbiotic noted by Oliveira et al. (2013). The symbiotic itself is of d-type, with dust making it rather faint already in the optical. [JD2002] 11 is of d-type and optically faint as well, and hence it is not surprising that it does not have a UIT counterpart. In order to see whether UIT could have detected the other SMC symbiotics, we estimated UIT magnitudes for those that have spectra in the IUE archive.² As can be seen from Table 3.2, all are around the detection limit of $m_{162} \simeq 14.5$ mag in UIT (for three of the four fields, the fourth going down to ~ 15.0 mag; Cornett et al. 1997).

From the above, we conclude that GALEX would detect all s-type symbiotics, while UIT might detect the brighter ones. To select candidate sources, we combined the GALEX and UIT catalogs with data from the Magellanic Cloud Photometric Survey (MCPS, Zaritsky et al., 2002) and from 2MASS via the SAGE-SMC catalog (Gordon et al. 2011; SAGE-SMC is already matched to the MCPS). For the GALEX points, we simply take the closest MCPS object within 2.5 arcsec; for the UIT objects, we follow the procedure described in Lepo & van Kerkwijk (2013), where we recalibrate the astrometry using the brighter sources before matching coordinates.

From this multi-wavelength photometric catalog of SMC objects, we developed a series of color cuts to identify objects that not only had evidence for a hot component – from the fact that they were detected in the ultraviolet – but also for a cool one, letting ourselves be guided by the colors of known MC symbiotics and detections from previous symbiotic star surveys like those of Corradi et al. (2008). Since multi-object spectrometers such as AAOmega offer a large number of allocatable fibers in each field, allowing one to observe a large number of objects fairly quickly, we can afford to include candidates with colors that have relatively large false-positive rates. We prioritized targets by the likelihood they are a symbiotic star, using the following color cuts:

²UIT magnitude estimates from IUE spectra should be fairly reliably, since IUE fluxes were used to calibrate UIT. Indeed, Parker et al. (1998) find that for SMC objects the difference in magnitudes obtained from IUE spectra and UIT photometry is 0.04 ± 0.25 mag.

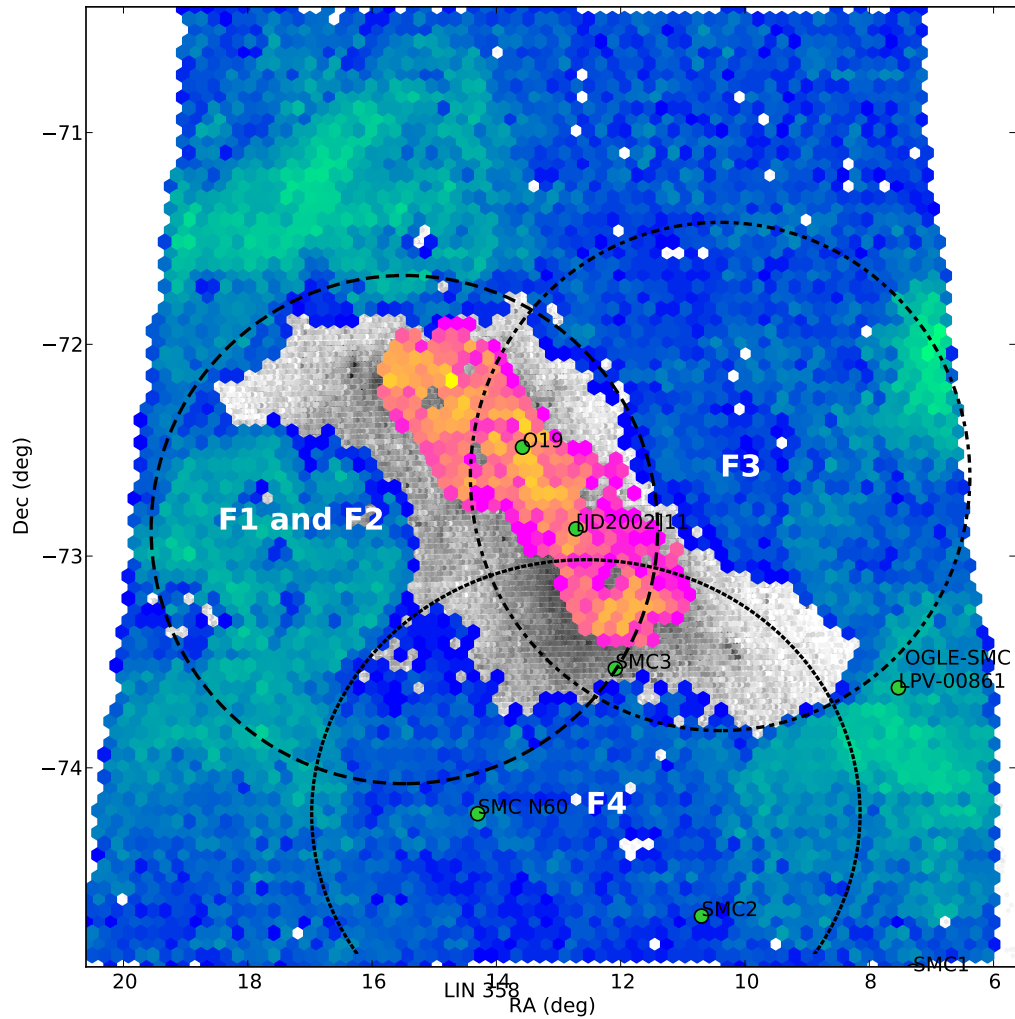


Figure 3.1

Overlap between ultraviolet and optical point source catalogs in the SMC. GALEX observed the outer part of the SMC (blue and green density map), while UIT surveyed the inner core (pink and yellow density map). The MCPS optical catalog (gray density map) covers the central 4.5×4 degrees of the SMC. The dashed lines represent fields observed by this survey. Known symbiotics are indicated with green points.

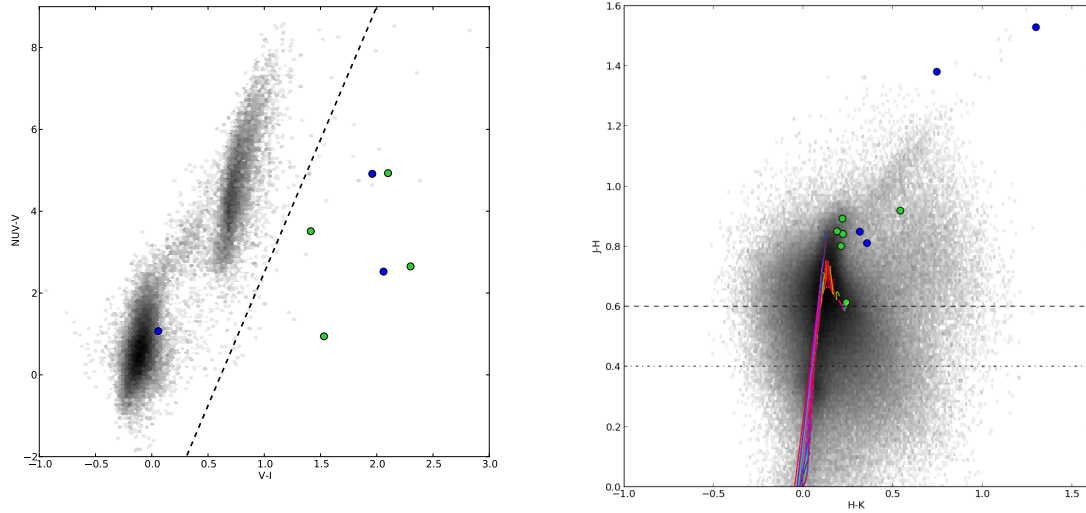


Figure 3.2

Color-color plots for objects in the SMC. **Left:** NUV-V vs. V-I colors for objects in the GALEX SMC point source catalog. Known symbiotics are shown with blue (SMC) and green (LMC, adjusted to SMC reddening and distance). Objects to the right of the line received a high fiber priority. **Right:** J-H vs. H-K color-color plot for 2MASS objects in the SMC. The dashed line shows the high priority $J-H > 0.6$ color cut, and the dot-dashed line shows the low priority $J-H > 0.3$ color cut. Solid lines show PARSEC isochrones (Bressan et al., 2012), showing the location of single main sequence and giant stars at SMC metallicities.

priority 8: Known or candidate symbiotic from previous observations;

priority 7: Sources with colours consistent with the known symbiotics: $J-H > 0.6$ and $V-I$ red-ward of the line in Fig. 4.3;

priority 6: Sources with colours reminiscent of the known symbiotics: $J-H > 0.3$, $V-I > 0.1$;

priority 5: Sources inconsistent with hot main-sequence stars, with $V-I > 0.1$ and a 2MASS detection;

priority 4: As above, but without a 2MASS detection;

priority 3: $0.6 > J-H$ (used primarily to fill the remaining fibers)

3.4 Observations

We took optical spectra of 719 symbiotic candidates using AAOmega on the Anglo-Australian Telescope (Pasquini et al., 2002; Sharp et al., 2006), on 2012 Aug. 3 (field 1), 2012 Aug. 4 (field 2), 2013 Sept. 23 (field 3) and 2013 Oct 18 (field 4). Each field is about two degrees in diameter. Fields 1 and 2 share a common center. Objects in F1 have a $V < 17$ and F2 have a $V > 17$, to allow different exposure times. We originally planned to use the same observing strategy for Fields 3 and 4, however the service

Table 3.3
New Candidate Symbiotics

ID	RA	Dec	UIT m_{162}	V	I	J	H	Other ID or Comment	Classification
F1 348	00 59 21.74	-72 11 10.8	13.590	16.713	16.789	15.113	13.529	NGC 346 MPG 710	False positive
F2 49	00 59 54.225	-72 07 59.55	14.360	17.022	17.137	16.714	16.278	Near NGC 346/N 66A	False positive
F2 282	00 58 12.8067	-72 29 38.00	14.720	17.365	17.500	16.820	16.351		Candidate
F2 446	00 59 25.71	-72 05 47.25	15.310	17.860	18.008	17.025	16.431	Near NGC 346/N 66A	False positive
F2 520	00 59 14.089	-72 10 42.02	13.500	17.209	16.910	16.248	15.732	NGC 346 MPG 632	False positive
F2 227	00 58 34.802	-72 11 56.29	15.100	17.592	17.800	14.841	14.169	NGC 346 MPG 127	False positive
F2 183	00 50 57.282	-72 46 22.3	14.810	17.014	17.176	14.997	14.390	Near N 37	False positive
F2 389	00 51 03.337	-72 47 54.56	14.800	17.405	17.639	14.985	14.519	Near N 37	False positive
F2 344	00 53 07.483	-72 44 19.14	14.740	17.379	17.545	16.134	15.589	Near nebulosity	False positive

Note. — MPG numbers in “Other ID” are from Massey et al. (1989). N numbers refer to LHA 115-N (Henize, 1956)

astronomer taking the Field 4 observations chose to offset the field to observe more high priority targets (see Fig. 3.1).

We covered the 3700–5800 Å region in the blue with the 580V grating, and the 5600–8800 Å in the red with the 385R grating. The resolving power in each band is ~ 1300 . The blue spectral region includes $H\beta$, several He I and He II lines (including He II at 4686 Å), [O III] at 4959 and 5007 Å as well as Ca I at 4227 Å and Fe I at 4405 Å. In the red spectra, the spectral range includes $H\alpha$ and He I at 5876 and 6678 Å, along with the Raman features at 6825 and 7088 Å, and TiO bands at 7054, 7088, 7126 and 7744 Å.

Since most of our targets are relatively bright, and we require only classification spectra, short integration times of 15 minutes for the bright fields and 75 minutes for the faint fields sufficed, even under mediocre conditions. Unfortunately, the 2013 observations were taken under conditions which were poorer than mediocre. The resulting low source counts made automatic sky subtraction difficult, making the red part of the spectra unusable for many sources, especially for the fainter F4 objects.

3.5 Results

Below, we describe sources for which we found possibly interesting spectra. We first discuss those which had already been classified as emission-line objects (with spectra shown in Figs. 3.5 and 3.6), and then turn to those that had not (Figs. 3.7 and 3.8).

3.5.1 Known Objects

LHA 115-N 60 (F4 1). Beside a marginal detection of the $H\alpha$ line, no other lines characteristic of a symbiotic are found, which means that our survey would not identify this object as a symbiotic star. This suggest that the magnitude limit for field 4 observations is $V \sim 17$. Unfortunately, since field 4 was comprised entirely of objects where $m_V > 17$, this means that there are few usable observations from this field.

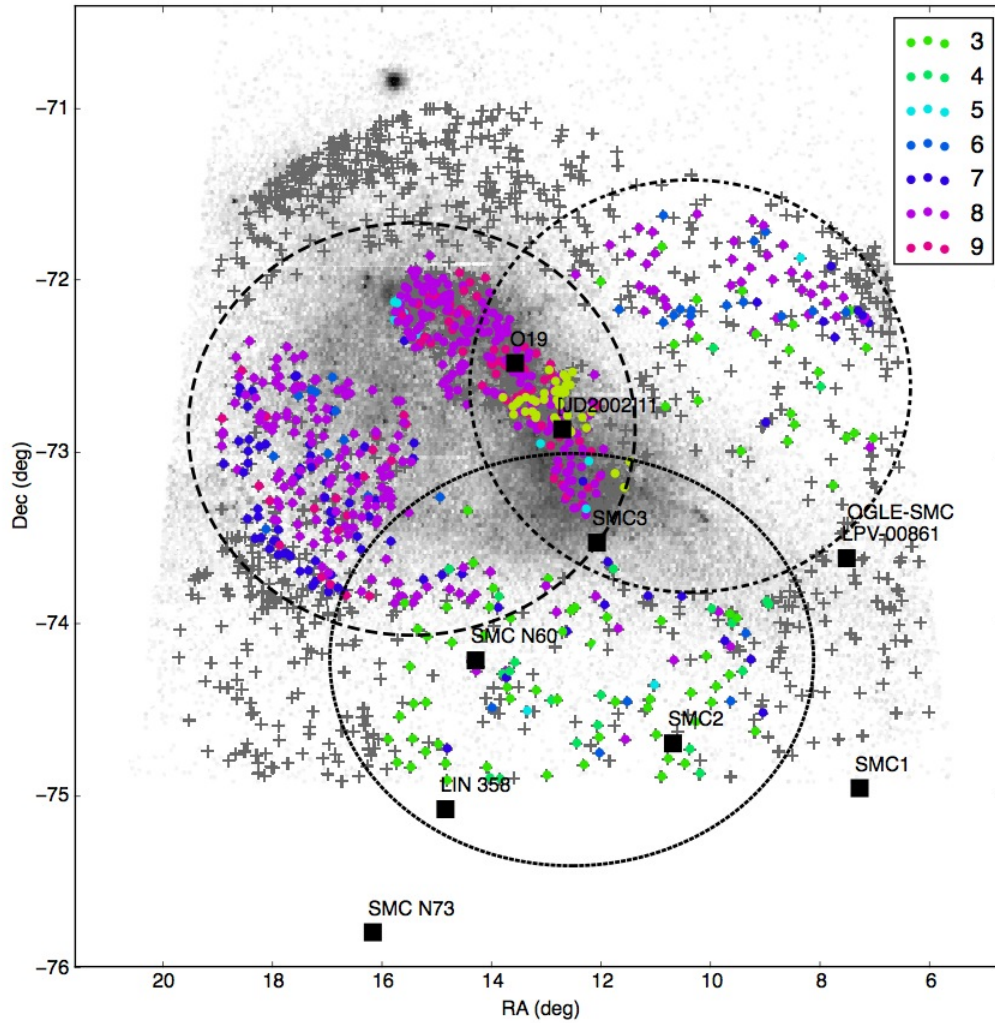


Figure 3.3

Objects observed for this survey. Colors represent priorities, red and purple objects are high priority targets. Green and blue objects are low priority targets. Unobserved targets are marked with grey Xs. The location of known symbiotic stars are marked with black squares. Most known symbiotic binaries are on the outskirts of the galaxy.

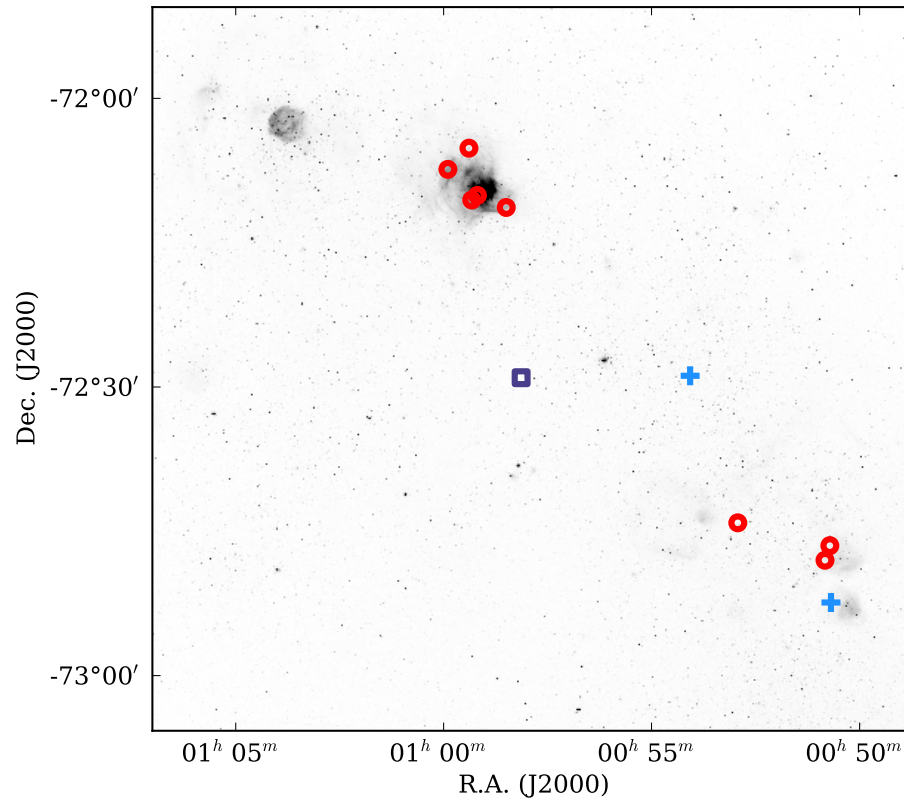


Figure 3.4

Location of objects in this survey. False positive objects are shown as red circles. The objects F2 49, F2 446, F2 520 and F2 227 are in the upper left near NGC 346. The objects F2 183 and F2 389 are in the bottom right near N 37. The symbiotic candidate F2 282 is shown with a purple square. The known symbiotics [OVS2013] 19 and [JD2002] 11 are shown with blue + signs. In the background is a [O III] 5007 Å image of the SMC from the MCEL survey (Smith et al., 2000), showing locations of ionized emission from the interstellar medium.

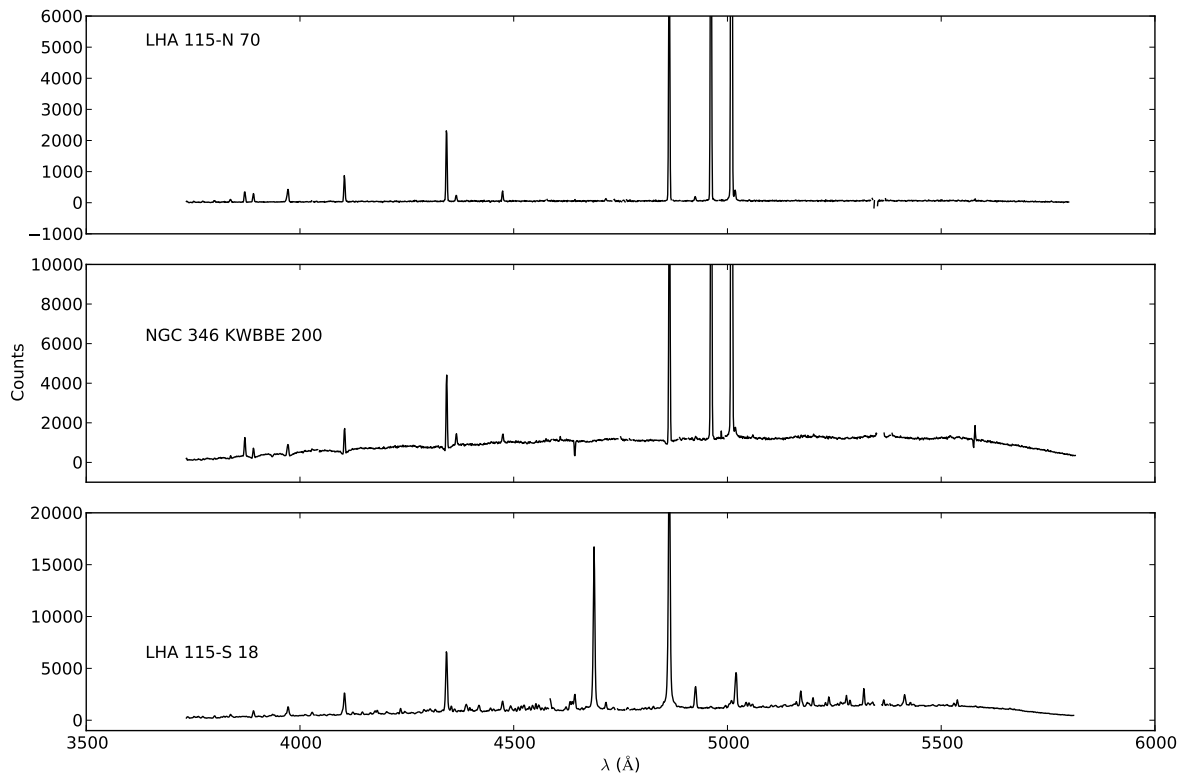


Figure 3.5

Blue spectra of three previously known objects observed in the survey. From top to bottom: LHA 115-N 70, a planetary nebula; NGC 346 KWBBE 200, a B[e] supergiant star; LHA 115-S 18, a peculiar, variable B[e] supergiant, showing a very strong He II line at 4686 \AA .

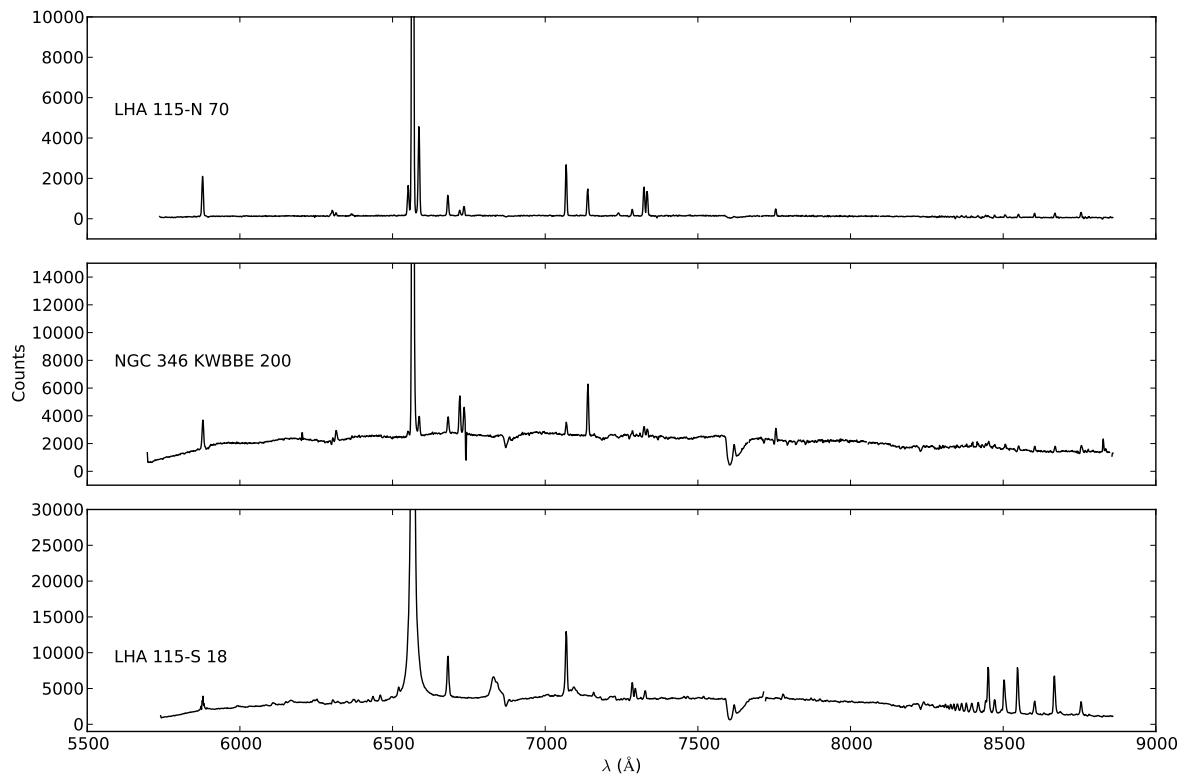


Figure 3.6

Like Fig. 3.5, but the red spectra. Note the strong Raman emission feature at 6825 \AA for LHA 115-S 18.

SMC 3 (F3 0). SMC 3 is a known symbiotic star and a super-soft X-ray source, with a $T_{\text{eff}} \simeq 500,000$ K white dwarf (Orio et al., 2007). Our spectra shows emission at $H\alpha$, $H\beta$ and, marginally, He II 4686, but no evidence for He I lines. This is consistent with previously published spectra (Muerstet et al., 1996; Munari & Zwitter, 2002). Unfortunately, problems with sky subtraction in the red spectrum prevent the identification of any other lines. Nevertheless, this symbiotic would have been identified as a candidate in our survey.

LHA 115-S 18 (F1 34). This source, also known as AzV 154 and Lin 250, is a peculiar, variable B[e] supergiant (Clark et al. 2013 and references therein). Our Aug 2012 observations of the object show the Raman 6825 emission feature, confirming their detection first reported by Torres et al. (2012). This suggests that in addition to the neutral hydrogen provided by the wind of the B[e] star, there is a source of O IV photons, indicating the presence of a hot, compact object. LHA 115-S 18 is discussed in more detail in Chapter 4.

NGC 346 KWBBE 200 (F2 30) is a known B[e] supergiant star (Wisniewski et al., 2007). Unlike LHA 115-S 18, there are no Raman emission lines, so it is likely a single object.

SMP 24 (F1 168), also known as LHA 115-N 70 is a known planetary nebula in the SMC. It shows Balmer, He I and [O III] emission lines, but no indication of a cool component, consistent with its classification as a PN. While with $J - H = 0.551$, it passed our near-infrared selection criteria, its blue $V - I = -1.084$ gave it a low rank.

3.5.2 Candidate New Emission Line Objects

We discovered nine stars which showed emission lines in their spectra, listed in Table 3.3. None of these were known as emission-line objects, and we investigated further to see if they might be symbiotics. The first five of these initially seemed very promising, and hence we discuss these in some detail.

As one can see from the spectra of the five most promising candidates in Figs. 3.7 and 3.8 (blue and red, respectively), the emission patterns are quite similar, including lines from hydrogen at $H\alpha$ 6562 and $H\beta$ 4862, He I at 5876, 6678 and 7065 Å, [O III] at 4959 and 5007 Å, and [Ne III] at 3869 Å. Of the five sources, F1 348 at first glance has a classic symbiotic spectrum, with TiO absorption bands in the red part (especially the 7054 Å band), which suggests it has a M-giant secondary. For the other four, a possible symbiotic nature is suggested by the presence of a weak Raman emission feature at 6825 Å (but no corresponding 7088 Å feature, not surprising given that it is about four times weaker intrinsically). However, given the presence of the Raman feature, which requires the presence of highly ionised oxygen, it is odd that otherwise the spectra are suggestive of a much lower ionisation object, showing no emission lines of He II and having [O III] emission that is much stronger than $H\beta$.

A closer look at our candidates suggests most are not symbiotics. In particular, F1 348 is in a very crowded region, inside NGC 346 (see Fig. 3.4). It is identified with cluster member MPG 710 (Massey et al., 1989), which was classified as a B2.5V (as quoted in Bonanos et al. 2010), i.e., emission was not noted before. In the cluster, *Hubble Space Telescope* observations show that it is only 2.3 arcsec removed from a much redder object, which has similar brightness in R (Gouliermis et al. 2006, their Table 2). Almost certainly, this object is responsible for the TiO features.

In Fig. 3.4, one sees that NGC 346 is surrounded by nebulosity. Almost certainly, this is responsible for the emission lines seen in the spectra of F1 348 – as well as in the spectra of sources near it (note that for multi-fiber spectrographs local emission will generally not be removed in the process of sky subtraction, since the sky emission is determined using fibers which may be quite distant). Indeed, even the Raman feature may originate in this nebulosity: NGC 346 is a young, bright cluster that excites a very bright H II region, LHA 115-N66 also contains two supernova remnants (for an overview and references, see Sabbi et al. 2007). One of the latter, SNR 0057–7226 shows strong O VI emission lines (Danforth et al., 2003). Combined with the large amounts of neutral hydrogen in the region, this might be responsible for the Raman features.

Now turning to all sources, and looking in more detail at Fig. 3.4, one sees that all but one of the sources are located near NGC 346 or other emission regions. Hence, most likely their emission spectra are from the local interstellar medium and none of these are symbiotics. The one exception is F2 282, which seems to be far from any source of nebular emission (see Fig. 3.4).

To check whether the candidates could be symbiotics or not, we followed Skopal (2011) in making two-component fits to the dereddened observed fluxes, using UV through IR photometry from the UIT, MCPS and SAGE catalogs. We estimated E_{B-V} for our candidates by using the mean reddening for objects in the MCPS Extinction Map (Zaritsky et al., 2002) in a radius of $\sim 2'$ from the object. These values ranged from $E_{B-V} = 0.061$ to 0.242. Then we applied the Gordon et al. (2003) reddening law for the SMC.

We fit the hot component with a blackbody curve and the cool component with the Atlas9 Stellar Atmosphere Models from Castelli & Kurucz (2004). The total flux is the sum of the flux from the hot and cool components. Results are shown in Table 3.4 and Fig. 3.10.

We find that most of our objects have a hot component with a radius between 1.25 and $4 R_{\odot}$ and a temperature between 27000 and 45000 K. Taking into account the substantial correlations between radius, temperature, and reddening, we conclude they are likely main-sequence OB stars. Our fits suggest the infrared emission is from objects at effective temperatures of 3750-5000 K and a radius of 10– 55 R_{\odot} (K and M giants). The difficulty fitting the I band suggests that the optical and IR fluxes come from independent objects that fall within the radius used to match the two catalogs and are not a genuine binary. However, given that many of these objects are very young, the IR emission might also be from circumstellar material around the OB star, in which the bad fit simply results from our two-component model not being the correct one. F2 520 likely is a miss-matched or viable object and thus has bad optical magnitudes. F2 282 has a SED consistent with a very hot object ($T_{eft} = 125000$ K), but a spectrum of a much cooler object. It may be a planetary nebula, though, again, we caution that given the strong correlations between radius, temperature, and reddening, it may also be that it simply is an object that is less reddened than stars near it, and therefore cooler and larger.

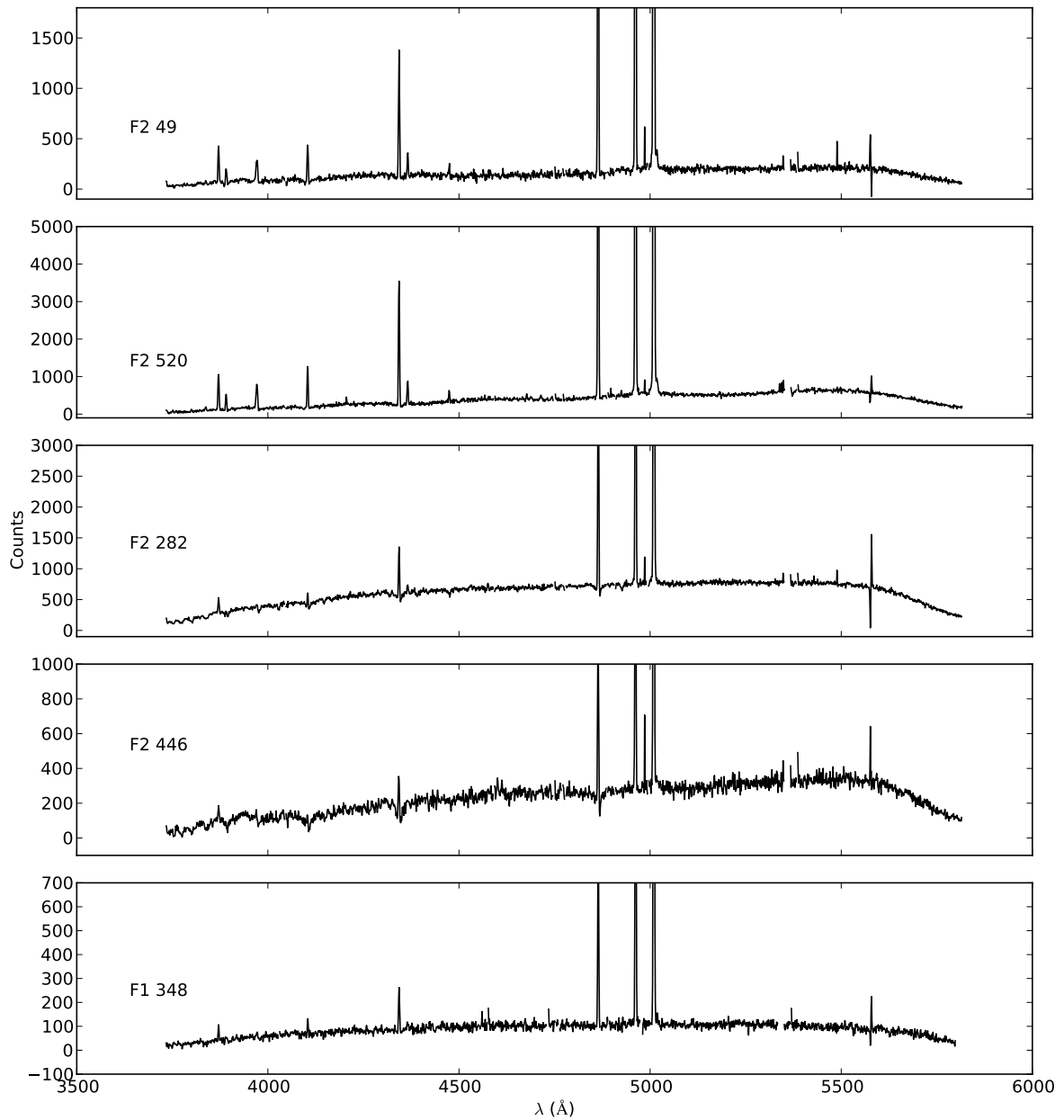


Figure 3.7

Blue spectra of new candidate symbiotics found in this survey (most of which are likely false positives). The most prominent emissions features are from $H\beta$ and $[O\ III]$ at 4959 and 5007 Å, but one also sees $Ne\ III$ at 3869 Å. The strong $[O\ III]$ lines along with the non-detection of $He\ II$ at 4686 Å suggest that the hot component is relatively cool.

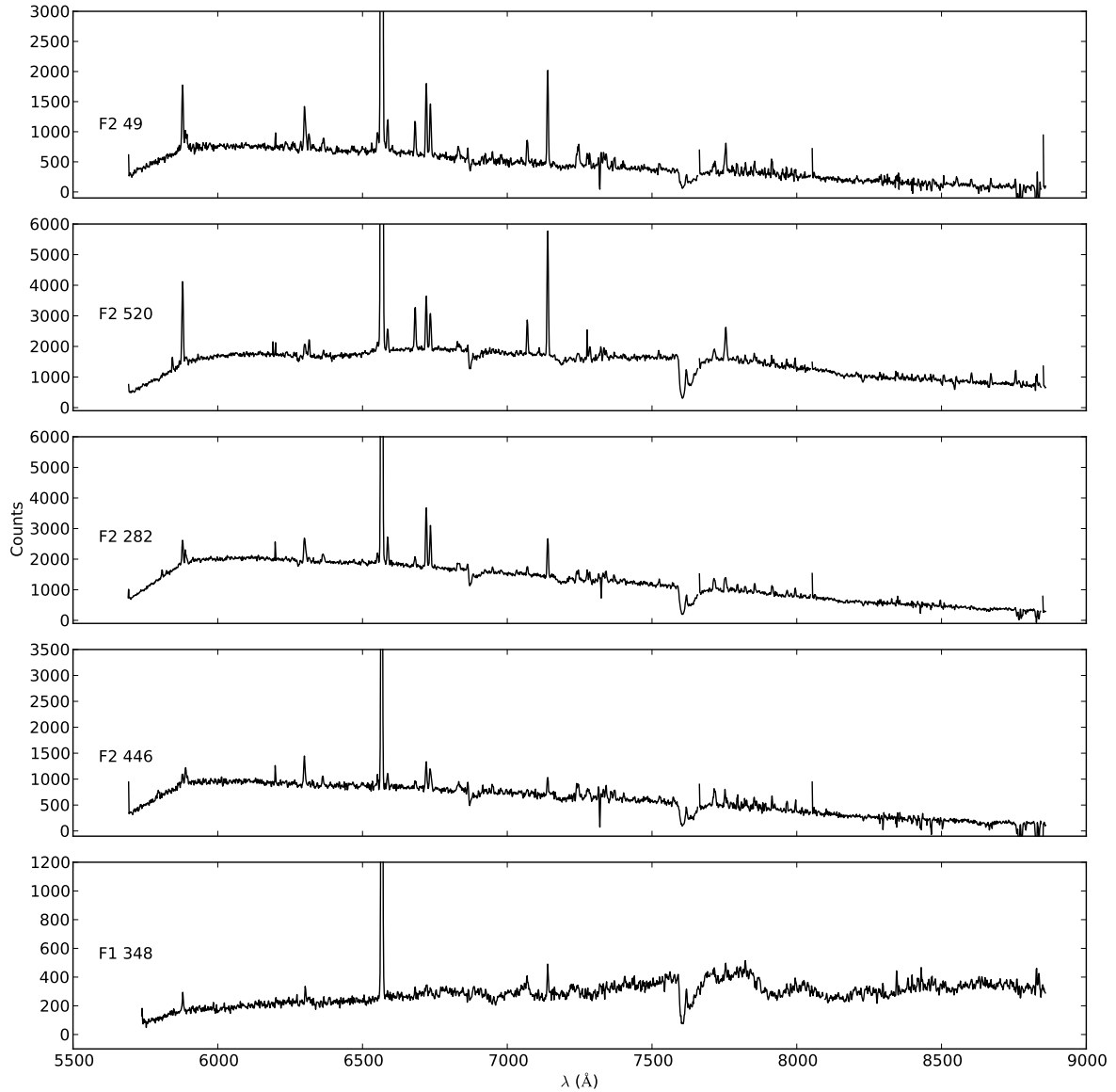


Figure 3.8

Red spectra of new candidate symbiotics found in this survey (most of which are likely false positives). F2 49, F2 282, F2 446, and F2 520 show a weak Raman 6825 emission feature (see also Fig. 3.9, while F1 348 shows weak TiO absorption bands (with the 7054 Å band most clearly visible).

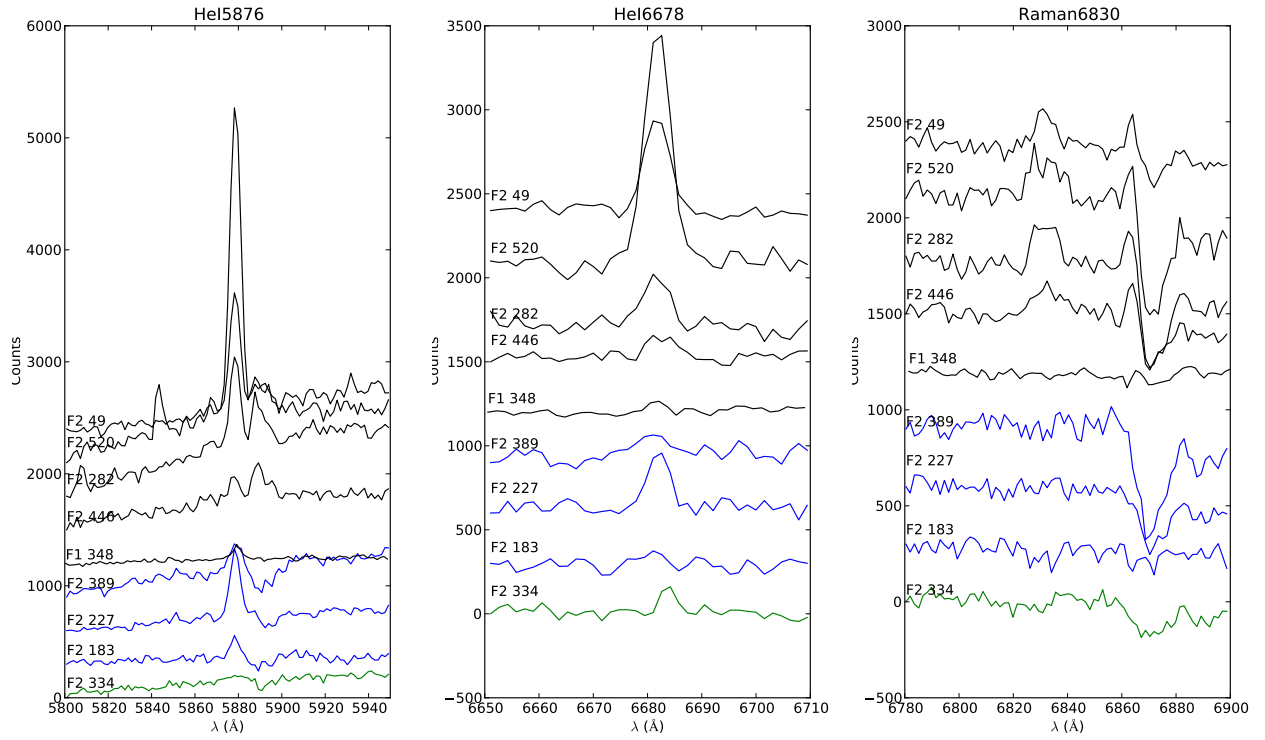


Figure 3.9

Lines from new suspected symbiotics (most of which likely are false positives). Flux is in units of counts with an arbitrary offset. F2 49, F2 282, F2 446, and F2 520 show a weak Raman 6825 Å feature while all other object have a flat spectrum in that area.

Table 3.4
Properties from SED fits of Objects in this survey

ID	E_{B-V} mag	T Hot K	R hot R_{\odot}	L hot L_{\odot}	T cool K	Rcool R_{\odot}	L cool L_{\odot}
F1 348	0.090	30000	3.75	10.0×10^3	< 3500		
F2 49	0.061	20000	4.0	3.4×10^3	3500	22	59
F2 282	0.242	125000	1.25	3400×10^3	4750	20	150
F2 446	0.129	29000	2.25	3.2×10^3	4750	10	89
F2 520	0.161	112000	1.5	3200×10^3	5000	25	410
F2 227	0.100	30000	2.0	2.9×10^3	3750	50	700
F2 183	0.142	28000	3.25	5.8×10^3	4000	50	570
F2 389	0.129	37000	2.0	6.7×10^3	3500	55	410

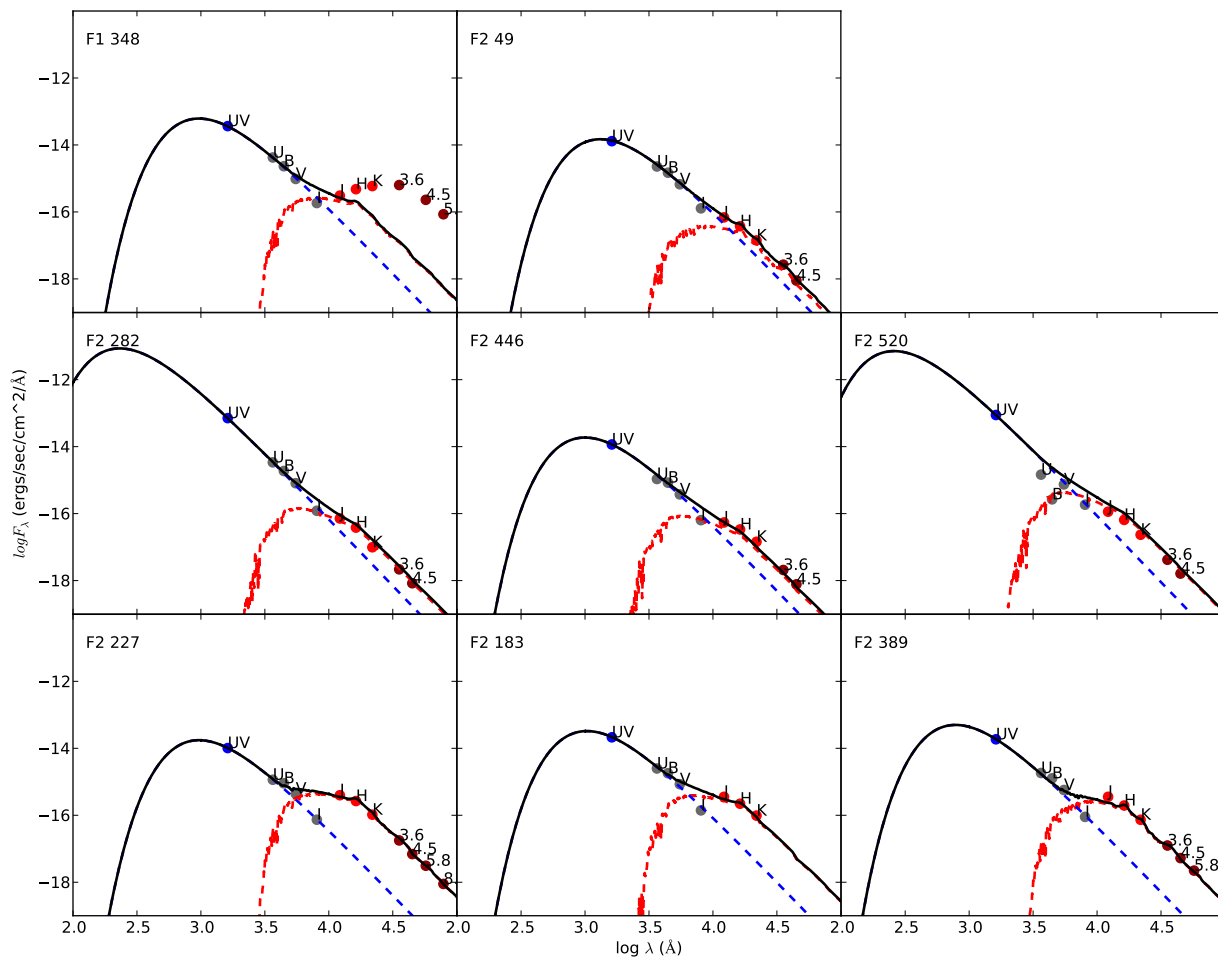


Figure 3.10

Spectral Energy Distributions of objects found in this survey using dereddened observed fluxes from the MCPS, 2MASS and SAGE SMC catalogs. Also shown are fits to the hot component with a blackbody curve (blue dashed line) and the cool component (red dashed line) with the Atlas9 Stellar Atmosphere Models from Castelli & Kurucz (2004). The total flux (solid black line) is the sum of the flux from the hot and cool components. None of the two-component fits match the I-band photometry well, suggesting that the model is wrong (e.g., because the infrared excess is due to a wind or disc and hence cannot be modeled well by a two-component spectrum) or that there was a mismatch between the optical and infrared photometry.

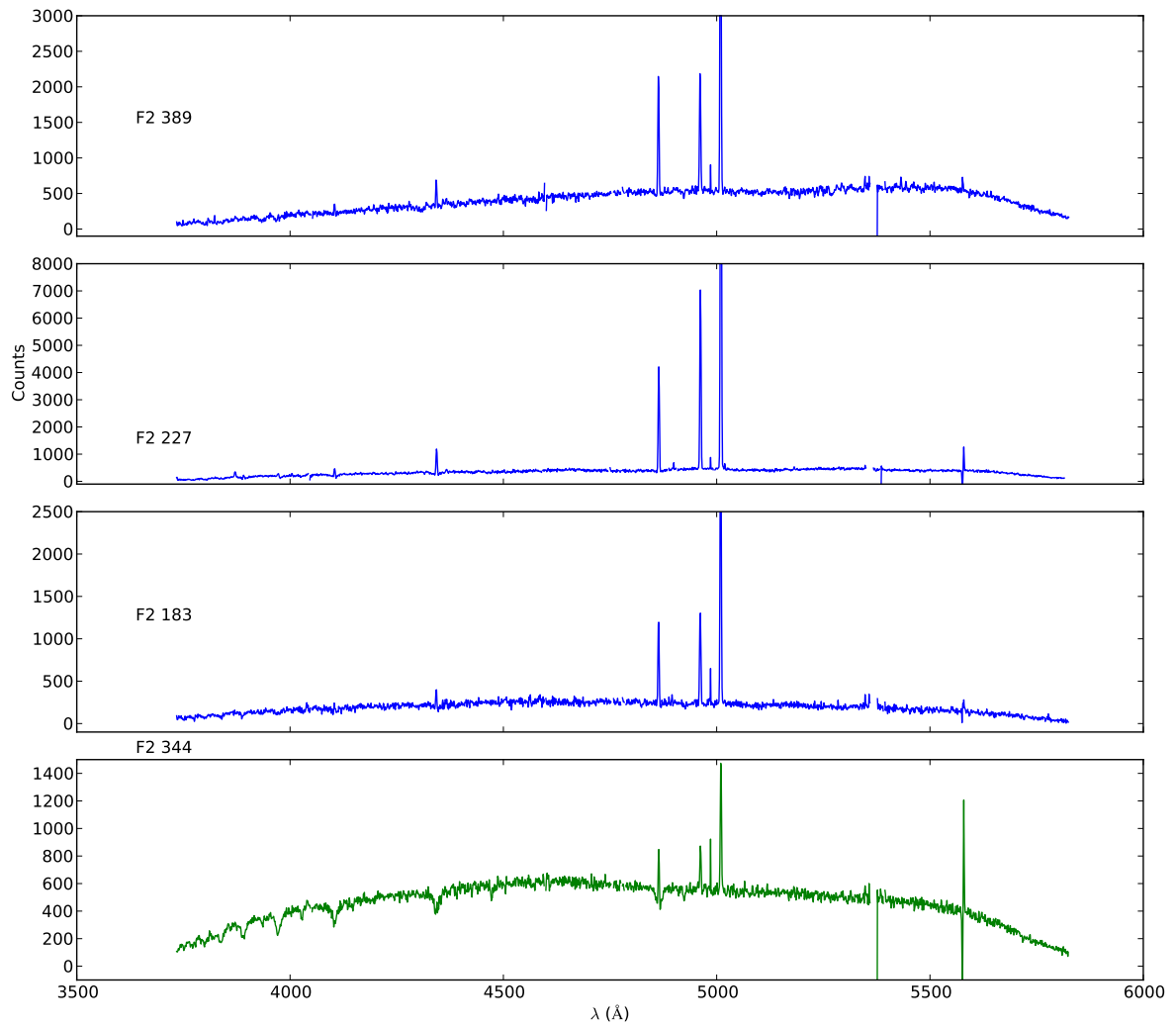


Figure 3.11
Blue spectra of other emission line objects found in this survey.

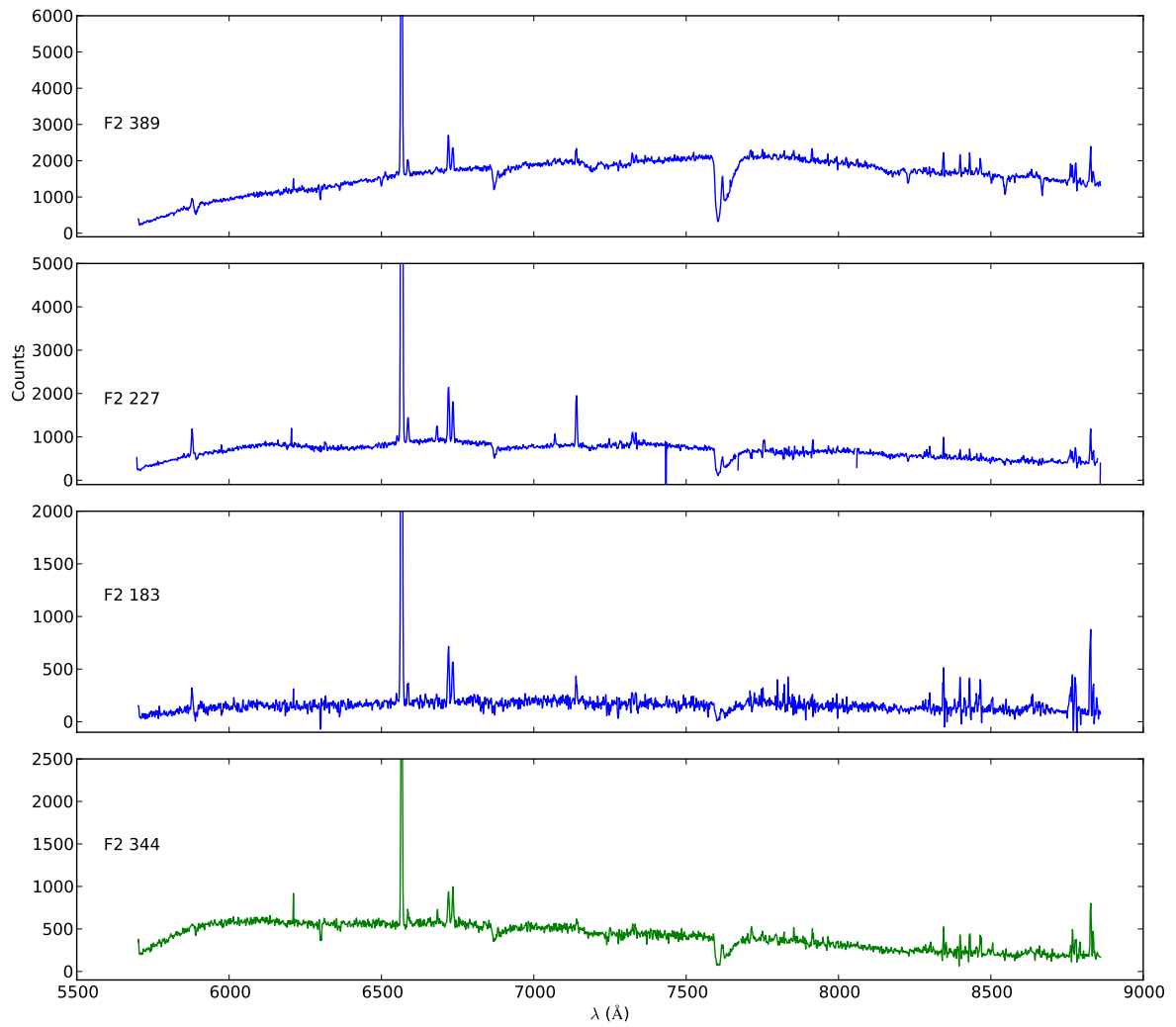


Figure 3.12
Red spectra of other emission line objects found in this survey.

Table 3.5
Symbiotic Fraction Near Known Symbiotics in the SMC

Name	Separation (deg)	ρ_{symb}
SMC 2	0.92	7.10×10^{-6}
SMC 3	0.68	2.34×10^{-6}
LHA 115-N 60	0.91	4.30×10^{-6}
[OVS2013] 19	0.46	3.57×10^{-6}
[JD2002] 11	0.46	3.21×10^{-6}
mean	0.69	4.1×10^{-6}

Note. — The symbiotic fraction for a given symbiotic is estimated as one per the number of stars in a circle with a radius equal to half the distance to the nearest other symbiotic.

3.6 The Fraction of Symbiotics in the SMC

We failed to find any new symbiotic stars in the SMC. For the outer regions of the SMC at least, this suggests the current sample of bright symbiotics is fairly complete, despite its heterogeneous origin. This is because those fields were covered by GALEX and we should have detected any similarly bright symbiotics, certainly in fields F1 and F2, where we obtained good spectra of candidates.

In the central regions covered by UIT, we cannot be sure we would have detected all symbiotics with properties similar to those known. Since the known symbiotics in this region were discovered only recently, it seems quite possible the sample here remains incomplete. But how incomplete? There seem to be two possibilities: (1) symbiotic systems preferentially form in the outer parts of the MC, perhaps following the older stellar populations; or (2) the fraction of symbiotics among all stars is roughly constant and symbiotics are simply easier to observe in the outer parts.

To test which one of these possibilities is more likely, we can compare the density of the known sample with that of the stars as a whole. The MCPS is a reasonably complete point source catalog of all objects with $V < 21$ in the central 4.5×4 degrees of the SMC (which is the majority of the dwarf galaxy). Thus, we can use star counts in MCPS as a reasonable proxy for the overall stellar number density. We will define the fraction of symbiotics among stars as the number of symbiotics in a given region divided by the total number of stars in the MCPS catalog in that region ($\rho_{\text{symb}} = N_{\text{symb}}/N_{\text{MCPS}}$). With that fraction, we can estimate the number of observable symbiotics in a given field by taking the above fraction times the number of observable stars. In our case, the latter is the number of stars in each field that are in the MCPS catalog and within the boundaries of fields covered by the UIT or GALEX surveys (and thus could have been identified as UV point sources).

We ran a Monty Carlo simulation where we randomly selected the coordinates of N_{symb} stars from the MCPS catalog to simulate the underlying population of symbiotic stars from the MCPS catalog (with $V < 21$), where N_{symb} is the true number of bright ($m_V < 17$) symbiotics in the SMC. We then counted the number of observable symbiotics in F1/F2 and F3 — simulated symbiotics that fall within the borders of the UIT or GALEX UV catalogs, the MCPS optics catalogs and our AAO fields. We found that the number of observable symbiotics follows a normal distribution, with the mean set only

Table 3.6
Number of bright symbiotics from Monty Carlo simulations

N_{symb}	ρ_{symb}	$N_{\text{F1/2}}$	Unobserved F1/2	N_{F3}	Unobserved F3	$N_{\text{GALEX/MCPS}}$	Unobserved GALEX/MCPS
9	5.0×10^{-6}	3.6	3.6 ± 2.5	2.3	1.3 ± 1.0	5.0	2.0 ± 2.5
10	5.6×10^{-6}	4.0	4.0 ± 2.6	2.6	1.6 ± 1.0	5.5	2.5 ± 2.6
11	6.2×10^{-6}	4.5	4.5 ± 2.7	2.9	1.9 ± 1.2	6.0	3.0 ± 2.7
13	7.1×10^{-6}	5.2	5.2 ± 2.8	3.2	2.2 ± 1.2	7.2	4.2 ± 2.8
15	8.3×10^{-6}	6.1	6.1 ± 3.0	3.8	2.8 ± 1.2	8.3	5.3 ± 3.0
18	1.1×10^{-5}	7.3	7.3 ± 3.2	4.6	3.6 ± 1.4	10.0	7.0 ± 3.2
20	1.1×10^{-5}	8.1	8.1 ± 3.6	5.1	4.1 ± 1.6		

by the stellar density within the field and the total number of symbiotics in the galaxy — in other words ρ_{symb} .

Table 3.6 shows the results of the Monty Carlo simulation. We list the number of symbiotics in the area covered by MCPS as well as the symbiotic fraction in that region. We include the number of symbiotics expected in F1/2, the number expected in F3 and the number in the entire region where the GALEX and MCPS catalogs overlap. We also list the number of unobserved symbiotics — the number of symbiotics predicted by the simulation minus the number of known bright symbiotics in that region.

- *Is ρ_{symb} from the known symbiotics consistent with observations?*

Yes. The symbiotic fractions of $3.2 - 7.1 \times 10^{-6}$ would suggest that there are between 0 and 1 unobserved bright ($m_V < 17$) symbiotic in F1/2, F3 and the GALEX/MCPS overlap region. Therefore, the distribution of known symbiotics is consistent with a population that follows the density of the SMC — there is no need to have symbiotics preferentially form in the outskirts of the galaxy. A $\rho_{\text{symb}} = 7.1 \times 10^{-6}$ is consistent with 15 symbiotics in the area covered by MCPS.

- *Assume our sample of symbiotics in the outer part of the galaxy (the area where the GALAX and MCPS catalogs overlap) is complete. If the number of bright symbiotics in the inner part of the galaxy has the same ρ_{symb} as those in the outer portion, how many total symbiotics should there be?*

It is reasonable to assume the number of symbiotics in the sparser region of the galaxy is fairly complete. Bright symbiotics are often also soft X-ray sources or recurrent novae. This makes them somewhat easy to detect, even at SMC distances. Outside of the nebular emission and dense fields of the inner bar of the SMC, bright, emission line objects will likely have been noted in earlier surveys.

The largest ρ_{symb} that is consistent with no unobserved objects in the GALEX/MCPS overlap region is 6.2×10^{-6} . This would mean there are 4.5 ± 2.7 unobserved bright symbiotics in F1/F2 and 11 bright symbiotics total in the area covered by MCPS.

- *Assume that there are no bright symbiotics in F1/F2 (which would be consistent with non-detections in our survey). What symbiotic fraction would we expect?*

For the number of bright symbiotics in F1/F2 to be consistent with zero, we would expect $\rho_{\text{symb}} = 5.0 \times 10^{-6}$ or 9 total bright symbiotics in the region covered by MCPS.

Thus, we can conclude that there are likely between 9 – 15 bright symbiotics in the area of the SMC covered by MCPS at a 95% confidence level. Adding in the three known symbiotics outside of the MCPS survey region, that gives us 12 – 18 total bright symbiotics in the SMC. The majority of the unobserved objects should be in the central bar of the galaxy.

To reproduce the type Ia supernova rate in the SMC, there should be about $N_{\text{acc}} = 33 - 132$ progenitors in the galaxy (Lepo & van Kerkwijk, 2013). Since there are only four (possibly five) known super-soft sources (the favored SD progenitor) in the SMC (Greiner, 2000; Sturm et al., 2011), there should be dozens of missing progenitors. From our work, the number of bright symbiotics would seem insufficient to make up this shortfall, even if the number of symbiotics is close to the upper limit we derived, and the number of progenitor systems is at the lower end.

While there is likely a population of unobserved, fainter symbiotics with low accretion rates, they will likely not be SN Ia progenitors. Thus, it seems that even with optimistic estimates, no more than 10 – 50 percent of the missing SD progenitors can come from symbiotic stars.

Chapter 4

New observations of the peculiar emission line supergiant S18

LHA 115-S 18 is a peculiar B[e] supergiant in the SMC, which is both photometrically and spectroscopically variable. In this chapter, we summarize historical observations of S18 and present two new spectra of the object. We speculate on the nature of what is probably a binary system. S18 likely contains a $\sim 12 M_{\odot}$ B supergiant, along with a hot compact object. The identity of the hot object remains unclear since either a neutron star or a white dwarf could be formed through normal stellar evolutionary processes around the B supergiant star. Both are also consistent with the properties of the hot object.

4.1 Introduction

LHA 115-S 18 = AzV 154, Lin 250 (hereafter S18) is a peculiar B[e] supergiant in the SMC. It has been seen in many surveys of emission line objects in the SMC, going back at least 60 years, with the first published account by Lindsay (1955) in their catalog of N₁ and N₂ nebular line ([OIII] 5007 and 4959, resp.) objects. They note that S18, object 40 in their catalog, had strong H α , H β , H γ , and He II 4686 emission lines.

The name S18 comes from the Henize (1956) catalog of H α emission line objects (where the ‘s’ stands for ‘star’, as opposed to ‘n’ for ‘nebulae’). It also appears in the Lindsay (1956, 1961) catalogs of emission line objects in the SMC, where it is listed as a very strong H α emitter. Sanduleak (1978) identify the star as a possible symbiotic binary due to the strong He II line the observe, but note that the “cool” object has the luminosity of a supergiant, rather than the late-type giant that is usually found in symbiotics stars. S18 was first identified as a B[e] supergiant by Zickgraf et al. (1989), who speculate that it has a unseen, hot ($\sim 10^5$ K), compact-object companion.

S18 came to our attention during a survey looking for new symbiotics stars in the SMC (see Chapter 3). Since it is a bright ultraviolet (UV) source and has an infrared (IR) excess, it was flagged as a symbiotic binary candidate. During our 2012 Aug 3 observation with AAOmega on the Anglo-Australian Telescope (Pasquini et al., 2002; Sharp et al., 2006), S18 had extremely unusual spectra (see Fig. 4.1), with a He II 4686 Å line almost as strong as the H β line, as well as prominent Raman scattered O VI emission features at 6825 and 7088 Å. At the time of the observation, no spectra of S18 with Raman scattered O VI had ever been published. Just as we realized we had discovered an unusual spectral

feature, Torres et al. (2012) published a paper announcing the discovery of the Raman scattered O VI lines, using data from 2000–2008. We were scooped.

We continued, however, as the system appeared to pose an interesting conundrum: the presence of O VI photons suggests a hot, compact object, like in symbiotic binaries, but given that S18 hosts a B-star it seemed hard to believe that, like in symbiotics, the compact object would be a white dwarf. Yet, for a neutron star X-ray emission would be expected, but at the time there were only relatively stringent upper limits. Then, again events caught up with us: Maravelias et al. (2013) found a faint X-ray source coincident with S18 in *XMM* observations, and Clark et al. (2013) published a detailed history of S18 observations and speculated on the nature of the system – having done much the same analysis that we had completed, but not yet published.

The study by Clark et al. (2013) left us unsatisfied, and hence here we revisit the information on S18, trying to determine what kind of binary it is. We first describe the properties of B[e] stars in general, and then the observed properties of S18. Next, we turn to the nature of S18, discussing separately what we can infer about the “cool” and “hot” components.

4.2 B[e] supergiant stars

B[e] supergiants are in a relatively short evolutionary phase of some massive stars, with zero-age main-sequence masses between ~ 7 and $85 M_{\odot}$, characterized by a spectrum that has both broad, high excitation emission lines and narrow, low excitation ones, along with luminosities from 10^4 to $10^6 L_{\odot}$ (Zickgraf, 2006). Most B[e] supergiant stars have been found in the Magellanic Clouds, due to the relatively low galactic extinction along the line of sight and the known distances, which simplifies luminosity calculations. Currently, there are 13 known B[e] stars in the LMC and 7 in the SMC (Zickgraf, 2006; Graus et al., 2012; Levato et al., 2014).

Zickgraf (2006) list five properties shared by all B[e] supergiants:

- 1 A continuum spectrum characteristic of an (early) B-star;
- 2 Strong Balmer emission lines;
- 3 Slow ($\sim 100 \text{ km s}^{-1}$), cool winds that produce low excitation emission lines (Fe II, [Fe II], [O I]);
- 4 Fast ($\sim 2000 \text{ km s}^{-1}$), hot, line-driven winds;
- 5 An IR excess caused by hot ($\sim 1000 \text{ K}$) circumstellar dust.

These properties suggests that B[e] supergiant stars have two distinct circumstellar regions – a cool, equatorial one and a hot polar one. The latter is likely similar to normal hot-star winds, but spectroscopic and interferometric observations suggest that the equatorial region is less like a wind and more like a viscously evolving, quasi-Keplarian disc, which is dense enough to contain both neutral hydrogen and dust (Kastner et al., 2006; Kraus et al., 2007; Wang et al., 2012; Thureau et al., 2009).

Kastner et al. (2010) find that the IR properties of these disks are similar to those around pre-main-sequence stars, including evidence for substantial dust processing, and hence argue that these disks are long-lived structures. From their fits to the spectral energy distribution, they infer somewhat puffed up disks, which they suggest indicates circumbinary disks, perhaps similar to those seen in some post-AGB-stars. If so, this would imply that B[e] stars are in a rather late evolutionary stage, following a major mass loss event (either as a red supergiant or perhaps a common-envelope stage).

4.3 Photometric and spectroscopic variability

4.3.1 Optical spectra and photometry

S18 shows considerable spectroscopic variations, as can be seen from a summary of historical spectroscopy shown in Table 4.1 (adapted from Clark et al., 2013). In particular, the Balmer series sometimes shows strong P Cygni profiles, yet at other times shows only single peaks. The switch between profiles can happen in less than 6 months (Shore et al., 1987). Intriguingly, when the Balmer series shows P Cygni profiles, He I emission lines do not, which suggests the hydrogen and helium lines arise in different regions.

There is also considerable variability in the strength of the He II 4686 line. Sometimes it is completely absent, sometimes it is relatively weak, and at other times it is comparable in strength with the nearby $H\beta$ line.

As first reported by Torres et al. (2012), S18 also shows emission features around 6825 and 7088 Å which are due to Raman scattering of strong O VI emission lines on H I Ly γ . The features are typically seen in symbiotic stars and indicate the presence of both a source of hot, ionizing photons and a large amount of neutral hydrogen. In S18, the Raman features only appear when there is also a strong He II 4686 line, but the reverse is not true: strong He II lines are not always accompanied by Raman emission features. Unfortunately, few published spectra include wavelengths redder than $H\alpha$, so other than a marginal detection by Shore et al. (1987), we are unable to verify the presence of Raman lines before the Dec. 2005 observation by Torres et al. (2012).

Here, we present two previously unpublished spectra of S18. The first, shown in Fig. 4.1, was taken as part of the symbiotics survey described in Chapter 3. We used AAOmega to take red and blue spectra of S18 on 2012 Aug. 3, covering the 3700–5800 Å region in the blue with the 580V grating, and the 5600–8800 Å in the red with the 385R grating, with a resolving power of ~ 1300 in each band. We observe an extremely strong He II 4686 line along with strong Raman scattered O VI emission features.

The second spectrum, shown in Fig. 4.2, comes from the SOAR Goodman Spectrograph, using the 1200 l/mm grating. This is the first in a series of spectra designed to search for radial-velocity variations in the He II 4686 Å line. At the time of this observation, the He II 4686 line was relatively weak.

From 1987.5 to 1989, van Genderen & Sterken (2002) monitored S18 in the Walraven system: optical V and B and near-UV L, U and W bands. They find short-term variability on the timescale of days and $\sim 0.1 - 0.2$ mag variations over a period of about 150 days. Ogle II-IV light curves from Clark et al. (2013) show I band magnitudes that range from $\sim 13.10 - 12.51$ mag. Variations in the light curve happen over periods of ~ 1 yr, but a Lomb-Scargle periodogram shows no evidence for periodicity. Clark et al. (2013) note that while He II 4686 Å may be in emission in any photometric state, it is absent only in brighter states.

4.3.2 UV spectra and photometry

Shore et al. (1987) present a series of IUE spectra. They note that while there are considerable variations in the strength of emission lines (including the almost complete disappearance of the Ly α line in an observation in 1981 March), the continuum flux remains relatively unchanged. They suggest the stable continuum is from the B[e] star but the strongly varying emission lines are excited by another component, which, from the strengths of the He II emission lines, must be much hotter, $\sim 10^5$ K.

S18 also appears in the Ultraviolet Imaging Telescope (UIT) SMC point source catalog. This catalog comes from observations during two space shuttle missions in late 1990 and early 1995, using the B5 filter at 162 nm (Cornett et al., 1997). The UIT magnitude $m_{162} = 13.30$ is consistent with the flux inferred from IUE observations, again suggesting that the UV continuum does not vary strongly.

4.3.3 X-ray photometry

S18 was not detected in any ROSAT or Einstein observations of the SMC, which suggests that the object had an X-ray luminosity of $L_X \lesssim 10^{35} \text{ erg s}^{-1}$ when those observations were made. On 2002 July 04, a Chandra observation detected an X-ray source with $L_X \simeq 3.5 \times 10^{33} \text{ erg s}^{-1}$ at the position of S18. On 2003 Dec. 18, an XMM-Newton observation detected S18 at $L_X \simeq 7.1 \pm 1.7 \times 10^{33} \text{ erg s}^{-1}$, but on 2006 November 01, it was not detected, to a limit of $L_X \lesssim 4.7 \times 10^{32} \text{ erg s}^{-1}$. Here, the measurements assumed a standard foreground column of $N_H = 6.23 \times 10^{20} \text{ cm}^{-2}$ and a power-law spectrum with a slope $\gamma = 1.7$ (Maravelias et al., 2013); the data are of insufficient quality to constrain the spectrum directly, though the intrinsic spectrum cannot be soft unless true column density is very high. The X-ray luminosities inferred from the two detections are well above those expected for a single, hot star — they require an extra source of hot photons (Clark et al., 2013). Thus, S18 is a faint, variable X-ray source which likely reflects emission from a hot component in the system.

4.4 Is S18 a Luminous Blue Variable?

Massey & Duffy (2001) compare their spectrum of S18 to that of S Dor, a luminous blue variable star (LBV), in its low state. They claim based on a superficial resemblance of the two spectra that S 18 is probably a LBV — another class of massive, evolved stars, the most famous of which is η Carinae.

According to Humphreys & Davidson (1994) LBVs share the following properties:

- 1 High luminosity ($\sim 10^6 L_\odot$);
- 2 H I, He I, Fe II and [Fe II] lines, often with P Cygni profiles;
- 3 Large photometric variability:
 - Giant eruptions, with brightness increases of > 2 mag (including some supernova mimics);
 - Normal eruptions, with brightness increases of 1–2 mag on 10–40 yr time scales;
 - Quasi-periodic oscillations of ~ 0.5 mag on timescales of months;
- 4 IR excess caused by hot circumstellar dust.

While these properties overlap with those of B[e] stars, it is unclear if LBVs and B[e] stars share more than that. S18 is under-luminous for a LBV and has photometric variations on much shorter timescales, suggesting it is smaller and denser. LBVs are bluer at minimum than maximum, because at the ends of their outburst, their photospheres retreat at roughly constant luminosity, i.e., they shrink and their effective temperature increases. Photometry from van Genderen & Sterken (2002) shows that the colors of S18 remain flat or even become slightly redder as the object leaves its optical high state. While the luminosity and timescale of variations are somewhat inconclusive, the color behavior is harder to dismiss. Thus, as both van Genderen & Sterken (2002) and Clark et al. (2013) conclude, while S18 is both luminous, blue and variable, it is likely not a LBV.

Table 4.1
Summary of historical S 18 spectroscopic observations

Date of observation	P Cygni profile Balmer line	HeII lines present	Raman Scattered O VI present	Reference
~1955	...	yes	...	L55
1967 Jul. 14	...	no	...	S78
1977 Sep. 17	...	yes	...	S78
1978 Jan. 27	yes	yes	...	A81
16 Jul. 1978	no	yes	no	S87
1981 Mar. 15	...	no	...	S87
1981 Jul. 13	...	yes	...	S87
1981 Sept. 29	...	yes	...	S87
1982 Mar. 22	...	yes	...	S87
1983 Mar. 02	...	yes	...	S87
1983 Dec. 20	yes	yes	yes? ^a	S87
1985 Apr. 27	...	no	...	IUE
1987 Nov. 7	yes	no	...	Z89
1991 Sep. 17-20	no	yes ^b	no	N96
1999 Oct. 25	...	yes ^c	...	M01
2000 Oct. 10	yes	no	...	M01
2000 Oct. 13	yes	no	no	T12
2001 Nov. 24	no	no	no	T12
2005 Dec. 10	no	yes	yes	T12
2007 Oct. 10	no	yes	yes	T12
2008 Nov. 13	no	yes	yes	T12
2010 Nov. 24	yes	no	...	C13
2011 Jul. 11	no	yes	...	C13
2011 Dec. 08	no	yes ^d	no	C13
2012 Jul. 07	no	yes	...	C13
2012 Aug. 03	no	yes	yes	This Work
2014 Feb. 08	no	yes	...	This Work

References. — L55: Lindsay (1955), S78: Sanduleak (1978), A81 Azzopardi et al. (1981), S87: Shore et al. (1987), Z89: Zickgraf et al. (1989), N96: Nota et al. (1996), M01: Massey & Duffy (2001), T12: Torres et al. (2012), C13: Clark et al. (2013). IUE: data from IUE archive.

^aPossibly a very weak Raman-scattered line at 6825 Å with the 7082 Å Raman-scattered line blended with He I 7065 Å.

^bThe line is double-peaked. In all other cases, the He II lines were single-peaked.

^cObserved in narrow band photometry, strong enough to flag the object as a 95σ candidate for a Wolf-Rayet star.

^dPresent but weak.

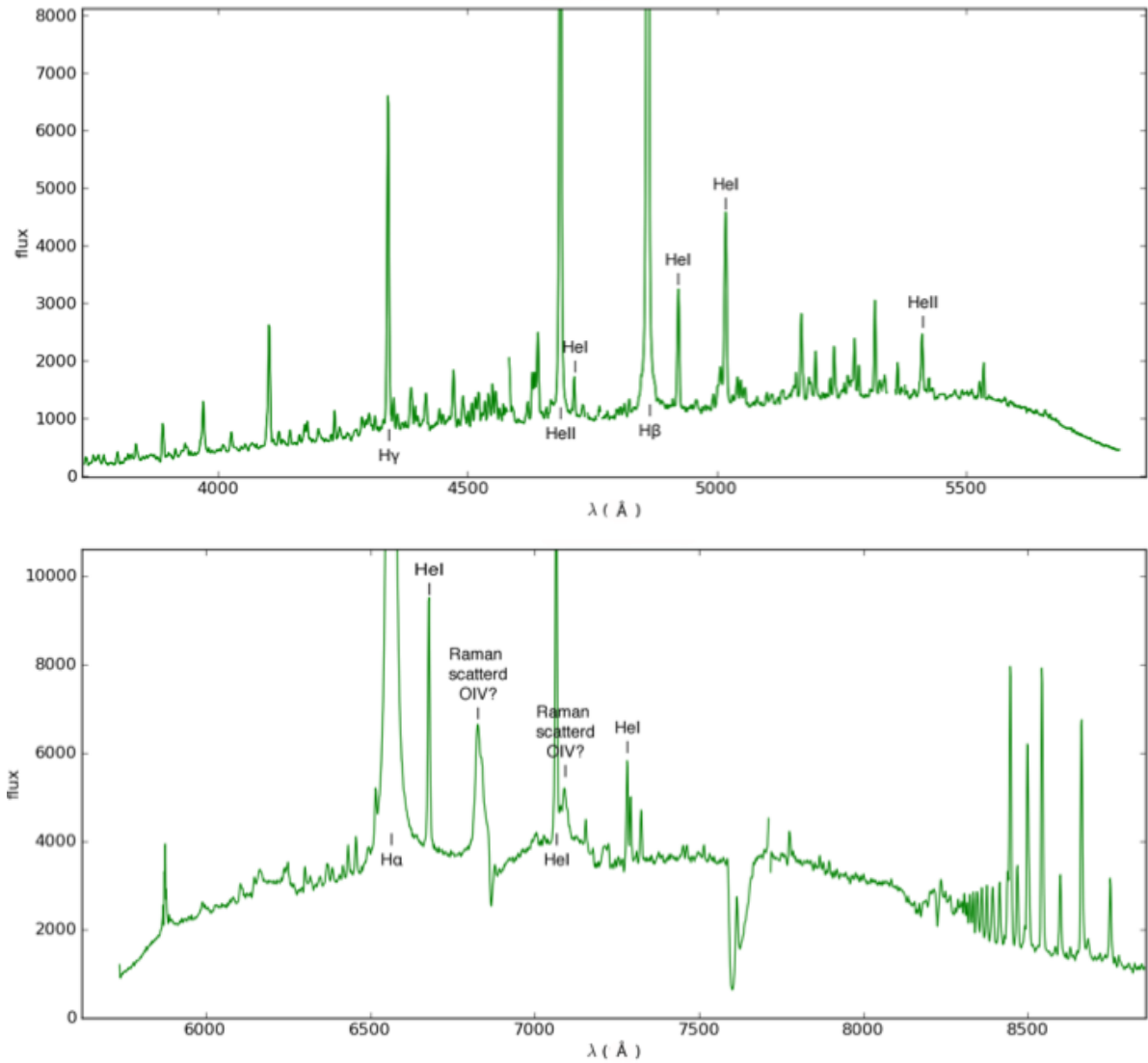


Figure 4.1
AAOMega spectra of S18 taken 2012 Aug. 3.

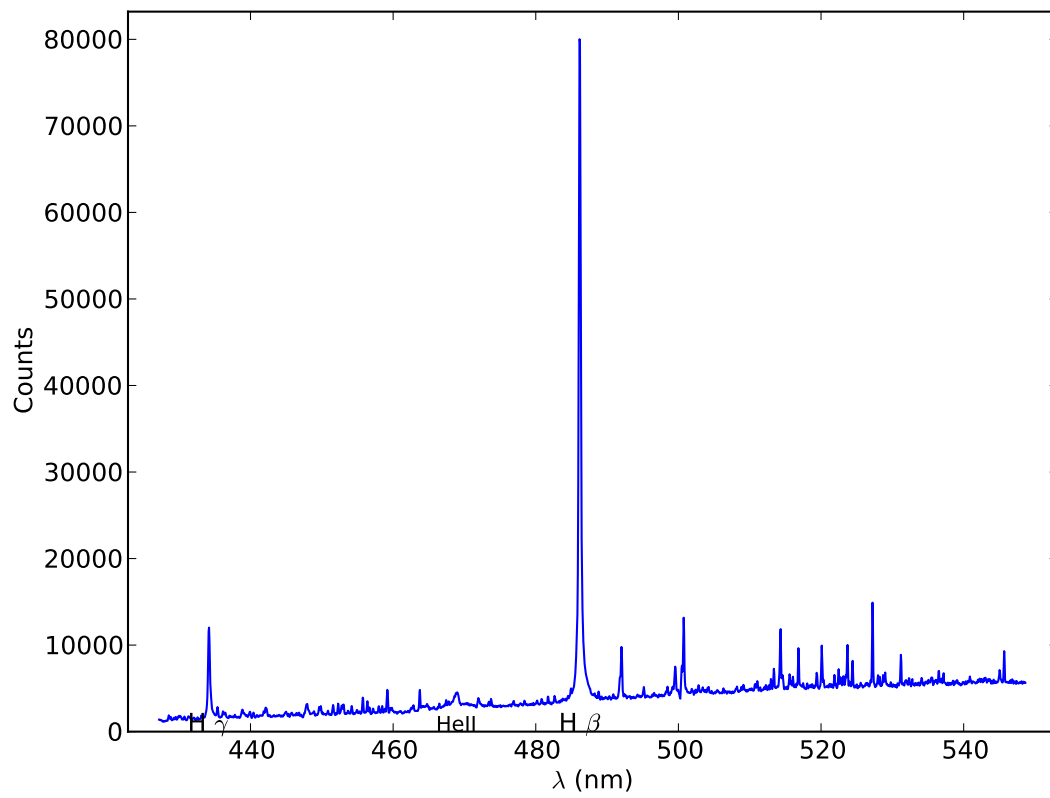


Figure 4.2
SOAR spectrum of S18 taken 2014 Feb, 8.

4.5 The nature of the cool star in S18

There are no absorption lines visible from the B supergiant in S18, making it difficult to determine its spectral type, and thus its evolutionary history. In the literature, the parameters most widely used are those from Zickgraf et al. (1989), who used a model atmosphere to fit the de-reddened spectral energy distribution (SED) of S18, noting that the object has both a UV and IR excess. They find the best fit at $T_{\text{eff}} = 25000$ K and $E_{B-V} = 0.4$ mag. The inferred effective temperature, however, is strongly correlated with the assumed extinction along the line of sight. Zickgraf et al. (1989) throw out all fit results with $E_{B-V} < 0.3$ mag, because this leads to temperatures $T_{\text{eff}} < 15000$ K, which they argue are inconsistent with the observed emission lines. However, all but one of the B[e] stars subsequently identified in the Magellanic Clouds have temperatures less than the 25000 K inferred for S18 (Zickgraf, 2006); indeed, the coolest LMC B[e] star, Hen S 93, has $T_{\text{eff}} \simeq 10000$ K.

Furthermore, a reddening $E_{B-V} = 0.4$ is rather large for the SMC. As was discussed in Chapter 2, SMC stars generally have E_{B-V} values of 0.02 to 0.12, with about 0.02 to 0.04 coming from the Milky Way foreground and the rest from internal reddening (Bessell, 1991; Cornett et al., 1997). Thus, it seems likely that S18 is less reddened than assumed in Zickgraf et al. (1989) and hence may be substantially cooler.

In order to verify this, we repeated the analysis done by Zickgraf et al. (1989), using modern stellar templates and reddening laws for the SMC. Specifically, we use the Gordon et al. (2003) reddening law for the SMC, using various assumptions for E_{B-V} and then fit the UV through IR photometry from the UIT, MCPS and SAGE-SMC catalogs using the Atlas9 Stellar Atmosphere models from Castelli & Kurucz (2004) with $\log g=3.0$ (the gravity also used by Zickgraf et al., 1989). We list our results in Table 4.3.

For our best estimate for the extinction to S18, we use the MCPS Extinction Map from Zaritsky et al. (2002): for hot objects in a 0.5 arcmin radius around S18, we find an average extinction of $\langle A_v \rangle = 0.48$ mag, corresponding to $E_{B-V} \simeq 0.15$ mag (for $R = 3.1$). For this E_{B-V} , our best fit yields $T_{\text{eff}} = 12250$ K, $R = 39 R_{\odot}$ and $L = 10^{4.49} L_{\odot}$. This luminosity suggests a zero-age main-sequence mass of $\sim 12 M_{\odot}$, rather than the mass of $\sim 40 M_{\odot}$ implied by the calculations of Zickgraf et al. (1989).

It is important to note here that S18 shows ~ 1 mag variations in its V and I-band measurements. Since the photometry used for these fits, collected from several SMC photometric catalogs, was taken during different epochs, the resulting parameters are unavoidably imprecise. It is clear, however, that S18 likely does not hold a very massive star, which is an important clue for the nature of its putative hot companion.

4.6 The nature of the hot component in S18

Three pieces of evidence suggest the presence of a hot component in S18: the X-ray emission, the strong He II lines, and the Raman emission features. All three components are strongly variable, in ways uncorrelated with the the UV, optical, and IR continua, suggesting they have a separate origin.

The implications for the nature of S18 were discussed in some detail by Clark et al. (2013). They suggest S18 is a binary, with the hot component either arising from accretion on a compact companion or from shocks from colliding winds from two massive stars (as is seen in, e.g., η Carinae). Such binaries have X-ray luminosities of $L_X \sim 10^{32} - 10^{35}$ erg s $^{-1}$ (Gagné et al., 2012). In principle, good X-ray

Table 4.2
S18 Photometry

Band	mag	source
m_{162}	13.30	UIT
U	13.097	MCPS
V	13.768	MCPS
B	13.816	MCPS
I	12.623	MCPS
J	12.349	2MASS
H	11.931	2MASS
J	11.109	2MASS
$m_{3.6}$	9.181	SAGE-SMC
$m_{4.5}$	8.329	SAGE-SMC
$m_{5.8}$	7.732	SAGE-SMC
$m_{8.0}$	6.935	SAGE-SMC

Table 4.3
Best fit Parameters for the Cool component of S18

E_{B-V}	T_{eff}	R/R $_{\odot}$	log(L/L $_{\odot}$)
0.01	9500	39	4.05
0.05	10250	37	4.13
0.10	11000	39	4.30
0.15	12250	39	4.49
0.20	14000	36	4.65
0.30	33000	13	5.25
0.40	50000	17	6.21

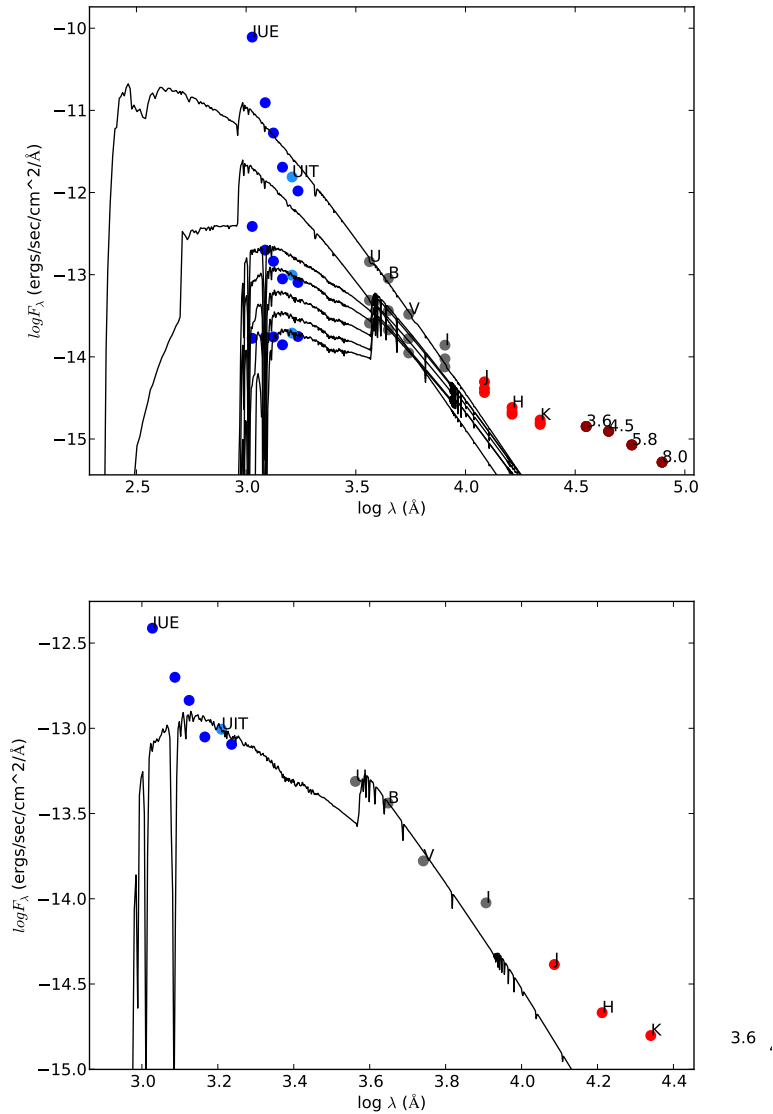


Figure 4.3

Dereddened Spectral Energy Distributions (SEDs) of S18 and best single-component fits to UV and optical photometry for various values of the extinction E_{B-V} : *top panel*: Best fit values for, from top to bottom, $E_{B-V} = 0.40, 0.30, 0.20, 0.15, 0.10, 0.05, 0.01$. Dereddened photometry is shown for $E_{B-V} = 0.40, 0.15$ and 0.01 . *bottom panel*: Best fit model spectra for $E_{B-V} = 0.15$, the best estimate for the extinction of S18 from nearby stars in the MCPS extinction map. For comparison, typically stars in the SMC have $E_{B-V} = 0.02-0.12$.

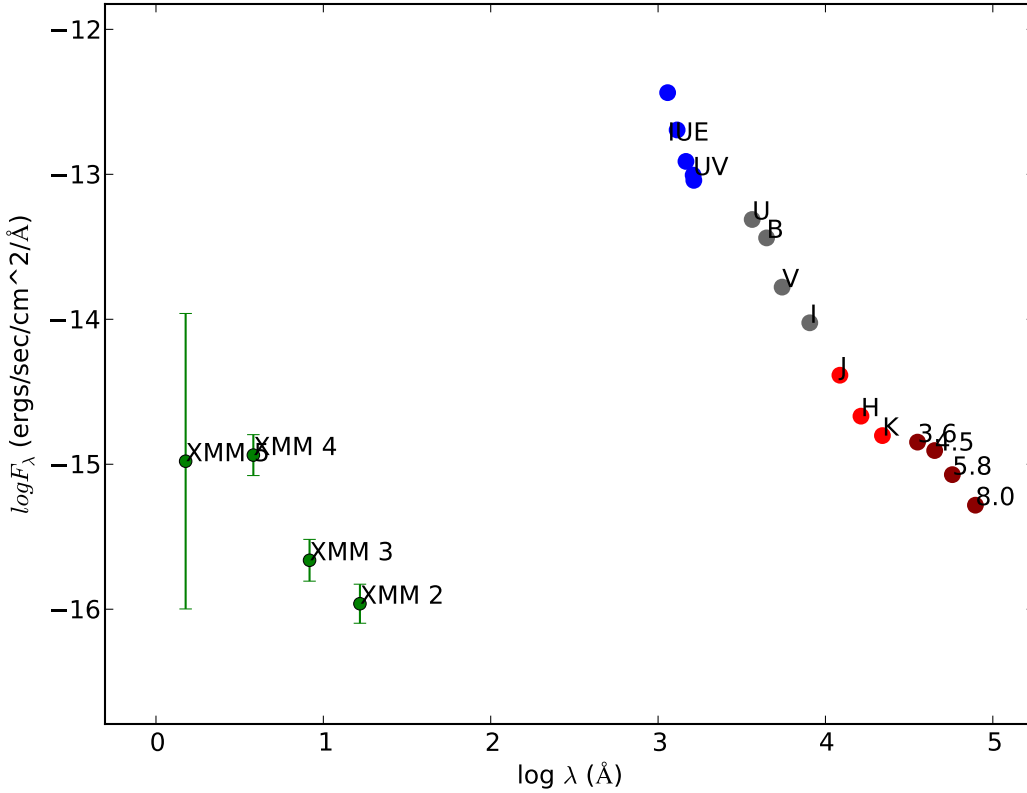


Figure 4.4

Spectral energy distribution of S18, including X-ray observations from *XMM*. UV through IR fluxes were dereddened using $E_{B-V} = 0.15$.

spectra could distinguish between the possibilities, as the spectrum from wind shocks (optically thin thermal emission with strong emission lines) is quite different from that expected from neutron stars or WDs (optically thick with fewer emission lines). Unfortunately, the current X-ray observations are of insufficient quality to do this.

A problem with the interpretation of the hot component as colliding winds is that both the very strong He II emission as well as the Raman features require a far-ultraviolet source that is of similar luminosity as the B[e] star (Shore et al., 1987). Indeed, this can be seen also by analogy with symbiotics, in which the hot source typically is near the Eddington luminosity for a $\sim 1 M_\odot$ compact object, of $\sim 10^{4.5} L_\odot$ – comparable to the luminosity we inferred for the B[e] star above.

Binary companions that could be directly responsible for the hot component would be hot helium stars or accreting compact objects. The strong variability suggests accretion on a compact object is more likely, so below we focus on the evidence for and against a white-dwarf or neutron-star companion.

4.6.1 A White Dwarf Companion?

Does the hot component in S18 arise from a white dwarf? Initially, it might seem unlikely that the B-star in S18 could have a white dwarf companion, since white dwarfs are the product of “low mass” stellar evolution. However, an evolved B-star with a white dwarf companion can form quite readily through normal stellar evolutionary processes.

B-stars have zero-age main-sequence masses ranging from ~ 2 to $16M_{\odot}$. Isolated late-type B-stars with masses of $\lesssim 8M_{\odot}$ should form white dwarfs at the end of their lifetimes — mostly with CO cores but some with ONe for stars with masses close to the upper cut-off (García-Berro, 2013). Thus, while it may be tempting to think of B-stars as “high mass” stars that end up as neutron stars, this is true only for the more massive ones; the vast majority of B-stars should form white dwarfs.

In addition, binary interactions can transfer mass from one star in a binary system to the other, prematurely stripping one star of its outer layers. For example, Shao & Li (2014) model binary interactions of stars between 1.5 and $60M_{\odot}$ that will form Be stars (rapidly rotating main sequence B-stars). They find that the majority of Be stars should have He star or white dwarf companions, confirming results that go back decades (e.g., Waters et al. 1989). The distribution of the periods of these binaries range from ~ 10 to 200 d, with a peak around 100 d. In the majority of these Be/WD pairs, the Be stars have masses between 1.5 and $10M_{\odot}$, although it is still possible to form white-dwarf companions for Be stars with masses up to about $15M_{\odot}$.

Thus, if the B-star in S18 is indeed $\sim 12M_{\odot}$, as is likely from the revised SED fits above, it does not need an exotic formation mechanism for it to have a white dwarf companion.

A white dwarf might naturally account for the fact that S18 shares, at least intermittently, many observational properties with symbiotic binaries — white dwarfs that accrete via winds from a low-mass giant companion. These properties include H I, He I and He II emission lines, as well as the emission features due to Raman-scattered O VI emission.

A white dwarf companion would also provide a natural explanation for the low observed X-ray luminosity, since it will have a larger radius than that of a neutron star. Indeed, Waters et al. (1989) model the X-ray luminosity from a Be/WD binary, where the WD is embedded in the equatorial winds of the Be star. They find $L_x = 10^{33}$ to 10^{29} erg/s, depending on the wind speed of the WD, the orbital separation and the masses of the components. This is consistent with XMM observations.

Maravelias et al. (2013) notes that there are too few counts in the XMM photometry of S18 to fit a good spectrum. Nevertheless, the fluxes in the four XMM bands give insight into the nature of the X-ray emitter and thus the type of hot object associated with the S18 system. Since the X-ray emission is brighter at harder X-rays (XMM bands 4 and 5) than at softer X-rays (XMM bands 2 and 3), it is not consistent with the soft X-ray spectrum expected of a hot, nuclear burning white dwarf, such as is often seen in symbiotics. The emission is consistent, however, with the type of spectra seen for magnetic white dwarfs in cataclysmic variables, as well as with sources such as the Be stars γ Cas and HD 110432, for which indeed a white dwarf companion is often invoked to explain the moderate-luminosity, strongly variable X-ray emission (e.g., Lopes de Oliveira et al. 2007).

4.6.2 A Neutron Star?

Is the hot object in S18 a neutron star? Since the progenitor of a neutron star companion would evolve more quickly than a B supergiant, one could form a neutron star companion for any reasonable mass of

the B-star in S18 through normal stellar evolutionary processes. In fact, this may be the only reasonable compact object companion if the B[e] star in S18 has a mass of $\gtrsim 15 M_{\odot}$.

A neutron star — or rather its accretion disk — could also provide a natural explanation for the intermittent features of the hot component, including possibly the Raman-scattered O VI features and the presence of X-rays. However, a puzzle would be that S18 has never been observed as a strong X-ray source. Maravelias et al. (2013) discuss this problem in some detail and find that to bring down the X-ray flux to the observed levels, not only do they have to invoke the neutron star only accreting from the fast, tenuous component of the wind (rather than the dense equatorial material), but also that the emission is absorbed by a rather large column density ($N_H = 1 \times 10^{24} \text{ cm}^{-2}$). These two constraints seem inconsistent with each other. Furthermore, it would imply a small accretion rate, which seems inconsistent with the requirement that the far-ultraviolet luminosity be very large. The only way out would seem to be that the accretion rate is in fact very large, but that the material does not reach the neutron star, perhaps because it is rotating too fast and material is ejected (i.e., it is in the so-called propellor phase; Illarionov & Sunyaev 1975).

4.7 A complete picture of the S18 system

Based on the available evidence, the most plausible scenario for the nature of the S18 system would seem to be that it contains both a B[e] supergiant star and a compact object. The latter is likely a white dwarf, though we cannot exclude a neutron star.

Following Zickgraf et al. (1989) and Zickgraf (2006), we will assume that there are three components to the emission from the S18 system. The first arises in an intrinsically variable B supergiant star, which like classical Be stars, undergoes large changes in its mass loss rate. Fast winds from the B-star contribute to the variable, high-excitation emission lines, including the strong Balmer emission lines, seen in the spectrum of S18.

The second component arises from a hot white dwarf and possibly an accretion disk. This is the source of the observed X-rays as well as the far-ultraviolet continuum that pumps the high-ionization emission lines, such as He II 4686, observed in S18. The white dwarf is the remnant of a B-star companion that likely was only slightly more massive than its companion, and transferred much of its mass to it (forming the current B[e] star). The luminosity of the white dwarf at least partially tracks what it accretes from the B-star, and thus the strength of the emission lines correspond to variations in the mass-loss rate of the B-star and in the region of the wind the white dwarf accretes from.

The third component is the quasi-stable Keplerian disk, which is the source of low ionization emission lines as well as the IR excess. The disk is likely created by outflows from the B-star (though it may be a circumbinary remnant) and is irradiated by the white dwarf, as well as by the O VI emission lines, causing the Raman features. The luminosity and position of the hot object relative to the disk determines how much energy is intercepted, and thus the strength of those features.

The white dwarf may well move in and out of the disk and could sometimes be obscured by disk material. Possibly, this corresponds to times when we fail to observe He II lines and X-ray emission. Since the disk geometry is likely variable, the visibility of the white dwarf does not have to be strictly periodic. The observed quasi-periodicities suggests the white dwarf remains visible for ~ 3 to 5 year periods and is obscured for ~ 1 year periods. Since the Raman emission should arise in neutral hydrogen

in the disk, they will only be visible when the white dwarf is active and visible (i.e., He II emission from near the white dwarf is observed), and it is close enough to the disk.

To test whether the above scenario is correct, we have begun a spectroscopic monitoring program of the He II line of S18 to look for the expected radial-velocity variations. If found, these would allow us to establish an orbital period for the source of hot photons. Unfortunately, since (at least the disk of) S18 has a low inclination (Zickgraf et al., 1989; Aret et al., 2012), the lack of RV variations would not conclusively rule out a hot companion object. Deeper X-ray spectra of S18 would also be useful to determine the nature of the hot component, to be sure there are no colliding winds, to check whether accretion-disk models fit, and to look for possible rotation periods.

4.8 Other B-star/White Dwarf Binaries

S18 likely provides an example of an interacting white dwarf / B-star binary. While there are many known high mass X-ray binaries that consist of a B- or Be-star and a neutron star (Liu et al., 2006; Sturm et al., 2013), there are fewer known X-ray binaries where the compact object is a white dwarf. γ Cas is a Be star with an X-ray luminosity of $\sim 10^{33}$ erg s $^{-1}$ with a hard spectrum similar to that of an accreting, magnetic white dwarf. Thus, it likely has a white dwarf companion (Murakami et al., 1986; Kubo et al., 1998; Owens et al., 1999). Torrejón & Orr (2001) show that two other Be stars, HD 110432 and HD 141926 are likely Be/X-ray binaries based on their X-ray spectra. These binaries likely resemble S18, but have main sequence Be stars instead of a B[e] supergiant companions.

More evidence for B-star/white dwarf X-ray binaries come from surveys that show a population of super-soft sources associated with the spiral arms of nearby galaxies (Di Stefano et al., 2003, 2010). These soft X-rays sources are likely too young to be what we typically think of as SSS. The “just right” super-soft sources that we consider SD progenitors can only occur during a fairly brief window after star formation — enough time must pass to form one white dwarf but not enough time for the $\sim 1 - 3 M_{\odot}$ main sequence star in the binary to evolve too much. One possibility is that these are B-stars with accreting white dwarf companions, the product of binaries consisting of nearly equal-mass B stars which evolve off of the main sequence fairly rapidly. Unlike S18 or γ -Cas, which have hard X-rays due to the magnetic fields of their white dwarfs, the white dwarfs in these binaries may not be strongly magnetic and accrete enough material from their B-star companions to sustain steady nuclear burning on their surfaces.

4.9 The fate of the S18 system

The ultimate fate of the S18 system depends on the orbital separation of the binary. If the B[e]/WD binary is very wide, the B[e] star will evolve independently, ultimately becoming a neutron star. The white dwarf will either be ejected from the system or orbit the young pulsar as part of a wide, eccentric binary.

If the B[e]/WD binary is only moderately wide, as the B[e] star expands in the final stages of its evolution, it will form a common envelope with the white dwarf. The white dwarf will spiral in but not merge with the core, creating a tight binary and ejecting the envelope. The core of the B[e] star will continue to evolve, and eventually undergo core collapse, forming a neutron star. This either unbinds the white dwarf or creates a young pulsar with a close, eccentric white dwarf companion. One example

of such a system is PSR B2303+46, a neutron star/white dwarf binary with a 12.3 day, highly eccentric ($e = 0.66$) orbit (Stokes et al., 1985; van Kerkwijk & Kulkarni, 1999). The cooling age of the white dwarf suggest that it formed before the neutron star due to binary interactions between similar mass companions — much like the S18 system (van Kerkwijk & Kulkarni, 1999).

If the B[e]/WD binary is fairly tight, again as the B[e] star expands in the final stages of its evolution, it will form a common envelope with the white dwarf. During its common envelope phase, the white dwarf will merge with the core of the B[e] star. This merger remnant may resemble a rapidly rotating, massive single star and may eventually form a rapidly rotating single neutron star. This can provide the right conditions to form a magnetar, a neutron star with an ultra-strong magnetic field, of $\gtrsim 10^{15}$ G (Duncan & Thompson, 1992).

It is difficult to know which one of these scenarios is the most probable, given the observational evidence that we have. However, it is likely that the WD in S18 is fairly close to its B[e] star companion, since the WD interacts with the supergiant's disk and accretes material. Thus, it seems likely that the ultimate fate of S18 will follow one of the last two scenarios, ending up as either a neutron star and an unbound white dwarf, a neutron star with a close, eccentric white dwarf companion or as a magnetar. Further observations to establish the orbital period and nature of the compact object will help us establish the most probable evolutionary path.

Chapter 5

Conclusion

The results presented in the previous chapters have a number of ramifications. Below, I first discuss the puzzling absence of RAWDs and ways in which we could improve our understanding of their observational properties. Next, I turn to suggestions for an improved symbiotics survey, able to find fainter objects and thus more strongly constrain the symbiotic population. Finally, I briefly discuss implications for the non-detections reported in this thesis for the ongoing debate about the nature of the progenitors of type Ia supernovae.

5.1 Understanding RAWDs

Our non-detection of rapidly accreting white dwarfs in the SMC is not only problematic for the single-degenerate progenitor scenario for type Ia supernovae, but also more generally for our understanding of white dwarf binary evolution. White dwarfs accreting rapidly from binary companions are a natural extension of the CV populations that we do observe, which include novae and SSS. Binaries with sufficiently high mass-transfer rates are also predicted by most population synthesis models (see, for example: Han & Podsiadlowski, 2004; Chen et al., 2014). Thus, unless we fundamentally misunderstand something about binary evolution or white-dwarf accretion physics, there should be at least some RAWD.

Given the above, it may be that we simply failed to find the RAWDs that exist in the SMC. While we strongly suspect that they would be both UV bright and have emission lines characteristic of a hot object, it is difficult to make good predictions in the absence of any confirmed RAWDs. Thus, it is important to study in greater detail the objects suspected to be RAWD, like V Sge and LHA 120-N 66. For instance, for V Sge, since the low-state is like that of a SSS, the mean accretion rate is likely at best modestly above that of a SSS, but it would be good to try to measure it. For N 66, the accretion rate may well be higher, but not even the binary nature of this source is secure. Might it be possible to confirm it through either photometric or spectroscopic time series? For example, one could look for signatures of either brightness changes due to an irradiated secondary or radial-velocity variations in irradiation-induced lines.

While we approached the RAWD problem from an observer's perspective, it may be necessary to attack it from a theorist's perspective as well. What should a RAWD look like? Will the expanding envelope around the white dwarf fill the Roche lobe? If so, how will this affect the orbital evolution? Are there important aspects of the accretion process that we are missing? Will the system emit strongly

in a wavelength regime that we are ignoring? More mundanely: What colors and luminosities should we expect? What will the light curves of these objects look like on short and long time scales? How will the color of a RAWD change if it undergoes an outburst?

It would also be useful to know to what extent the cooler companion in a RAWD system would be visible. It is likely that RAWD have 2–3 M_{\odot} main sequence star companions (Hachisu & Kato, 2003a). If we could determine the mass and radius of the companion observationally, it would help us constrain the mass of the white dwarf in these proposed RAWD systems, along with the accretion rate. V Sge has almost a hundred years of detailed photometric observations. Using models of the system (that go beyond the extremely simple one used for the RAWD in Chapter 2), could we disentangle the contributions of the hot white dwarf, the cooler main sequence companion and the (circumbinary?) accretion disk? If so, we might much better constrain the system parameters and help address the questions raised above.

5.2 Designing a better symbiotic survey

It is clear, looking back at our survey looking for new symbiotics in the SMC, that several changes to the observational design would have increased the probability of detecting new objects.

5.2.1 Selecting hot objects

While at first it would seem that UV surveys should be fairly good at identifying the hot component of SMC symbiotics, in practice there are several major problems. The first is the surveys presently available: the UV coverage of the central bar of the SMC — which contains the vast majority of the galaxy’s stars — is fairly shallow. The known symbiotics in the SMC are at the magnitude limit of the UIT survey, meaning they would be marginal detections at best. There is also an annoying gap between the UIT and GALEX survey fields of the SMC, which further limits our ability to identify objects in the denser parts of the SMC.

Instead of UV photometry, suitable candidates might be found using narrow-band imaging, looking for point sources that emit strongly in the emission lines characteristic of symbiotic binaries. Lines in the Balmer series, such as $H\alpha$ are probably not a good choice, since many sources have them and there is strong nebular emission from the interstellar medium, particularly in the central core of the SMC. Imaging using a filter centered around the 6825 Å Raman emission feature, perhaps using a filter meant for $H\alpha$ detections on redshifted galaxies, may be able to detect candidate symbiotic stars. While the presence of the 6825 Å Raman emission feature is not sufficient to characterize an object as a symbiotic star (see the false-positive detections in Chapter 3 and the strong Raman feature in S 18), the conditions that give rise to Raman scattered O VI lines occur infrequently outside of symbiotic systems.

Using the de-reddened flux of the Raman emission feature from galactic symbiotic stars reported in Birriel et al. (2000), we would expect Raman emission lines to have a flux of $(1.5\text{--}8.0) \times 10^{-13} \text{ erg cm}^{-2} \text{ s}^{-1}$ for the 6825 Å feature and $(0.33\text{--}2.2) \times 10^{-13} \text{ erg cm}^{-2} \text{ s}^{-1}$ for the 7082 Å feature at SMC distances and extinctions. Symbiotics with cooler white dwarfs will have fainter Raman lines (see the detection in faint symbiotics in M31 in Mikolajewska et al., 2014). Since the features reflect Raman-scattered O VI emission, their strength decreases rapidly with temperature. Thus, a narrow-band imaging survey would only detect fairly hot ($\gtrsim 41000$ K) white dwarfs.

Another possibility is to use a filter centered around the He II 4686 Å line. While He II 4686 surveys of the SMC have been performed (for example in the Massey & Duffy, 2001, survey looking for Wolf-Rayet

stars), they have been shallow and no He II point source catalogs of the SMC have been published. While, the He II 4686 line is not unique to symbiotic stars (it is also seen in RAWD, SSS, Wolf-Rayet stars and X-ray binaries), it is a good marker for rare, hot objects. It also suffers less from contamination from nebular emission surrounding clusters than does H α . Indeed, reversing the logic on the non-uniqueness, a He II 4686 Å survey would be useful for identifying other objects that are either interesting in their own accord or are possible SD type Ia progenitors. As with the 6825 Å Raman emission feature, however, a 4686 Å survey will only find symbiotic binaries with relatively hot ($\gtrsim 54000$ K) white dwarfs.

5.2.2 Better candidate identification

Since we were using large, multi-object spectrometers, we assumed that we would handle large false-positive rates, and were fairly liberal with the color cuts that we used to select candidate objects. In hindsight, a somewhat smarter survey design might have helped to identify better high-priority targets. In particular, our $V - I$ color cuts were designed to find objects that had optical colors similar to those of the giant companions of known symbiotics in the SMC. However, given the uncertainty over which optical bands are dominated by the white dwarf’s flux and which are dominated by the giant’s flux, this selection may have excluded symbiotic stars with cooler, optically fainter secondaries.

Since UV through IR photometry is available for all objects in the survey, it is possible (if a bit computationally intensive) to fit model spectra to some or all of the objects in our multi-wavelength SMC catalog — identifying objects that show more concrete evidence for having both a hot, compact object and a cool giant component.

5.2.3 Deeper Spectroscopy

Our survey was designed to take quick classification spectra of a large number of objects under fairly poor conditions. This was partially because of practical considerations — applications for short observing programs are more appealing to time allocation committees and are more likely to be observed even with low queue priorities. We were also confident that even with quick integration times and poor conditions, the observations would yield spectra with a sufficient signal to noise ratio to identify new symbiotics.

In practice, however, identifying a cool component either through the presence of TiO bands or the Raman emission feature seems to require higher-quality spectra than the ones that we obtained. In the poor conditions in which our data were taken, our short integration times were only useful for identifying bright, $V \lesssim 17$ symbiotic stars; fainter objects require deeper spectra. It is a little difficult to estimate exactly how much longer our integration time would have to be since we are dealing with a two-component system. However, according to the AAOmega integration time calculator, a S/N of 15 could be achieved for an object with a $I = 19$ (approximately the value observed for the faint SMC symbiotic [JD2002] 11a) with a 231 minute integration during grey time, i.e., significantly longer than the 75 minutes used in the faint fields in our original survey, but not an insurmountable amount of time.

5.3 Implications for Type Ia Supernova Progenitors

To match the expected type Ia supernova rate in the SMC, based on the galaxy’s blue luminosity, we expect that there should be 33–132 actively accreting type Ia progenitors in the SMC. Since there are

between four and five known accreting white dwarfs visible as super-soft sources in the SMC, there are still between 28 and 128 missing progenitors.

In the RAWD survey presented in Chapter 2, we find that there is an upper limit of 10–14 RAWD in the SMC, assuming that they resemble LHA 120-N 66 or fainter versions of Wolf-Rayet stars. In Chapter 3, we find that the numbers and distribution of the known symbiotic systems, combined with our non-detection of any new ones, are consistent with a total of about 12–18 bright symbiotic stars in the SMC.

Assuming that all of the bright symbiotic stars in the SMC are SD progenitors and that most RAWD resemble N 66, we can thus set an upper limit of 26–37 SD progenitors in the SMC. This is only marginally consistent with the expected number of progenitors in the galaxy, though more work must be done to establish whether these assumptions are valid.

A more likely scenario, given our non-detections, is that SD progenitors are rare. This is consistent with other recent evidence (see Chapter 1) that suggests that SD progenitors are not responsible for most type Ia supernovae, and that they can account for only $\lesssim 20\%$ of the total progenitor population. If they do create some explosions, they may produce atypical type Ia supernovae.

Another possibility is that the ultimate fate of a SD system is not an explosion at all. For instance, even if a white dwarf can steadily accumulate hydrogen, if the helium layer that accumulates is unstable (which seems not unlikely based on our understanding of AGB stars) the white dwarf may lose all of its accumulated mass to a nova-like helium flash (as was seen in the simulations of Iban et al., 2013). Thus, even if a new census were to discover a hitherto hidden population of SD progenitors, this would be no guarantee that the SD channel is responsible for type Ia supernovae.

Bibliography

- Allen, D. A. 1980, MNRAS, 190, 75
- Aret, A., Kraus, M., Muratore, M. F., & Borges Fernandes, M. 2012, MNRAS, 423, 284
- Ashok, N. M., & Banerjee, D. P. K. 2003, A&A, 409, 1007
- Azzopardi, M., Breysacher, J., & Muratorio, G. 1981, A&A, 95, 191
- Azzopardi, M., & Vigneau, J. 1982, A&AS, 50, 291
- Badenes, C., Hughes, J. P., Bravo, E., & Langer, N. 2007, ApJ, 662, 472
- Badenes, C., & Maoz, D. 2012, ApJ, 749, L11
- Baella, N. O., Pereira, C. B., & Miranda, L. F. 2013, AJ, 146, 115
- Barlow, M. J. 1987, MNRAS, 227, 161
- Belczyński, K., Mikołajewska, J., Munari, U., Ivison, R. J., & Friedjung, M. 2000, A&AS, 146, 407
- Bessell, M. S. 1991, A&A, 242, L17
- Bianchi, L., Conti, A., Shiao, B., Keller, G. R., & Thilker, D. A. 2014, in American Astronomical Society Meeting Abstracts, Vol. 223, American Astronomical Society Meeting Abstracts 223, 254.09
- Birriel, J. J., Espey, B. R., & Schulte-Ladbeck, R. E. 2000, ApJ, 545, 1020
- Bonanos, A. Z., Lennon, D. J., Köhlinger, F., et al. 2010, AJ, 140, 416
- Bressan, A., Marigo, P., Girardi, L., et al. 2012, MNRAS, 427, 127
- Brown, P. J., Dawson, K. S., Harris, D. W., et al. 2012, ApJ, 749, 18
- Castelli, F., & Kurucz, R. L. 2004, ArXiv Astrophysics e-prints
- Chen, H.-L., Woods, T. E., Yungelson, L. R., Gilfanov, M., & Han, Z. 2014, MNRAS, 445, 1912
- Chomiuk, L., Soderberg, A. M., Moe, M., et al. 2012, ApJ, 750, 164
- Chomiuk, L., Nelson, T., Mukai, K., et al. 2014, ApJ, 788, 130
- Clark, J. S., Bartlett, E. S., Coe, M. J., et al. 2013, A&A, 560, A10
- Cornett, R. H., Greason, M. R., Hill, J. K., et al. 1997, AJ, 113, 1011

- Corradi, R. L. M., Rodríguez-Flores, E. R., Mampaso, A., et al. 2008, *A&A*, 480, 409
- Corradi, R. L. M., Valentini, M., Munari, U., et al. 2010, *A&A*, 509, A41
- Danforth, C. W., Sankrit, R., Blair, W. P., Howk, J. C., & Chu, Y.-H. 2003, *ApJ*, 586, 1179
- Di Stefano, R. 2010a, *ApJ*, 712, 728
- . 2010b, *ApJ*, 719, 474
- Di Stefano, R., Kong, A., & Primini, F. A. 2010, *New Astron. Rev.*, 54, 72
- Di Stefano, R., Kong, A. K. H., VanDalsen, M. L., et al. 2003, *ApJ*, 599, 1067
- Drew, J. E., Hartley, L. E., Long, K. S., & van der Walt, J. 2003, *MNRAS*, 338, 401
- Duncan, R. C., & Thompson, C. 1992, *ApJ*, 392, L9
- Fitzpatrick, E. L. 1986, *AJ*, 92, 1068
- Foellmi, C. 2004, *A&A*, 416, 291
- Foellmi, C., Moffat, A. F. J., & Guerrero, M. A. 2003, *MNRAS*, 338, 360
- Gagné, M., Fehon, G., Savoy, M. R., et al. 2012, in *Astronomical Society of the Pacific Conference Series*, Vol. 465, *Proceedings of a Scientific Meeting in Honor of Anthony F. J. Moffat*, ed. L. Drissen, C. Rubert, N. St-Louis, & A. F. J. Moffat, 301
- Gänsicke, B. T., van Teeseling, A., Beuermann, K., & de Martino, D. 1998, *A&A*, 333, 163
- García-Berro, E. 2013, in *IAU Symposium*, Vol. 281, *IAU Symposium*, ed. R. Di Stefano, M. Orío, & M. Moe, 52–59
- Gilfanov, M., & Bogdán, Á. 2010, *Nature*, 463, 924
- Gordon, K. D., Clayton, G. C., Misselt, K. A., Landolt, A. U., & Wolff, M. J. 2003, *ApJ*, 594, 279
- Gordon, K. D., Meixner, M., Meade, M. R., et al. 2011, *AJ*, 142, 102
- Gouliermis, D. A., Dolphin, A. E., Brandner, W., & Henning, T. 2006, *ApJS*, 166, 549
- Graur, O., Maoz, D., & Shara, M. M. 2014, *MNRAS*, 442, L28
- Graus, A. S., Lamb, J. B., & Oey, M. S. 2012, *ApJ*, 759, 10
- Greiner, J. 2000, *New A*, 5, 137
- Hachisu, I., & Kato, M. 2003a, *ApJ*, 598, 527
- . 2003b, *ApJ*, 590, 445
- . 2006, *ApJS*, 167, 59
- Hachisu, I., Kato, M., & Nomoto, K. 1996, *ApJ*, 470, L97
- . 2008, *ApJ*, 679, 1390

- . 2010, *ApJ*, 724, L212
- Hachisu, I., Kato, M., & Schaefer, B. E. 2003, *ApJ*, 584, 1008
- Hajduk, M., Gładkowski, M., & Soszyński, I. 2014, *A&A*, 561, A8
- Hamann, W.-R., Peña, M., Gräfener, G., & Ruiz, M. T. 2003, *A&A*, 409, 969
- Han, Z., & Podsiadlowski, P. 2004, *MNRAS*, 350, 1301
- Hayden, B. T., Garnavich, P. M., Kasen, D., et al. 2010, *ApJ*, 722, 1691
- Henize, K. G. 1956, *ApJS*, 2, 315
- Humphreys, R. M., & Davidson, K. 1994, *PASP*, 106, 1025
- Iben, Jr., I. 1988, *ApJ*, 324, 355
- Iben, Jr., I., & Tutukov, A. V. 1994, *ApJ*, 431, 264
- . 1996, *ApJS*, 105, 145
- Idan, I., Shaviv, N. J., & Shaviv, G. 2013, *MNRAS*, 433, 2884
- Iijima, T., & Nakanishi, H. 2008, *A&A*, 482, 865
- Illarionov, A. F., & Sunyaev, R. A. 1975, *A&A*, 39, 185
- José, J., & Hernanz, M. 1998, *ApJ*, 494, 680
- Kastner, J. H., Buchanan, C., Sahai, R., Forrest, W. J., & Sargent, B. A. 2010, *AJ*, 139, 1993
- Kastner, J. H., Buchanan, C. L., Sargent, B., & Forrest, W. J. 2006, *ApJ*, 638, L29
- Kato, M. 2005, in *Astronomical Society of the Pacific Conference Series*, Vol. 330, *The Astrophysics of Cataclysmic Variables and Related Objects*, ed. J.-M. Hameury & J.-P. Lasota, 311
- Kato, M., & Hachisu, I. 2003, *ApJ*, 598, L107
- . 2009, *ApJ*, 699, 1293
- . 2011, *ApJ*, 743, 157
- Kato, M., Hachisu, I., Cassatella, A., & González-Riestra, R. 2011, *ApJ*, 727, 72
- Kato, M., Hachisu, I., Kiyota, S., & Saio, H. 2008, *ApJ*, 684, 1366
- Kato, M., Saio, H., & Hachisu, I. 1989, *ApJ*, 340, 509
- Kerzendorf, W. E., Childress, M., Scharwächter, J., Do, T., & Schmidt, B. P. 2014, *ApJ*, 782, 27
- Kerzendorf, W. E., Schmidt, B. P., Laird, J. B., Podsiadlowski, P., & Bessell, M. S. 2012, *ApJ*, 759, 7
- Kovetz, A., & Prialnik, D. 1985, *ApJ*, 291, 812
- Kraus, M., Borges Fernandes, M., & de Araújo, F. X. 2007, *A&A*, 463, 627

- Kubo, S., Murakami, T., Ishida, M., & Corbet, R. H. D. 1998, PASJ, 50, 417
- Lepo, K., & van Kerkwijk, M. 2013, ApJ, 771, 13
- Levato, H., Miroshnichenko, A. S., & Saffe, C. 2014, A&A, 568, A28
- Lindsay, E. M. 1955, MNRAS, 115, 248
- . 1956, MNRAS, 116, 649
- . 1961, AJ, 66, 169
- Liu, J., Di Stefano, R., Wang, T., & Moe, M. 2012, ApJ, 749, 141
- Liu, Q. Z., van Paradijs, J., & van den Heuvel, E. P. J. 2006, A&A, 455, 1165
- Lopes de Oliveira, R., Motch, C., Smith, M. A., Negueruela, I., & Torrejón, J. M. 2007, A&A, 474, 983
- Lynch, D. K., Russell, R. W., & Sitko, M. L. 2001, AJ, 122, 3313
- Mader, J., & Shafter, A. 1997, PASP, 109, 1351
- Maoz, D., & Mannucci, F. 2012, PASA, 29, 447
- Maoz, D., Mannucci, F., & Nelemans, G. 2014, ARA&A, 52, 107
- Maravelias, G., Zezas, A., Antoniou, V., & Hatzidimitriou, D. 2013, ArXiv e-prints
- Massey, P., & Duffy, A. S. 2001, ApJ, 550, 713
- Massey, P., Olsen, K. A. G., & Parker, J. W. 2003, PASP, 115, 1265
- Massey, P., Parker, J. W., & Garmany, C. D. 1989, AJ, 98, 1305
- McLaughlin, D. B. 1960, in *Stellar Atmospheres*, ed. J. L. Greenstein, 585
- Mikolajewska, J. 2010, ArXiv e-prints
- Mikolajewska, J., Caldwell, N., & Shara, M. M. 2014, ArXiv e-prints
- Miszalski, B., Jones, D., Rodríguez-Gil, P., et al. 2011, A&A, 531, A158
- Miszalski, B., & Mikołajewska, J. 2014, MNRAS, 440, 1410
- Miszalski, B., Mikołajewska, J., & Udalski, A. 2013, MNRAS, 432, 3186
- . 2014, ArXiv e-prints
- Muerset, U., Nussbaumer, H., Schmid, H. M., & Vogel, M. 1991, A&A, 248, 458
- Muerset, U., Schild, H., & Vogel, M. 1996, A&A, 307, 516
- Munari, U., & Zwitter, T. 2002, A&A, 383, 188
- Murakami, T., Koyama, K., Inoue, H., & Agrawal, P. C. 1986, ApJ, 310, L31
- Mürset, U., & Schmid, H. M. 1999, A&AS, 137, 473

- Nahar, S. N. 1999, *ApJS*, 120, 131
- Napiwotzki, R., Yungelson, L., Nelemans, G., et al. 2004, in *Astronomical Society of the Pacific Conference Series*, Vol. 318, *Spectroscopically and Spatially Resolving the Components of the Close Binary Stars*, ed. R. W. Hilditch, H. Hensberge, & K. Pavlovski, 402–410
- Napiwotzki, R., Karl, C. A., Nelemans, G., et al. 2007, in *Astronomical Society of the Pacific Conference Series*, Vol. 372, *15th European Workshop on White Dwarfs*, ed. R. Napiwotzki & M. R. Burleigh, 387
- Nelson, T., Chomiuk, L., Roy, N., et al. 2014, *ApJ*, 785, 78
- Nomoto, K., Nariai, K., & Sugimoto, D. 1979, *PASJ*, 31, 287
- Nomoto, K., Saio, H., Kato, M., & Hachisu, I. 2007, *ApJ*, 663, 1269
- Nota, A., Pasquali, A., Drissen, L., et al. 1996, *ApJS*, 102, 383
- Nugent, P. E., Sullivan, M., Cenko, S. B., et al. 2011, *Nature*, 480, 344
- Oliveira, J. M., van Loon, J. T., Sloan, G. C., et al. 2013, *MNRAS*, 428, 3001
- Orio, M., Nelson, T., Bianchini, A., Di Mille, F., & Harbeck, D. 2010, *ApJ*, 717, 739
- Orio, M., Zezas, A., Munari, U., Siviero, A., & Tepedelenlioglu, E. 2007, *ApJ*, 661, 1105
- Orio, M., Behar, E., Gallagher, J., et al. 2013, *MNRAS*, 429, 1342
- Osborne, J. P., Page, K. L., Beardmore, A. P., et al. 2011, *ApJ*, 727, 124
- Owens, A., Oosterbroek, T., Parmar, A. N., et al. 1999, *A&A*, 348, 170
- Pakmor, R., Kromer, M., Taubenberger, S., & Springel, V. 2013, *ApJ*, 770, L8
- Panagia, N., Van Dyk, S. D., Weiler, K. W., et al. 2006, *ApJ*, 646, 369
- Parker, J. W., Hill, J. K., Cornett, R. H., et al. 1998, *AJ*, 116, 180
- Pasquini, L., Avila, G., Blecha, A., et al. 2002, *The Messenger*, 110, 1
- Patterson, J., Kemp, J., Shambrook, A., et al. 1998, *PASP*, 110, 380
- Patterson, J., Oksanen, A., Monard, B., et al. 2013, *ArXiv e-prints*
- Peña, M., Hamann, W.-R., Ruiz, M. T., Peimbert, A., & Peimbert, M. 2004, *A&A*, 419, 583
- Peña, M., Peimbert, M., Torres-Peimbert, S., Ruiz, M. T., & Maza, J. 1995, *ApJ*, 441, 343
- Peña, M., Ruiz, M. T., Rojo, P., Torres-Peimbert, S., & Hamann, W.-R. 2008, *ApJ*, 680, L109
- Pena, M., Ruiz, M. T., & Torres-Peimbert, S. 1997, *A&A*, 324, 674
- Pickles, A. J. 1998, *PASP*, 110, 863
- Prialnik, D. 1986, *ApJ*, 310, 222
- Pritchett, C. J., Howell, D. A., & Sullivan, M. 2008, *ApJ*, 683, L25

- Sabbi, E., Sirianni, M., Nota, A., et al. 2007, *AJ*, 133, 44
- Sahman, D. I., Dhillon, V. S., Marsh, T. R., et al. 2013, *MNRAS*, 433, 1588
- Sanduleak, N. 1978, *Information Bulletin on Variable Stars*, 1389, 1
- Schaefer, B. E. 2005, *ApJ*, 621, L53
- . 2009, *ApJ*, 697, 721
- . 2010, *ApJS*, 187, 275
- . 2011, *ApJ*, 742, 112
- Schaefer, B. E. 2013, in *American Astronomical Society Meeting Abstracts*, Vol. 221, *American Astronomical Society Meeting Abstracts* 221, 233.06
- Schaefer, B. E., & Pagnotta, A. 2012, *Nature*, 481, 164
- Schaefer, B. E., Pagnotta, A., & Shara, M. M. 2010, *ApJ*, 708, 381
- Schaefer, B. E., Landolt, A. U., Linnolt, M., et al. 2013, *ApJ*, 773, 55
- Schmid, H. 2001, in *Astronomical Society of the Pacific Conference Series*, Vol. 242, *Eta Carinae and Other Mysterious Stars: The Hidden Opportunities of Emission Spectroscopy*, ed. T. R. Gull, S. Johansson, & K. Davidson, 347
- Schmid, H. M. 1989, *A&A*, 211, L31
- Schwab, J., Shen, K. J., Quataert, E., Dan, M., & Rosswog, S. 2012, *MNRAS*, 427, 190
- Schwarz, G. J., Ness, J.-U., Osborne, J. P., et al. 2011, *ApJS*, 197, 31
- Seaton, M. J. 1979, *MNRAS*, 187, 73P
- Selvelli, P., González-Riestra, R., Gilmozzi, R., & Cassatella, A. 2010, *Mem. Soc. Astron. Italiana*, 81, 388
- Shao, Y., & Li, X.-D. 2014, *ArXiv e-prints*
- Shappee, B. J., Kochanek, C. S., & Stanek, K. Z. 2013, *ApJ*, 765, 150
- Shara, M. M., Prialnik, D., & Kovetz, A. 1993, *ApJ*, 406, 220
- Sharp, R., Saunders, W., Smith, G., et al. 2006, in *Society of Photo-Optical Instrumentation Engineers (SPIE) Conference Series*, Vol. 6269, *Society of Photo-Optical Instrumentation Engineers (SPIE) Conference Series*
- Shen, K. J., & Bildsten, L. 2009, *ApJ*, 692, 324
- . 2014, *ApJ*, 785, 61
- Shen, K. J., Idan, I., & Bildsten, L. 2009, *ApJ*, 705, 693
- Shore, S. N., Sanduleak, N., & Allen, D. A. 1987, *A&A*, 176, 59

- Shore, S. N., Schwarz, G. J., De Gennaro Aquino, I., et al. 2013, *A&A*, 549, A140
- Simons, R., Thilker, D., Bianchi, L., & Wyder, T. 2014, *Advances in Space Research*, 53, 939
- Skopal, A. 2005, *A&A*, 440, 995
- Skopal, A. 2011, in *Astronomical Society of the Pacific Conference Series*, Vol. 447, *Evolution of Compact Binaries*, ed. L. Schmidtobreick, M. R. Schreiber, & C. Tappert, 233
- . 2014, ArXiv e-prints
- . 2015, *New A*, 34, 123
- Smith, C., Leiton, R., & Pizarro, S. 2000, in *Astronomical Society of the Pacific Conference Series*, Vol. 221, *Stars, Gas and Dust in Galaxies: Exploring the Links*, ed. D. Alloin, K. Olsen, & G. Galaz, 83
- Sokoloski, J. L., Crofts, A. P. S., Lawrence, S., & Uthas, H. 2013, *ApJ*, 770, L33
- Steiner, J. E., & Diaz, M. P. 1998, *PASP*, 110, 276
- Stokes, G. H., Taylor, J. H., & Dewey, R. J. 1985, *ApJ*, 294, L21
- Sturm, R., Haberl, F., Pietsch, W., et al. 2011, ArXiv e-prints
- . 2013, *A&A*, 558, A3
- Sullivan, M., Le Borgne, D., Pritchett, C. J., et al. 2006, *ApJ*, 648, 868
- Szymanski, M. K. 2005, *Acta. Astron.*, 55, 43
- Thoroughgood, T. D., Dhillon, V. S., Littlefair, S. P., Marsh, T. R., & Smith, D. A. 2001, *MNRAS*, 327, 1323
- Thureau, N. D., Monnier, J. D., Traub, W. A., et al. 2009, *MNRAS*, 398, 1309
- Torrejón, J. M., & Orr, A. 2001, *A&A*, 377, 148
- Torres, A. F., Kraus, M., Cidale, L. S., et al. 2012, *MNRAS*, 427, L80
- Tutukov, A. V., & Iungelson, L. R. 1976, *Astrofizika*, 12, 521
- Udalski, A., Kubiak, M., & Szymanski, M. 1997, *Acta. Astron.*, 47, 319
- Uthas, H., Knigge, C., & Steeghs, D. 2010, *MNRAS*, 409, 237
- van den Heuvel, E. P. J., Bhattacharya, D., Nomoto, K., & Rappaport, S. A. 1992, *A&A*, 262, 97
- van Genderen, A. M., & Sterken, C. 2002, *A&A*, 386, 926
- van Kerkwijk, M. H., Chang, P., & Justham, S. 2010, *ApJ*, 722, L157
- van Kerkwijk, M. H., & Kulkarni, S. R. 1999, *ApJ*, 516, L25
- Wagner, R. M., Foltz, C. B., & Starrfield, S. G. 2001, *IAU Circ.*, 7556, 2
- Wallerstein, G. 1981, *The Observatory*, 101, 172

- Wang, Y., Weigelt, G., Kreplin, A., et al. 2012, *A&A*, 545, L10
- Warner, B. 1995, *Cambridge Astrophysics Series*, 28
- Waters, L. B. F. M., Pols, O. R., Hogeveen, S. J., Cote, J., & van den Heuvel, E. P. J. 1989, *A&A*, 220, L1
- Williams, R. 2012, *AJ*, 144, 98
- Wisniewski, J. P., Bjorkman, K. S., Bjorkman, J. E., & Clampin, M. 2007, *ApJ*, 670, 1331
- Wolf, W. M., Bildsten, L., Brooks, J., & Paxton, B. 2013, *ApJ*, 777, 136
- Woods, T. E., & Gilfanov, M. 2013, *MNRAS*, 432, 1640
- Woosley, S. E., & Weaver, T. A. 1994, *ApJ*, 423, 371
- Woudt, P. A., Steeghs, D., Karovska, M., et al. 2009, *ApJ*, 706, 738
- Yamashita, Y., Maehara, H., & Norimoto, Y. 1982, *PASJ*, 34, 269
- Yaron, O., Prialnik, D., Shara, M. M., & Kovetz, A. 2005, *ApJ*, 623, 398
- Zaritsky, D., Harris, J., Thompson, I. B., Grebel, E. K., & Massey, P. 2002, *AJ*, 123, 855
- Zickgraf, F.-J. 2006, in *Astronomical Society of the Pacific Conference Series*, Vol. 355, *Stars with the B[e] Phenomenon*, ed. M. Kraus & A. S. Miroshnichenko, 135
- Zickgraf, F.-J., Wolf, B., Stahl, O., & Humphreys, R. M. 1989, *A&A*, 220, 206